

**INVESTIGATION OF PROPERTIES,  
CORROSION AND BIOACTIVITY OF NOVEL  
BaO ADDED PHOSPHATE GLASSES AND  
GLASS-CERAMIC COATING ON  
BIOMEDICAL METALLIC IMPLANT  
MATERIALS**

Thesis

Submitted in partial fulfillment of the requirements for the degree of

**DOCTOR OF PHILOSOPHY**

by

**AKHILA B EDATHAZHE**



DEPARTMENT OF PHYSICS

NATIONAL INSTITUTE OF TECHNOLOGY KARNATAKA,

SURATHKAL, MANGALORE - 575025

OCTOBER, 2018

**INVESTIGATION OF PROPERTIES,  
CORROSION AND BIOACTIVITY OF NOVEL  
BaO ADDED PHOSPHATE GLASSES AND  
GLASS-CERAMIC COATING ON  
BIOMEDICAL METALLIC IMPLANT  
MATERIALS**

Thesis

Submitted in partial fulfillment of the requirements for the degree of

**DOCTOR OF PHILOSOPHY**

by

**AKHILA B EDATHAZHE**



DEPARTMENT OF PHYSICS

NATIONAL INSTITUTE OF TECHNOLOGY KARNATAKA,

SURATHKAL, MANGALORE - 575025

OCTOBER, 2018

## **DECLARATION**

*by the Ph.D. Research Scholar*

I hereby *declare* that the Research Thesis entitled “**Investigation of properties, corrosion and bioactivity of novel BaO added phosphate glasses and glass-ceramic coating on biomedical metallic implant materials**”, which is being submitted to the **National Institute of Technology Karnataka, Surathkal** in partial fulfillment of the requirements for the award of the Degree of **Doctor of Philosophy** in **Physics** is a *bonafide report of the research work carried out by me*. The material contained in this Research Thesis has not been submitted to any University or Institution for the award of any degree.

**Akhila B Edathazhe**

Register No. 123009PH12F04

Department of Physics

National Institute of Technology Karnataka, Surathkal

Place: NITK-Surathkal

Date:

## CERTIFICATE

This is to *certify* that the Research Thesis entitled “**Investigation of properties, corrosion and bioactivity of novel BaO added phosphate glasses and glass-ceramic coating on biomedical metallic implant materials**”, submitted by **Akhila B Edathazhe** (Register No. 123009PH12F04) as the record of the research work carried out by her, is *accepted as the Research Thesis submission* in partial fulfillment of the requirements for the award of degree of *Doctor of Philosophy*.

**Dr. H. D. Shashikala**

Research Guide

Professor, Department of Physics

National Institute of Technology Karnataka, Surathkal

**Chairman- DRPC**

(Signature with Date and Seal)

**DEDICATED TO MY BELOVED FAMILY**

## **ACKNOWLEDGEMENT**

I would like to acknowledge National Institute of Technology (NIT) Karnataka, Surathkal, India for providing Ph.D. fellowship from Ministry of Human Resource Development (MHRD), Government of India.

I am grateful to my research supervisor, Prof. H. D. Shashikala, Department of Physics, NIT Karnataka, Surathkal for giving me an opportunity to conduct my research. I would like to thank for her valuable suggestions, discussions and encouragement throughout my research work. Her sincere approach to both research and personal life teach me to keep the rhythm and harmony between professional and personal life as a woman.

I would like to thank Prof. G. Umesh and Prof. N K Udayashankar, Department of Physics, NIT Karnataka for their smiling faces and supporting words which filled me with enormous pleasure and strength during my research.

I would like to express my deepest appreciation to Research Progress and Assessment Committee Members, Dr. S M Murigendrappa, Department of Mechanical Engineering and Dr. Partha Pratim Das, Department of Physics, NIT Karnataka for their valuable suggestions and support.

A special regards to all the faculty members in the Department of Physics, NIT Karnataka, Dr. M. N. Satyanarayan, Prof. Kasturi. V. Bangera, Dr. H. S. Nagaraja, Dr. Ajith K M, Dr. Deepak Vaid, Dr. T. K. Shajahan and Dr. Kartick Tarafder for all the help and support provided at different stages of research. I acknowledge the help and cooperation of the non-teaching staffs of Department of Physics, NIT Karnataka in successful execution of my daily activities in the department.

A special mention of thanks to all my colleagues especially Amudha A, NIT Karnataka for their friendly approaches and helps at the different stages of my research work.

I would like to extend my gratitude to Prof. Nithyanandha Shetty, Department of Chemistry and Prof. Narendranath, Department of Mechanical Engineering, NIT Karnataka for giving corrosion and hardness test facilities respectively. Sincere thanks to Sophisticated Test and Instrumentation Center (STIC) Cochin, Innovation center (MIT Manipal) and IIT Roorkee for giving me FTIR, SEM and DTA analysis facilities respectively.

I would like to express my deepest gratefulness to all my beloved teachers from St. Mary's Nursery School Kottayadu, St. Joseph's U P School Vayattuparamba, Santhome H S S Kolakkadu, Nirmalagiri College Kuthuparamba, P K R Arts and Science College for Women Gobichettipalayam, and Vivekanandha College of Arts and Sciences for Women Tiruchengode for their supports, love, encouragement and especially for helping me to come forward in both curricular and extracurricular activities. Special mention of thanks to all my teachers from Catechism Schools associated with Little Flower Church Karuvanchal, St. Sebastian's Church Nedumpuramchal and St. Joseph's Church Thondiyl for their unforgettable support and enormous love during my studies. Notable thanks to all my friends from all the above mentioned institutes for their helps and friendly behavior.

Special record of gratitude to Fr. Mathew Alamkottu from Archdiocese of Tellicherry and Sr. Annie George from S. H. Convent for their spiritual guidance and love, which made my childhood as awesome.

I would like to express my sincere gratitude to my Grandparents especially to Late. Mrs. Elikkutty Kurivinalpakuthiyil for her motherly love and supports. Without her support and care, I never reach up to here. Tearful eyes of thankfulness to Late. Mr. Joseph Kurivinalpakuthiyil, Late. Mr. George and Mr. Chacko Kurivinalpakuthiyil for the wealth and things that help me to reach up to here.

I would like to thank my uncle Late. Adv. Georgekutty Edathazhe, who directed me to the world of Physics. I am grateful to his enormous support and timely help in my life.

I would like to express my sincere gratitude to my parents Mr. Billy Thomas Edathazhe and Mrs. Leena Billy who paved the path before me upon whose shoulders I stand. Sincere thanks to them for brought me up well especially when they were struggled a lot in life. Wholehearted appreciation to my beloved parents for holding me closer when I am unable to move forward in my life.

Sincere thanks to my beloved younger sister Ms. Aparna Billy and my cousin brother Mr. Abijith Sebastin Mundackal for their kind love, prayer and supports all through my life. Special thanks to my aunties Rosamma Joseph, Lincy Alikalthazhe and Anu Pathalil for their maternal love and helps.

I express my heart-felt gratitude to my dearest husband, Mr. Sijo Kaviyil Joseph who brought me an idea initially and inspire me to carry out Ph.D. and M.Phil. studies. His infallible love and support flourish my day today life and professional life always with joy and wellness especially when I face the difficulties. Since his grate love to all my drawbacks along with my strengths make me what I am today.

My special word of thanks to my parents-in-law Mr. Jose Kaviyil and Mrs. Elsy Jose for loving me as your own daughter. Notable regards to their supports in my struggles and prayers to reach at my goals. Heart-full thanks to them to give me a second home where I feel that I am still at my loving parent's laps and my beloved better half.

Above all, my grateful acknowledgement to the God Almighty, Mary Matha and all the Saints for all the blessings and make me a better person in each day. Sincere thanks to fill the hopes and divine love in me when I was fallen apart. Special regards to my Lord for giving me a wonderful family and friends who groomed me to reach up to this stage of life.

**Akhila B Edathazhe**



## ABSTRACT

This thesis deals with the synthesis, characterization and investigation of properties of phosphate glasses with composition  $(26-x)\text{Na}_2\text{O}-x\text{BaO}-29\text{CaO}-45\text{P}_2\text{O}_5$  ( $x = 0, 5, 10, 15$  mol%) and coating of  $11\text{Na}_2\text{O}-15\text{BaO}-29\text{CaO}-45\text{P}_2\text{O}_5$  glass on biomedical metallic implant materials such as stainless steel 316 L, duplex stainless steel (DSS) 2205 and Ti6Al4V alloy. Glasses were prepared by melt-quenching technique and glass was coated by thermal enamelling technique. Effect of BaO addition on the structural, mechanical, thermal, optical, dissolution and *in vitro* bioactivity properties of bioactive  $\text{Na}_2\text{O}-\text{CaO}-\text{P}_2\text{O}_5$  glasses was the main subject of study. The glasses were synthesized at three melting temperatures such as 1000, 1100, 1200°C. Glasses prepared at 1200°C were having lower brittleness attributing to the plastic flow of deformation. Brittleness of glasses prepared at higher melting temperatures has decreased with BaO addition, whereas thermal stability, glass forming ability and optical band gap energy have increased. Dissolution rate of glasses in deionized water was reduced by three orders of magnitude with BaO content of 15 mol %. *In vitro* bioactivity studies of glasses were carried out in Phosphate buffer saline (PBS) and Hank's balanced salt (HBS) solutions for 28 days. Bioactivity of glasses was improved with BaO content. Faster hydroxyapatite (HAp) formation was observed in HBS solution in comparison with PBS. All the coatings have glass-ceramic nature with porous morphology. DSS and coated 316 L were having higher electrochemical corrosion resistance in HBS solution among uncoated and coated substrates respectively. DSS 2205 can be an alternative for 316 L and Ti6Al4V for biomedical applications due to its better corrosion resistance. *In vitro* bioactivity test of glass coated samples were conducted in HBS solution for 14 days and formation of amorphous calcium-phosphate (ACP) layer on coatings was noticed.

**Keywords:** Phosphate glass; glass-ceramic coating; structural property; mechanical property; thermal property; optical property; dissolution rate; bioactivity; electrochemical corrosion resistance; biomedical application

# Contents

<b>List of Figures</b>	<b>v</b>
<b>List of Tables</b>	<b>viii</b>
<b>Nomenclature</b>	<b>x</b>
<b>1 INTRODUCTION</b>	<b>1</b>
1.1 GLASS	1
1.2 PHOSPHATE GLASSES	3
1.2.1 Structure of phosphate glasses	3
1.2.2 Properties and application of phosphate glasses	4
1.3 GLASS – AS A BIOMATERIAL	5
1.3.1 History of bioactive glasses	6
1.3.2 Properties of bioactive glasses	7
1.3.3 Behavior of therapeutic ions in the glass matrix	8
1.3.4 Applications of bioactive glasses	9
1.4 GLASS – AS A COATING MATERIAL	11
1.4.1 Properties of glass coating	11
1.4.2 Details of different coating methods	11
1.5 BIOMEDICAL IMPLANTS (BMI)	12
1.5.1 Metals – as implant materials	14
1.5.2 Glass coating for biomedical implants	17
1.6 CaO-Na <sub>2</sub> O-P <sub>2</sub> O <sub>5</sub> GLASSES	17
1.7 SCOPE AND OBJECTIVES OF THE PRESENT WORK	18
1.7.1 Scope	18
1.7.2 Objectives	22

1.8	Organization of the thesis	22
<b>2</b>	<b>MATERIALS AND METHODS</b>	<b>25</b>
2.1	PREPARATION OF GLASSES	26
2.1.1	Materials used for glass preparation	26
2.1.2	Methods used for glass preparation	27
2.1.3	Surface polishing of glass samples	27
2.2	CHARACTERIZATION TECHNIQUES OF GLASSES	29
2.2.1	X-ray diffraction (XRD) studies	30
2.2.2	Fourier transform infra-red (FTIR) spectroscopy	31
2.2.3	Scanning electron microscopy (SEM) and energy dispersive X-ray spectroscopy (EDS)	32
2.2.4	Density, molar volume and theoretical structural parameters	33
2.2.5	Mechanical properties	36
2.2.6	Thermal analysis	40
2.2.7	Optical properties	41
2.2.8	Dissolution studies	44
2.2.9	In-vitro bioactivity test of glasses	46
2.3	PREPARATION OF GLASS COATINGS	48
2.4	CHARACTERIZATION TECHNIQUES OF GLASS COATINGS	49
2.4.1	Structural and compositional studies	49
2.4.2	Electrochemical corrosion study	50
2.4.3	In-vitro bioactivity test of glass coatings	52
2.5	ERROR ANALYSIS	53
2.5.1	Standard deviation of mean (SDOM)	54
2.5.2	Quadrature sum of uncertainty	54

<b>3</b>	<b>EFFECT OF BaO ADDITION ON THE STRUCTURAL AND MECHANICAL PROPERTIES OF Na<sub>2</sub>O-CaO-P<sub>2</sub>O<sub>5</sub> GLASSES</b>	<b>56</b>
3.1	RESULTS AND DISCUSSION	56
3.1.1	Structural investigations of synthesized glasses	57
3.1.2	Mechanical properties of synthesized glasses	64
3.1.3	Effect of melting temperature on the properties of synthesized glasses	68
3.2	SUMMARY	69
<b>4</b>	<b>EFFECT OF BaO ADDITION ON THE THERMAL AND OPTICAL PROPERTIES OF Na<sub>2</sub>O-CaO-P<sub>2</sub>O<sub>5</sub> GLASSES</b>	<b>70</b>
4.1	RESULTS AND DISCUSSION	70
4.1.1	Thermal properties of synthesized glasses	71
4.1.2	Optical properties of synthesized glasses	75
4.2	SUMMARY	78
<b>5</b>	<b>EFFECT OF BaO ADDITION ON THE DISSOLUTION AND IN-VITRO BIOACTIVITY PROPERTIES OF Na<sub>2</sub>O-CaO-P<sub>2</sub>O<sub>5</sub> GLASSES</b>	<b>80</b>
5.1	RESULTS AND DISCUSSION	80
5.1.1	Dissolution studies of synthesized glasses	81
5.1.2	In-vitro bioactivity tests of synthesized glasses	92
5.2	SUMMARY	105
<b>6</b>	<b>ELECTROCHEMICAL CORROSION AND IN-VITRO BIOACTIVITY PROPERTIES OF BaO CONTAINING Na<sub>2</sub>O-CaO-P<sub>2</sub>O<sub>5</sub> PHOSPHATE GLASS-CERAMIC COATING ON 316 L, DUPLEX STAINLESS STEEL 2205 AND Ti6Al4V</b>	<b>107</b>

6.1	RESULTS AND DISCUSSION	108
6.1.1	Structural and compositional studies of coatings	108
6.1.2	Electrochemical corrosion studies	112
6.1.3	In-vitro bioactivity test of coatings	122
6.2	SUMMARY	126
<b>7</b>	<b>SUMMARY AND CONCLUSIONS</b>	<b>127</b>
7.1	SUMMARY	127
7.2	CONCLUSIONS	129
7.3	SCOPE FOR THE FUTURE WORK	131
	<b>References</b>	<b>132</b>
	<b>List of publications</b>	<b>150</b>
	<b>Curriculum vitae</b>	<b>153</b>

## List of Figures

1.1	Structure of (a) crystalline and (b) amorphous SiO <sub>2</sub>	2
1.2	Schematic diagram of phosphorous tetrahedral sites in phosphate glasses	4
1.3	Implants in the human body structure	13
1.4	Schematic diagram of stent located inside the arterial structure	16
2.1	Flow chart of the steps involved in preparation and processing of glasses	28
2.2	Images of synthesized glasses	29
2.3	Furnaces used for glass preparation	29
2.4	XRD machine used for analysis of synthesized glasses	31
2.5	Density measurement setup used for the synthesized glasses	34
2.6	Schematic diagram of residual impression formed on surface of sample by Vickers indentation	39
2.7	Schematic diagram of cracks propagating from four corners of Vickers indentation	39
2.8	Flow chart of process involved in glass coating synthesis and processing	49
2.9	Potentiodynamic polarization curve or tafel plot and (b) schematic diagram of electrochemical polarization cell	51
3.1	XRD pattern of glasses prepared at (a) 1000°C, (b) 1100°C, (c) 1200°C	57
3.2	FTIR spectrum of glasses prepared at (a) 1000°C, (b) 1100°C and (c) 1200°C	58
3.3	SEM images of synthesized glasses (a) C0 and (b) C15	61
3.4	EDS spectra of synthesized glasses (a) C0 and (b) C15	61

3.5	SEM images of synthesized glasses after indentation (a) A5, (b) A15 and (c) C15	65
4.1	DTA thermograms of glass samples (a) without (C0) & (b) with BaO (C5)	72
4.2	(a) $(\alpha h\nu)^{1/2}$ and (b) $\ln(\alpha)$ as a function of photon energy, $h\nu$ of $\text{Na}_2\text{O-BaO-CaO-P}_2\text{O}_5$ glasses	76
5.1	Ionic concentration of (a) $\text{PO}_4^{3-}$ , (b) $\text{Ca}^{2+}$ , (c) $\text{Na}^+$ and (d) pH in deionized water	83
5.2	SEM images of (a) untreated C15 and treated (b) C0, (c) C5, (d) C10 and (e) C15 in deionized water for 28 days and (f) grain structure of white layer on C 5	86
5.3	XRD spectra of $\text{Na}_2\text{O-BaO-CaO-P}_2\text{O}_5$ glasses after the immersion in deionized water for 28 days	88
5.4	FTIR spectra of $\text{Na}_2\text{O-BaO-CaO-P}_2\text{O}_5$ glasses after immersion in deionized water for 28 days	89
5.5	Ionic concentration of (a) $\text{PO}_4^{3-}$ , (b) $\text{Ca}^{2+}$ , (c) $\text{Na}^+$ and (d) pH measurements in PBS solution	92
5.6	Ionic concentration of (a) $\text{PO}_4^{3-}$ , (b) $\text{Ca}^{2+}$ , (c) $\text{Na}^+$ and (d) pH measurements in HBS solution	93
5.7	XRD pattern of (a) C0 and (b) C5 after immersion in PBS for 28 days	96
5.8	XRD pattern of (a) C0 and (b) C15 after immersion in HBS for 28 days	97
5.9	SEM images of (a) C0, (b) C10 and (c) C15 after immersion in PBS for 28 days	98
5.10	SEM images of (a) C0 and (b) C15 and (c) grain structure of layer formed on C15 after immersion in HBS for 28 days	99
5.11	FTIR spectra of $\text{Na}_2\text{O-BaO-CaO-P}_2\text{O}_5$ glasses after immersion in (a) PBS and (b) HBS solutions for 28 days	102

6.1	XRD spectra of glass coated and uncoated (a) 316 L, (b) DSS and (c) Ti6Al4V	109
6.2	SEM images of glass coated Ti6Al4V (a) & (b) at different magnifications and (c) cross-sectional view of coating	110
6.3	Polarization curves of (a) uncoated & (b) glass coated substrates	112
6.4	XRD image of glass coated and uncoated 316 L after the electrochemical corrosion studies	114
6.5	SEM images of (a) glass coated Ti6Al4V and (b) magnified image of needle shaped particles formed on it after the electrochemical corrosion studies	115
6.6	SEM image of uncoated Ti6Al4V after electrochemical corrosion test and (b) weight losses of uncoated samples after in-vitro bioactivity test	118
6.7	SEM images of coated Ti6Al4V after HBS immersion for 14 days	122
6.8	(a) pH (b) $\text{PO}_4^{3-}$ (c) $\text{Ca}^{2+}$ and (d) $\text{Na}^+$ ion release rate from coated substrates after immersion in HBS for 14 days	125



## List of Tables

1.1	Applications of biomedical metallic implants	15
2.1	Batch composition of synthesized Na <sub>2</sub> O-BaO-CaO-P <sub>2</sub> O <sub>5</sub> glasses	26
2.2	Ionic composition of Human blood plasma and simulated body fluids	47
3.1	Assigned vibrational bands in FTIR spectra of Na <sub>2</sub> O-BaO-CaO-P <sub>2</sub> O <sub>5</sub> glasses	59
3.2	Mass % of elements calculated from batch composition and obtained from EDS analysis for glasses prepared at 1200°C. Minimum and maximum values are reported	62
3.3	Density ( $\rho_{mes}$ ), molar volume ( $V_m$ ), oxygen packing density ( $\rho_{ox}$ ), oxygen molar volume ( $V_o$ ) and cross-link density (CLD) values of Na <sub>2</sub> O-BaO-CaO-P <sub>2</sub> O <sub>5</sub> glasses	63
3.4	Number of bonds ( $N_b$ ), inter ionic distance between Ba <sup>2+</sup> [R(Ba <sup>2+</sup> )] and Na <sup>+</sup> [R(Na <sup>+</sup> )] ions, phosphorous molar volume ( $V_m^P$ ), average phosphorous-phosphorous distance ( $\langle d_{p-p} \rangle$ ) values of Na <sub>2</sub> O-BaO-CaO-P <sub>2</sub> O <sub>5</sub> glasses	64
3.5	Measured microhardness ( $H_v$ ), calculated brittleness ( $\chi$ ), fracture toughness ( $K_{IC}$ ) and measured half crack-length (c) of Na <sub>2</sub> O-BaO-CaO-P <sub>2</sub> O <sub>5</sub> glasses	66
3.6	Theoretically calculated mechanical properties of Na <sub>2</sub> O-BaO-CaO-P <sub>2</sub> O <sub>5</sub> glasses	68
4.1	Thermal properties obtained from DTA analysis and density of Na <sub>2</sub> O-BaO-CaO-P <sub>2</sub> O <sub>5</sub> glasses	71
4.2	Refractive index, optical band gap energy and Urbach energy of Na <sub>2</sub> O-BaO-CaO-P <sub>2</sub> O <sub>5</sub> glasses	77
4.3	Optical properties of Na <sub>2</sub> O-BaO-CaO-P <sub>2</sub> O <sub>5</sub> glasses calculated from molar volume and optical band gap energy values	78
5.1	Weight losses and dissolution rates of Na <sub>2</sub> O-BaO-CaO-P <sub>2</sub> O <sub>5</sub> glasses in deionized water	81

5.2	Mass % of elements on Na <sub>2</sub> O-BaO-CaO-P <sub>2</sub> O <sub>5</sub> glasses before and after immersion in deionized water for 28 days	87
5.3	Assigned vibrational bands in FTIR spectra of Na <sub>2</sub> O-BaO-CaO-P <sub>2</sub> O <sub>5</sub> glasses before and after the immersion in deionized water for 28 days	91
5.4	Mass % of elements on glass samples after immersion in PBS and HBS solutions for 28 days	100
5.5	Assigned vibrational bands in FTIR spectra of Na <sub>2</sub> O-BaO-CaO-P <sub>2</sub> O <sub>5</sub> glasses after the immersion in PBS and HBS solutions for 28 days	103
6.1	Mass % of elements present on coated substrates and glass. Column I, II and III indicate top surface, interface (~ 20-30 μm between coating & substrate) and substrate respectively	111
6.2	Corrosion current (I <sub>COR</sub> ), corrosion potential (E <sub>COR</sub> ), anodic (β <sub>A</sub> ) & cathodic (β <sub>C</sub> ) Tafel slope and polarization resistance (R <sub>P</sub> ) derived from the polarization curve	113
6.3	Mass % of elements on the surface of glass coated substrates as determined from EDS after the electrochemical corrosion test along with the thickness of coatings before and after the electrochemical corrosion test	116
6.4	Mass % of elements from EDS on uncoated 316 L and DSS before and after electrochemical corrosion test	119
6.5	Mass % of elements measured using EDS on uncoated Ti6Al4V before and after electrochemical corrosion test	121
6.6	Mass% of elements on coated substrates after HBS immersion for 14 days	123

## Nomenclature

$\text{Å}^\circ$	Angstrom
$^\circ\text{C}$	Degree Celsius
$\alpha$	Alfa
$\alpha(\nu)$	Absorption coefficient
$\alpha_m$	Molar polarizability
$\alpha_o$	Anion polarizability
$\beta_a$	Anodic tafel slope
$\beta_c$	Cathodic tafel slope
$\beta$	Beta
$\chi$	Brittleness
$\rho_{\text{mes}}$	Measured density
$\rho_l$	Density of xylene
$\rho_{\text{ox}}$	Molar oxygen packing density
$\sigma$	Poisson's ratio
$\lambda$	Optical basicity
ACP	Amorphous calcium phosphate
Al	Aluminum

ASTM	American Society for Testing and Materials
ATP	Adenosine tri-phosphate
B	Boron
Ba	Barium
BaCO <sub>3</sub>	Barium carbonate
BaO	Barium oxide
Ba(PO <sub>3</sub> ) <sub>2</sub>	Barium phosphate
BMD	Bone mineral density
BMI	Biomedical implant
BSE	Back scattered electron
C	Carbon
<i>C</i>	Ionic concentration
<i>c</i>	Half crack-length
Ca	Calcium
CaCO <sub>3</sub>	Calcium carbonate
CaO	Calcium oxide
CaP	Calcium phosphate
Ca(PO <sub>3</sub> ) <sub>2</sub>	Calcium triphosphate
Ca <sub>2</sub> P <sub>2</sub> O <sub>7</sub>	Calcium pyrophosphate

$\text{Ca}_{10}(\text{PO}_4)_6(\text{OH})_2$	Hydroxyapatite
Ce	Cerium
Cl	Chlorine
cm	Centimeter
Co	Cobalt
$\text{CO}_2$	Carbon dioxide
$\text{CO}_3^{2-}$	Carbonate ion
CLD	Cross link density
Cr	Chromium
CRG	Controlled release glass
DBO	Double bonded oxygen
DCP	Direct current polarization
$d_{\text{p-p}}$	Average distance between phosphorous ions
DSS	Duplex stainless steel
DTA	Differential thermal analysis
E	Yong's modulus
EBS	Diffacted back scattered electron
ECM	Extra cellular matrix
$E_{\text{COR}}$	Corrosion potential
EDS	Energy dispersive X-ray spectroscopy

$E_g$	Optical band gap energy
EIS	Electrochemical impedance spectroscopy
$E_{OC}$	Open circuit potential
Er	Erbium
etc.	et cetera
$E_u$	Urbach energy
ERMI	Endosseous ridge maintenance implant
F	Fluorine
FDA	Food and Drug Administration, U.S.
Fe	Iron
$Fe_2O_3$	Iron oxide
$f_i$	Elemental concentration from EDS
FTIR	Fourier transform Infra-red
gm	Gram
GF	Growth factor
$G_i$	Dissociation energy
H	Hydrogen
$h$	Plank's constant
HAp	Hydroxyapatite
HBS	Hank's balanced salt solution

$\text{HCO}_3^{2-}$	Bi-carbonate ion
$\text{HPO}_4^{2-}$	Hydrogen phosphate ion
hr.	Hour
$H_v$	Vickers hardness
HVOF	High velocity oxy fuel
I	Current
$I_{\text{COR}}$	Corrosion current
ICSD	Inorganic crystal structure database
IR	Infra-red
ISO	International Organization for Standardization
JCPDS	Joint committee on powder diffraction standards
K	Bulk modulus
KBr	Potassium bromide
k/cal	Kilo calorie
$K_{1C}$	Fracture toughness
$K_{gl}$	Hruby's parameter
L	Liter
M	Modifier cation

Mw	Molecular weight
$M_c$	Metallization criteria
mM	Milli molar
MEP	Middle ear replacement prosthesis
Mg	Magnesium
MGP	Matrix gla protein
$\mu\text{m}$	Micrometer
min.	Minute
mg	Milligram
Mn	Manganese
Mo	Molybdenum
mV	Milli-volt
N	Nitrogen
Na	Sodium
NaBaP	Sodium barium phosphate
$N_{\text{avg}}$	Avogadro's number
$\text{Na}_2\text{CO}_3$	Sodium carbonate
$\text{Na}_2\text{O}$	Sodium oxide
$\text{NaPO}_3$	Sodium phosphate
$n(A)$	Ionic concentration



Nb	Niobium
$n_f$	Coordination number
$n_i$	Number of cations
NH <sub>3</sub>	Ammonia
NH <sub>4</sub> H <sub>2</sub> PO <sub>4</sub>	Ammonium dihydrogen phosphate
NH <sub>4</sub> OH	Ammonium hydroxide
Ni	Nickel
$n(O)$	Number moles of oxygen
$N_o$	Number of oxygen ions
O	Oxygen
OH	Hydroxide
P	Phosphorous
<i>P</i>	Load
PBS	Phosphate buffer saline solution
PID	Proportional-Integral-Derivative
PLD	Pulsed laser deposition
P <sub>2</sub> O <sub>3</sub>	Phosphorous trioxide
P <sub>2</sub> O <sub>4</sub>	Phosphorous tetraoxide
P <sub>2</sub> O <sub>5</sub>	Phosphorous pentoxide
ppm	Parts/million

PS	Plasma spray
R(A)	Inter ionic distance
R <sub>m</sub>	Molar refraction
RNA	Ribonucleic acid
R <sub>p</sub>	Polarization resistance
S	Surface area
S	Sulfur
SBF	Simulated body fluid
SCL	Super cooled liquid
SE	Secondary electron
sec.	Second
SEM	Scanning electron microscope
SDOM	Standard deviation of mean
Si	Silicon
SiO <sub>2</sub>	Silicon dioxide
Sm	Samarium
SO <sub>4</sub> <sup>2-</sup>	Sulphate ion
Sr	Strontium
Ta	Tantalum
T <sub>g</sub>	Glass transition temperature

Ti	Titanium
$T_m$	Melting temperature
$T_x$	Onset of crystallization temperature
$\Delta T$	Thermal stability
UV	Ultra-violet
V	Volume of solution
V	Vanadium
$V_m$	Molar volume
$V_m^p$	Phosphorous molar volume
$V_m$	Oxygen molar volume
V-P <sub>2</sub> O <sub>5</sub>	Vitreous- phosphorous pentoxide
$V_t$	Packing density
$W_a$	Weight in air
$W_l$	Weight in liquid
$W_L$	Weight loss
$W_o$	Initial weight
$W_t$	Weight at time, t
wt	Weight
x	Modifier concentration
X	Mole fraction

XRD

X-ray diffraction

Zn

Zinc

Zr

Zirconium

## **Chapter 1**

### **INTRODUCTION**

Materials have influenced the fascinating history of human era and especially their heroic actions behind the transformation of human culture from stone age divulges their inspiring role in the society. Solid materials can be classified generally as crystalline and amorphous. According to Dembovsky and Chechetkina (1982), the two basic classes of amorphous solids are amorphous metals and glasses. The amorphous metals are good electrical conductors whereas most of the common glasses are good insulators. The journey of glass starts from old age weapons to modern energy harvesting materials. The naturally occurring volcanic glass or obsidian was used by ancient people for making weapons. Glass was synthesized by Egyptians at first in the form of beads about 4000 BC. The manufacturing of glass was started in Europe and Middle East about 200 BC under the ruling of Roman Empire. During the nineteenth century, the scientists like Abbe, Scott etc. started to research on glasses for optical applications. The introduction of float glass production by Sir Alistair Pilkington in 1950's is a greatest event in glass history (Burling 2006). The latest arguments show that we are living in a 'glass age' (Morse and Evenson 2016) and it is an indication of versatile role of glass in the metamorphosis of modern civilization due to its enormous technical capabilities. The property based applications of any material define its future and the special characteristic properties of glasses are key enabler of its practical usages from kitchen to space and from house wife to a scientist.

#### **1.1 GLASS**

Glass can be defined as an amorphous solid completely lacking in long range,

periodic atomic structure, and exhibiting a region of glass transformation behavior. Any material, inorganic, organic, or metallic, formed by any technique, which exhibits glass transformation behavior is a glass (Shelby 2007). According to the material scientists E D Zanotto and J C Mauro (2017) glass is a non-equilibrium, non-crystalline condensed state of matter that exhibits a glass transition. The structure of glasses is similar to that of their parent supercooled liquids (SCL), and they spontaneously relax towards the SCL state. The ultimate fate, in the limit of infinite time, is to crystallise. Debates are going on the classification of glass as a frozen liquid and its redefinition as liquid from solid due to the structural similarity of glass to its parent supercooled liquid. Glasses can relax and deform like liquids under the action of gravity alone, whereas the solids deform under only external pressure (Zanotto and Mauro 2017, Welch et al. 2013).

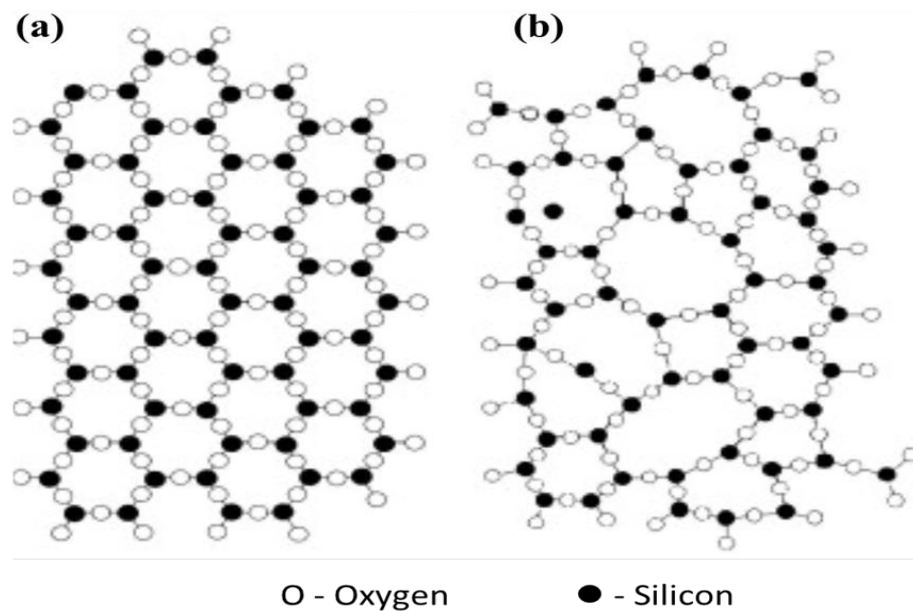


Figure 1.1: Structure of (a) crystalline and (b) amorphous SiO<sub>2</sub> (Jiang and Zhang 2014)

Short range order of glasses originates from the similarity of bond length and bond angles between atoms at some positions of entire structure. The bond length and

angle are similar throughout the whole structure of crystals, which leads to its long range periodic order. The schematic diagram of crystalline and glassy forms of  $\text{SiO}_2$  is given in Figure 1.1.

## 1.2 PHOSPHATE GLASSES

### 1.2.1 Structure of phosphate glasses

Phosphate glasses contain network forming oxide as  $\text{P}_2\text{O}_5$ . Among the three known form of Phosphorous (P) such as  $\text{P}_2\text{O}_3$ ,  $\text{P}_2\text{O}_4$ ,  $\text{P}_2\text{O}_5$ , only  $\text{P}_2\text{O}_5$  can form glasses. Formation of tetrahedral network of glass is possible for  $\text{P}_2\text{O}_5$  due to the cation to anion ratio of 0.256 according to Goldschmidt rule of glass formation.

The basic structural unit of phosphate glasses is  $\text{PO}_4^{3-}$  tetrahedra. P- atom in each tetrahedra forms covalent bond to three bridging oxygens which can link to other tetrahedra to form various phosphate anions and one place is occupied by terminal double bonded oxygen (DBO). Phosphate tetrahedra are represented using  $Q^i$  terminology, where, 'i' indicates the number of bridging oxygen per tetrahedra as shown in Figure 1.2. Addition of network modifying oxides into  $\text{P}_2\text{O}_5$  breaks the bridging P—O—P bonds and forms P—O—M linkages (M- modifier cation) which leads to the formation of non-bridging oxygens. Thus, the structure of cross-linked  $Q^3$  tetrahedra of vitreous  $\text{P}_2\text{O}_5$  (V- $\text{P}_2\text{O}_5$ ) converts into polymer-like metaphosphate chains of  $Q^2$  tetrahedra and then into invert glasses based on small pyro ( $Q^1$ ) as well as orthophosphate ( $Q^0$ ) anions. Depending on the glass composition, phosphate glasses are classified into three groups as follows. Metaphosphate glasses with modifier concentration,  $x=0.50$  and  $[\text{O}]/[\text{P}]=3.0$  entirely consists of  $Q^2$  tetrahedra that form chains and rings. The term metaphosphate is reserved for cyclic anions of  $(\text{PO}_3^-)_n$  composition. The glasses with modifier concentration,  $x>0.50$  come under polyphosphate glasses and they contain  $Q^2$  chains terminated by  $Q^1$  tetrahedra. Pyro ( $x=0.67$ ,  $[\text{O}]/[\text{P}]=3.5$ ) and ortho ( $x = 0.75$ ,  $[\text{O}]/[\text{P}]>3.5$ ) phosphate glasses are classified under the polyphosphate glasses category, and contain  $Q^1$

and isolated  $Q^0$  tetrahedra respectively. The ultraphosphate glasses are based on  $Q^3$  and  $Q^2$  tetrahedra with  $x < 0.50$  and  $2.5 \leq [O]/[P] < 3$  (Brow 2000).

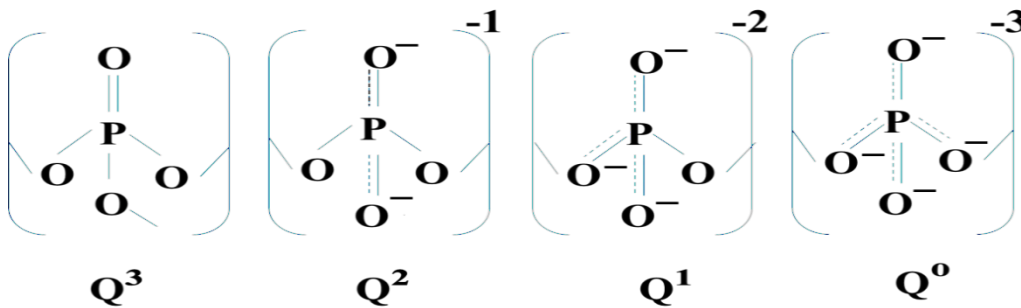


Figure 1.2: Schematic diagram of phosphorous tetrahedral sites in phosphate glasses (Brow 2000)

### 1.2.2 Properties and applications of phosphate glasses

Among other oxide glasses, phosphate glasses have unique thermal and optical properties like low melting temperature, low glass transition temperature, low softening temperature, high thermal expansion coefficient, high refractive index and high ultraviolet (UV) transmission. It can be used for optical fiber, solid state lasers, nuclear waste disposals, solid state batteries, solar energy concentrators, glass-to-metal sealing and biomedical applications. Hygroscopic nature, poor chemical durability and lower thermal stability limit their broad range of technical applications.

Alkali and alkaline-earth ions added phosphate glasses have interesting optical properties (Dayanand et al. 1996). The binary calcium phosphate glasses are chemically durable than barium phosphate glasses due to the higher field strength of  $Ca^{2+}$  ions. The refractive index of CaP glasses initially is found to decrease with the addition of CaO and then it increases with further addition, whereas addition of BaO to phosphate glasses increases the refractive index monotonically. Thermal expansion coefficient of CaP and



BaP glasses increase with modifier contents (CaO and BaO) and  $dn/dT$  (thermo-optic coefficient) changes to negative values (Lee and Taylor 2006). The amount of CaO and Na<sub>2</sub>O in CaO-Na<sub>2</sub>O-P<sub>2</sub>O<sub>5</sub> glasses can control the solubility and thermal properties of those glasses (Franks et al. 2001, Maheswaran et al. 2014). Rare-earth ions doped CaO-BaO-P<sub>2</sub>O<sub>5</sub> glasses can be used for laser applications (Chanthima et al. 2017). Sm<sup>3+</sup> ions doped CaO-BaO-P<sub>2</sub>O<sub>5</sub> glasses show photoluminescence properties, which can be used for high density optical storage devices, solid state lasers, fluorescence devices and under sea communication devices (Tariwong et al. 2016). The replacement of alkali oxides (Na<sub>2</sub>O) with alkaline-earth oxides (BaO) improved the physical, thermal and chemical durability properties of Na<sub>2</sub>O-CaO-ZnO-P<sub>2</sub>O<sub>5</sub> glasses which are ionic conductors (Hafid et al. 2002). A monovalent alkali ion can link to only one non bridging oxygen, whereas a divalent alkaline-earth ion bond to neighbouring two non-bridging oxygens. So, the addition of divalent ions improves the strength of cross-linking in the glass structure and thus enhances thermal and mechanical properties (Shelby 2007). The immobile divalent ions can retard the mobile alkali ions due to the effective cross-linkages in the structure and thus prevent the dissolution or improve the chemical durability of glasses (Hafid et al. 2002). Na<sub>2</sub>O can reduce the processing temperature of glasses, whereas CaO increases these temperatures (Shelby 2007).

### **1.3 GLASS – AS A BIOMATERIAL**

Biomaterials are classified into four different groups. They are (a) natural or synthetic polymers, (b) metals, (c) composites and (d) ceramics (bioglasses). The poor mechanical strength of polymers limits their wide range of applications. Though metals have higher mechanical strength, their higher corrosion rate in comparison with polymers and lower biocompatibility are the main drawbacks. Composites have higher elastic strength and less corrosion rate, whereas its chemical durability is very less. Ceramics have better biocompatibility and corrosion resistance among the four groups, whereas

their higher brittleness, higher density and low fracture strength adversely affect their usages (Kaur et al. 2014).

### 1.3.1 History of bioactive glasses

History of bioactive glasses started from 1969 by the father of bioglass invention, Larry L Hench. The first bioactive glass, 45S5 Bioglass® with composition  $\text{SiO}_2\text{-CaO-Na}_2\text{O-P}_2\text{O}_5$  was invented by Hench and team at university of Florida. According to Hench (2006), a biomaterial is the one that elicits a specific biological response at the interface of the material which results in the formation of a bond between the tissues and the material.

There are four eras in the history of bioactive glasses (Hench and Jones 2015),

- i. Era of discovery (1969-1979)
- ii. Era of clinical application (1980-1995)
- iii. Era of tissue regeneration (1995-2005)
- iv. Era of innovation (2005-2025)

In the first era, *in vitro* studies of 45S5 glasses reported that HAp (Hydroxy apatite) crystals formed on the surface of glasses during immersion in physiological solutions. A strong chemical bonding was observed between HAp and layers of collagen fibrils which was produced by osteoblast (Beckham et al. 1971, Hench and Paschall 1973). Later, Wilson et al. (1981) lead the historical path of bioglass to clinical applications and they reported the ability of bioglass to bond with soft tissues also. Middle ear replacement prostheses (MEP) (Merwin et al. 1982) and Endosseous ridge maintenance implants (ERMI) (Stanley et al. 1997) was discovered with an objective to bond with soft and bone tissues. FDA (Food and Drug Administration, U.S.) regulatory approval was obtained for using bioglass in periodontal repair of patients at the University of Florida followed by the successful experiments of bone regeneration in

periodontal defects created in monkey model (Wilson and Low 1992). BonAlive® (BonAlive Biomaterials, Turku, Finland) was the first non-45S5 composition introduced into the market for orthopedic applications.

The studies carried out on bioactive silicate glasses with composition  $\text{SiO}_2\text{-CaO-Na}_2\text{O-P}_2\text{O}_5$  (Rajendran et al. 2002) showed that the addition of more than 45 mol%  $\text{SiO}_2$  decreases the strength of glasses. Though the research on silicate glasses is widely conducted for biomedical applications, the long term existence of Silicon (Si) in the human body is still a topic of debate. Gali et al. (2018) have studied about yttria stabilized zirconia added mica-based glass-ceramics for dental restorations. The hardness and toughness of those ceramics have increased without degrading its brittleness and solubility, which is suitable for developing machinable ceramics. Xiang et al. (2007) have reported that mica-based glass ceramics showed higher bioactivity with the very fast growth of needle like fluorapatite crystals. High fracture toughness and Vickers hardness have obtained for mica-based glass ceramics with higher amount of CaO and  $\text{P}_2\text{O}_5$  due to their microstructure and presence of needle shaped crystals.

### **1.3.2 Properties of bioactive glasses**

The properties of bioactive glasses are related to their reactivity in tissue fluids, resulting in the formation of HAp [i.e.,  $\text{Ca}_{10}(\text{PO}_4)_6(\text{OH})_2$ ] layer on it. HAp is an analogue to the mineral form of bone with Ca/P molar ratio  $\sim 1.67$ . Releasing of Calcium ( $\text{Ca}^{2+}$ ) and orthophosphate ( $\text{PO}_4^{3-}$ ) ions from the glass surface leads to the calcium-phosphate (HAp) layer formation on it. HAp layer can interact with collagen molecules resulting in the biological bond formation between tissue and the glass material. Dissolved ions from glass surface such as Silicon and Calcium etc. can enhance the osteogenic properties which stimulate osteogenic cells to form bone matrix (Jones 2013, Kaur et al. 2014).

The first stage of bioactivity mechanism is the ion exchange reactions where Sodium ( $\text{Na}^+$ ) ions are released from the glass surface after immersion in physiological

solutions and it leads to the dissolution of network linkages such as Si—O—Si and P—O—P. The released  $\text{Ca}^{2+}$  and  $\text{PO}_4^{3-}$  ions accumulate on glass surface giving rise to calcium-phosphate layer formation. Finally the crystalline HAp layer will be formed by the incorporation of ions which are already present in the solution such as  $\text{OH}^-$ ,  $\text{CO}_3^{2-}$  in to amorphous calcium-phosphate (ACP) layer.

Glasses can be used for soft/hard tissue repair and regenerations. Certain compositions of bioactive glasses are showing osteoconductive responses such as differentiation of osteoprogenitor cells to osteoblasts and enhance bone proliferation. The possibility of tailoring the properties and formation of rapid bonding with tissues make the glasses an effective biomaterial in comparison with ceramics and glass-ceramics. Poor mechanical properties such as brittleness and bending-tensile rigidity in the range of 40-60 MPa limit their usages in load bearing applications. Embedding of bioglasses in biomaterials improve their mechanical properties and make them suitable for orthopedic and orthodontic prosthetics applications. Bioactive glasses with macroporous structure are favorable for bone regeneration due to their large surface area. The behavior of bioactive glass mainly depends on composition, surrounding pH, temperature and surface layer formed on it. Porosity levels in bioglasses are helpful for bone resorption and bioactivity. The adequate mechanical strength and controlled reaction or dissolution rate are the important properties for the successful bioactive glass product.

### **1.3.3 Behavior of therapeutic ions in the glass matrix**

Addition of various therapeutic ions into the glass matrix beneficially affects its role in medicine and treatments. The various studies have been reported about the role of ions in bioactive glasses (Hoppe et al. 2011, Ali et al. 2014) as mentioned below.

Silicon (Si) – It is essential for metabolic processes, formation and calcification of bone tissue. Dietary intake of silicon increases bone mineral density (BMD). Release of

Si from glasses induces HAp nucleation. It can induce formation of collagen I fibrils and thus osteoblastic differentiation.

Phosphorous (P) – Release of  $\text{PO}_4^{3-}$  is necessary for HAp nucleation on glass surface. It stimulates expression of matrix gla protein (MGP) which is a main regulator in bone formation.

Boron (B) – Dietary intake of Boron is needed for bone formation and it stimulates RNA synthesis in fibroblast cells.

Calcium (Ca) – It is essential for HAp nucleation on glass surfaces, osteoblast proliferation and differentiation. Calcium can induce mineralization of extra cellular matrix (ECM). It can increase expression of growth factors such as IGF-I and IGF-II.

Zinc (Zn) – It can activate protein synthesis in osteoblasts and thus stimulate bone formation. It has anti-inflammatory effect and enhances the ATPase activity. It is beneficial for transcription of osteoblastic differentiation genes such as collagen I, osteocalcin, osteopontin etc.

Magnesium (Mg) – It can enhance the adhesion of bone cell and thus stimulate new bone formation

Strontium (Sr) – It is a therapeutic agent for treatment of osteoporosis. And it is needed for bone cells and bone formation.

Fluorine (F) – Fluorine can inhibit demineralization of enamel and dentin. It can prevent bacterial enzyme and support oral health by preventing dental decay.

### **1.3.4 Applications of bioactive glasses**

**Bioglass as bone graft material** – Bone grafting is a surgical procedure which fixes problems with bones or joints. Bone graft fills voids where bone is absent and offer

biological repair of bone defects or provide structural stability. Autografts and allografts are two types of bone grafts. Bioactive glasses which are biocompatible, bioresorbable and osteogenic materials come under synthetic graft materials. Bioactive glass with interconnected porosity is useful for hard tissue prosthesis, which supports tissue in/out growth. Bioactive glass bone graft materials showed more repair response to human periodontal osseous defects than open flat debridement.

**Dental applications** – Bioglasses are used in dentistry for periodontal bone defects and ridge preservation. Endosseous Ridge Maintenance Implant<sup>®</sup> which is the simple cones of 45S5 bioglass reached the market around November 1988 to support labial and lingual plates in tooth roots and provide a stable ridge for denture construction following tooth extraction. Dentifrices contain Novamin<sup>®</sup> bioglass particulates which can support oral health according to the study of Tai et al. (2006). Bioactive glasses are used for remineralization and hypersensitivity treatments. Particles or granules of such glasses come into picture instead of monoliths due to the ease of filling the bone defects by pressing. Perio-Glas<sup>®</sup> (NovaBone Products LLC, Alachua, Florida) is the first particulate bioactive glass with particle size 90-710  $\mu\text{m}$  to repair the bone defects of jaws and bone loss arising from periodontal disease. NovaMin<sup>®</sup> (NovaMin Technology, GlaxoSmithKline, Florida, UK) prepared from Bioglass<sup>®</sup> particles with 18  $\mu\text{m}$  size is used as an active repair agent in toothpaste which can reduce hypersensitivity by filling the holes in the teeth. Remineralization of teeth can be obtained by the release of Calcium and Phosphorous ions from bioactive glasses. Such glasses can be used as antibacterial agents to reduce the pathogens in enamel, root and periodontics etc.

**Bioglass in drug delivery** – Bioglasses can be used for delivering drugs for patients. The first drug delivery vehicle was MCM-41 used in 2001. Bioglass carriers are used successfully to deliver Vancomycin for treating osteomyelitis (Krishnan and Lakshmi 2013). Mesoporous silicate bioactive glasses carry considerable amount of drugs and better drug diffusion kinetics is investigated by many researchers (Li et al. 2013).

**Bioactive glass scaffolds** – The composition and microstructure determine the properties of scaffolds. Bioactive glass scaffolds can be used for load bearing bone defects and repair due to its better mechanical strength. Lower fracture toughness and mechanical reliability of these scaffolds limit their practical usages. An ideal scaffold should mimic the morphology, structure and function of bone (Fu et al. 2011).

## **1.4 GLASS – AS A COATING MATERIAL**

### **1.4.1 Properties of glass coatings**

Among various coating materials, glass and glass-ceramics have several advantages of superior mechanical properties (abrasion, impact etc.), good adherence, thermal stability, chemical inertness and defect free surfaces. Crystallization can be induced within the glass phase of coating material by using the required heat treatment process, which helps to increase the resistance towards the abrasion, impact, high temperature, corrosion and thermal shock. The poor adhesion and/or degradation of material property during heat treatments is the main drawback of glass coatings (Majumdar and Jana 2001). Glass coatings are used for tribiological, electrical, chemical, metallurgical, high temperature resistant and aerospace engineering applications.

### **1.4.2 Details of different coating methods**

**Thermal spray technique** - In this technique, glass particles are injected in to high temperature gas flow where they melt and accelerate towards substrate at high speed. The molten or semi-molten particles solidify on the substrate as thin slices which are called as ‘splats’ resulting in typical lamellar microstructure. The thickness of coating produced by this method can be varied from 50  $\mu\text{m}$ -2 mm. Plasma spray (PS) and high velocity oxyfuel (HVOF) methods are commonly used thermal spray techniques.

**Laser cladding method** - In laser cladding, the powdered glass particles are injected by nozzle on to a substrate and glass powder is melted by hitting this flow with laser beams. Thus melt is formed and coated on a substrate. The lack of direct exposure of substrates to higher temperatures and better deposition rate are the advantages of this coating method.

**Pulsed Laser Deposition (PLD) technique** - It is a thin film technique in which the high power pulsed laser beam hits the target material which then vaporises and gets coated on a substrate. The target and substrate materials are placed in a high or low vacuum mode and the reactive or inert gases also can be used under necessary conditions. The thickness of coating can be varied between tens of nanometer to several microns.

**Enamelling method** - Enamelling is a traditional technique used for coating, which is simple and cheap. The suspension of glass powder is sedimented on the surface of substrates and then it is glazed by heat treatment processes. The temperatures are selected between glass transition and onset of crystallization temperature of glasses to avoid the crystallization of glass as well as degradation of substrates during coating process. The thickness of coating can be varied between tens of microns to few microns. The thermal expansion coefficient of substrates and coating materials (glass) should match to avoid thermal residual stresses in the coating, which cause crack generation and delamination of coating from substrates. Formation of byproducts due to the reaction between substrates and glasses at higher temperatures is one of the drawbacks of this method.

## **1.5 BIOMEDICAL IMPLANTS (BMI)**

Medical bionic implants are the artificial systems which can replicate the functions of biological systems. Biomedical implants are in wide spread usage over the past decades for various orthopedic and orthodontic applications. Silver and gold were used in olden days for implantation, whereas expenses and poor mechanical properties



limit their usages. The first biomedical implant ‘Sherman Vanadium Steel’ developed for humans failed due to corrosion. It is said that the number of revision hip surgery has increased by 26% and it will reach 137% in the year 2030. Good mechanical properties, tribiological properties and biocompatibility are the main properties required for a biomedical implant. Various implants used in the human body structure are given in Figure 1.3.

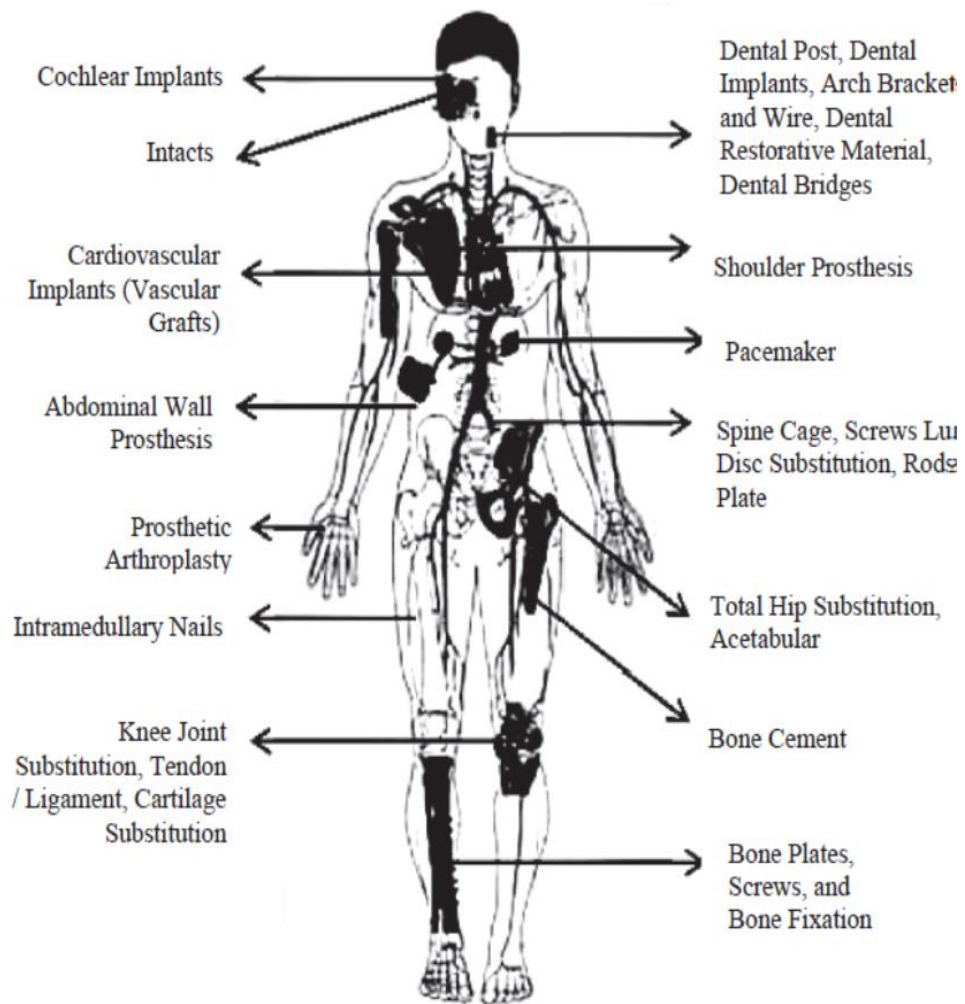


Figure 1.3: Implants in the human body structure (Manam et al. 2017)

### 1.5.1 Metals – as implant materials

Metals are bio-inert materials which can not directly bond with living tissues. Release of toxic ions from metallic implants due to the corrosion can cause severe health issues such as toxicity, swelling of tissues and finally even death. The various metals used for biomedical applications are given below. Biomedical applications of some metallic implants are given in Table 1.1 (Manam et al. 2017) .

**316 L stainless steel** - Conventional stainless steels are highlighted for its corrosion resistance by the formation of chromium oxide which prevents further oxidation. Addition of Nickel and reduction of Carbon content in this conventional stainless steel resulted in 316 L steel with superior corrosion resistance. 316 L has been approved by US FDA (Food and Drug Administration) due to its accepted mechanical, tribological and biocompatible properties. Ease of preparation and cost effectiveness make them attractive for various applications. Release of Nickel from 316 L causes toxicity (Ibrahim et al. 2017).

**Cobalt-Chromium (Co-Cr) alloys** - Cobalt is the base metal in these alloys and they have excellent mechanical properties, corrosion and wear resistance. This alloy was used in 1940's for the first time for medical application in dentistry. Nowadays it is used in orthopedics and jaws. Though Cobalt, Chromium and Nickel are highly toxic elements, the lower corrosion rate make them biocompatible by preventing the dissolution of these toxic ions. Excellent wear resistance makes them suitable for joint replacement instead of 316 L. But its long term existence in human body causes severe health problems due to Cobalt and Chromium ions. Low osseointegration and bioactivity besides their high cost limit the usages of these alloys (Manam et al. 2017).

**Titanium alloys** - Ti-alloys were used in 1950's for the first time for dental applications after which it is used in orthopedics also. Even higher doses of Ti are non-toxic in human body.  $\alpha$ ,  $\alpha$ - $\beta$ ,  $\beta$ -phase alloys are the main categories of Ti-alloys and Ti6Al4V is the one which contains both  $\alpha$  and  $\beta$  phases. The excellent mechanical -

Table 1.1: Applications of biomedical metallic implants (Manam et al. 2017)

Metals/alloys	Applications	Implants
Stainless steel	Orthopedic	Femoral prosthesis, acetabular cup applications, noble metal ion implantation, reconstructive surgery
	Dentistry	Dental implants, orthodontic wire leads
	Cardiovascular	Cardiovascular stents, heart valve parts, coronary stents.
Co-Cr alloys	Orthopedic	Total hip arthroplasty, total hip implant, total knee substitution joint, femoral stems
	Dentistry	Dental implants, removable partial dentures, orthodontic wire leads
	Cardiovascular	Vascular stents, heart valve parts
Ti and its alloys	Orthopedic	Orthopaedic prostheses, total hip implant, acetabular cup, reconstruction of craniofacial defects, skeletal prostheses
	Dentistry	Dental implants, orthodontic wire leads.
	Cardiovascular	Cardiovascular stents, heart valve parts.

properties, corrosion resistance and biocompatibility are the main features of Ti6Al4V alloy. Allergic reactions caused by Aluminum and Vanadium lead to the inventions of other Ti-based alloys such as Ti6Al7Nb, Ti5Al2.5Fe, Ti15Zr4Nb2Ta etc. (Manam et al. 2017).

**Duplex stainless steel (DSS) 2205** - DSS contains both austenitic and delta-ferritic phases. Delta ferritic phases are hard and less ductile, whereas the austenitic is soft and more ductile. The combination of both phases results in a steel which is harder than single-austenitic phase and more ductile than single-phase ferritic steel. The presence of higher Chromium, Molybdenum and Nitrogen in DSS offers them higher pitting corrosion resistance in chloride solutions. Chromium and Molybdenum support passive film formation during corrosion (Kocijan et al. 2011). Ferritic phase inhibits crack propagation and pit initiation (Sivakumar et al. 1993). Currently duplex stainless steels are replacing austenitic stainless steel due to their better mechanical properties, corrosion resistance and cost effectiveness.

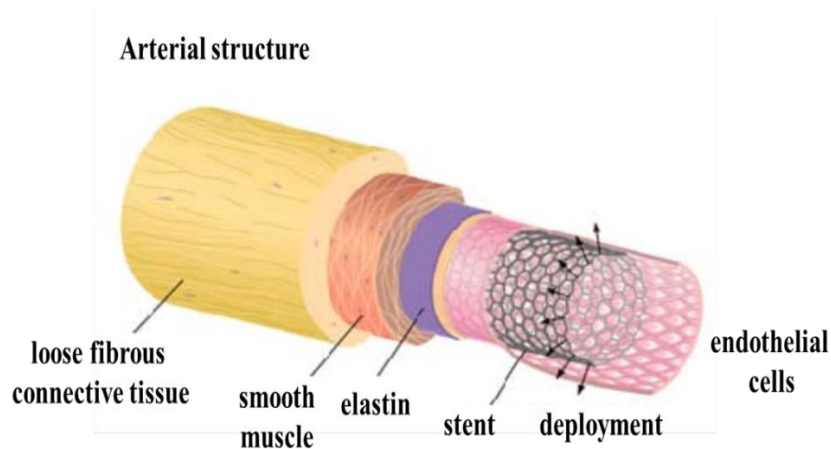


Figure 1.4: Schematic diagram of stent located inside the arterial structure (Dunn et al. 2007)

They can be used for endoprosthesis devices such as magnetic stents (Uthamaraj et al. 2015, Tefft et al. 2013, Sandhu et al. 2011). The schematic diagram of stent placed in the

artery is shown in Figure 1.4. Research on other orthopaedic and orthodontic applications of DSS 2205 is going on world wide (Kocijan and Conradi 2010).

### **1.5.2 Glass coating for biomedical implants**

Glasses are unsuitable for load bearing applications due to their poor mechanical properties such as higher brittleness, lower fracture toughness and bending strength. Coating of glasses on substrate can provide sufficient mechanical strength for various biomedical applications. There is a possibility of encapsulation of uncoated metallic implants with fibrous tissues and corrosion after implantation adversely affects the health. Metals are bioinert materials which can not directly bond with human tissues and the coating of bioactive glasses on such biomedical metallic implants help to make them bioactive and corrosion resistant. The corrosion of toxic ions from metallic implant materials leads to the swelling of tissues and ultimate death. Thermal expansion coefficient of substrate and glass should match to avoid the delamination of coating and crack generation during heat treatment processes.

Glass coated 3-D porous scaffolds induce tissue regeneration and dissolve fully after the completion of their functional role. Glasses are coated on metallic and polymeric implants for orthopedic, dental, endoprosthesis devices, surgical fixation, soft tissue repair (wound healing) and ocular applications etc. Transparent biocompatible glasses are used in ocular implants to provide angiogenesis and antibacterial properties (Baino and Verné 2017).

### **1.6 CaO-Na<sub>2</sub>O-P<sub>2</sub>O<sub>5</sub> GLASSES**

Chemical composition of calcium-phosphate glasses is similar to human bone and they are having bioresorbable, biocompatible properties and less toxicity. Bioresorbable

materials dissolve over time in body fluids and are replaced by regenerated tissues. The conventional silicate glasses with poor solubility results in risk of surgery for removing the implants and longer recovery time, whereas the soluble phosphate glasses avoid the risk of surgery due to their bioresorbable nature (Carta et al. 2007, Da Costa et al. 2006). Phosphate glasses with composition,  $\text{CaO-Na}_2\text{O-P}_2\text{O}_5$  are widely accepted for soft and hard tissue repair/regenerations. The chemical affinity of these glasses with bone can stimulate new bone formation by the release of ions (Franks et al. 2001). Such glasses are used for dental implants, scaffold for bone tissue engineering, vehicles for antimicrobial ion delivery and drug release. The higher degradation rate of these glasses resulting in large changes of pH of solution is the limiting factor of their broad usages. So, the studies are going on to control the dissolution rate by changing their composition thereby obtaining highly dissolved to stable glasses (Lee et al. 2013).

The increase in CaO content gives rise to less soluble glasses with minimum level of cyto-toxicity, whereas the decrease in  $\text{P}_2\text{O}_5$  content causes cyto-toxicity (Uo et al. 1998). Glasses with high CaO/ $\text{Na}_2\text{O}$  ratio are less soluble and enhance bone cell growth as well as antigen expression (Ahmed et al. 2005, Salih et al. 2000). The controllable addition of  $\text{Na}_2\text{O}$  can regulate the solubility, which works as a flux resulting in easier homogenization and casting of melt (Maheswaran et al. 2014). Glass transition, crystallization and melting temperature of these glasses can be reduced by decreasing  $\text{Na}_2\text{O}$  content (Lee et al. 2013).

## **1.7 SCOPE AND OBJECTIVES OF THE PRESENT WORK**

### **1.7.1 Scope**

Glass is an impactful material for shaping the modern human civilization. The inevitable role of glasses to transform the modern technology and engineering such as architecture, transportation, medicine, energy, science exploration, communication and display of information can be experienced in our day-to-day life. Phosphate glasses have

unique physical, thermal and optical properties among other oxide glasses, which make them suitable for solid state lasers, solid state batteries, sensors, solar energy concentrators, data transmission, sealants and biomedical applications. The hygroscopic nature, poor thermal stability and chemical durability of these glasses limit their technical capabilities and addition of various metal oxides to phosphate glasses is necessary for developing new glasses with special properties.

As long as humans exist in the earth, the importance of biomaterials and biomedical devices is expected to grow. Health and health care techniques are the primary concern of human species from the ancient days. So, the research work is going on globally to design new materials or devices for better treatment of health issues and fulfilling various demands of patients. Phosphate glasses are smart materials for biomedical applications called as 'third generation biomaterials'. They are controlled release glasses (CRG) whose solubility can be tailored by changing the composition from days to several months and it is beneficial for reducing toxicity. Among various phosphate glasses, CaO-Na<sub>2</sub>O-P<sub>2</sub>O<sub>5</sub> is the one which is broadly attracted for soft/hard tissue repair and regenerations. All the elements present in this composition of glass are essential for growth of bone and teeth tissues as well as they all have their own biological functional roles in human body conditions.

Glasses with 45 mol% P<sub>2</sub>O<sub>5</sub> can be melted and cast easily. It is biocompatible or less toxic in physiological conditions. CaO and P<sub>2</sub>O<sub>5</sub> can support bioactivity by helping the formation of hydroxyapatite (HAp) due to the release of Ca<sup>2+</sup> and PO<sub>4</sub><sup>3-</sup> ions from glass surfaces. The replacement of low field strength monovalent ions with high field strength divalent ions can improve the strength of effective cross-linking in the glass structure and thus it enhances the mechanical, thermal, optical and dissolution properties of glasses. In order to reduce the fast dissolution rate or improve the chemical durability of Na<sub>2</sub>O-CaO-P<sub>2</sub>O<sub>5</sub> glasses, Na<sub>2</sub>O is replaced with divalent oxide, BaO. It is expected to control the release of ions from glasses during dissolution and improve the mechanical properties such as fracture toughness, brittleness etc. as well as thermal properties such as

thermal stability, crystallization temperature of glasses due to the addition of higher field strength  $Ba^{2+}$  ions. Later research work shows that low doses of  $Ba^{2+}$  can act as a muscle stimulant (Moore 1964) and also its presence in the early life dietary transitions in primates (Austin et al. 2013). It can replace  $Ca^{2+}$  ions in HAp crystal lattice due to the same valency of both ions (Arepalli et al. 2015). Barium can increase the surface adherence by reducing surface tension and Barium crystals can perform as opacifier in bone cements (Kaur et al. 2012). The synthesized glasses can be used as base glasses for the addition of  $Fe_2O_3$  which can generate magnetic properties with bioactivity and it might make them suitable material for cancer treatments. It is reported that magnetic properties of  $BaO-Fe_2O_3$  added 45S5 bioglass can be used for magnetic hyperthermia treatments of cancer (Leenakul et al. 2013). Such glasses can be used as thermoseeds which can be implanted near the deep seated tumors and the heat generation from such magnetic glasses using certain magnetic field can burn such tumors. Though some Barium compounds are toxic, its role in amorphous state is worth to study to design a new class of glass materials for biomedical applications. The amount of Barium which is added to the glass composition can be varied based on different applications and functional roles in biomaterials. The enhancement effect of  $BaO$  on the bioactivity of silicate, borosilicate and phospho-silicate glasses have been reported already, whereas it is being reported for the first time in phosphate glasses in the present research work.

Calcium phosphate glasses which possess suitable biocompatibility, higher thermal stability and better optical properties can be promising materials for biomedical optical applications such as photodynamic therapy, opto-genetics and biosensing (Cecchi-Ginistrelli et al. 2016). The glasses which resorb fully in the body after the diagnostic treatments eliminate the need of explant surgery. Synthesized glasses can be used as base glasses to add rare earth ions ( $Sm^{3+}$ ,  $Ce^{2+}$ ,  $Nb^{2+}$  and  $Er^{2+}$ ) for biomedical optical applications (Pugliese et al. 2016).

Glasses can be coated on metallic materials for various purposes such as aerospace, metallurgical, chemical and biomedical applications. It is important to coat



glasses on metallic substrate materials for improving the mechanical strength for load bearing applications. The bioinert nature and corrosion of metallic biomedical implant materials can be overcome by the bioactive glass coating on it. The porous nature of glass coating helps to circulate body fluids through out the material and it leads to fast HAp nucleation and tissue growth. The control over porosity is necessary for better corrosion resistance

Among the four compositions of synthesized glasses that are studied here, glass with high BaO content (45P<sub>2</sub>O<sub>5</sub>-29CaO-11Na<sub>2</sub>O-15BaO) having better mechanical, thermal, dissolution and bioactive properties was selected for coating on metallic biomedical implant materials. Stainless steel 316 L, duplex stainless steel (DSS) 2205, Ti6Al4V are the important metallic materials used for orthopaedic and orthodontic implant applications (Gnanavel et al. 2018, K. et al. 2018, Hammood et al. 2017). The magnetizable nature of DSS 2205 due to the presence of ferritic phase makes it suitable for endoprosthesis devices such as magnetic stent materials. Such stents can be used for capturing endothelial cells which contain magnetic components leading to the fast healing of damages or blockages in the arteries (Tefft et al. 2017). DSS 2205 can be an alternative for 316 L and Ti6Al4V in biomedical implant applications due to its better corrosion resistance.

Hence, the present research work is taken up to enhance the mechanical, thermal, optical, dissolution and bioactive properties of ternary Na<sub>2</sub>O-CaO-P<sub>2</sub>O<sub>5</sub> glasses by adding BaO for developing new composition of glasses with improved properties for technological applications. The selected glass is coated on biomedical metallic implant materials to evaluate their corrosion resistance and bioactive properties. Further biocompatibility studies are required in future for developing practically successful implant materials with glass coating.

### 1.7.2 Objectives

The main objective of this research is to “synthesize, characterize and study the properties of BaO added bioactive Na<sub>2</sub>O-CaO-P<sub>2</sub>O<sub>5</sub> glasses and glass-ceramic coating on biomedical metallic implant materials.” This research focusses on

- the synthesis of phosphate glasses with composition (26-x)Na<sub>2</sub>O-xBaO-29CaO-45P<sub>2</sub>O<sub>5</sub> by varying x as 0, 5, 10, 15 mol% at different melting temperatures such as 1000, 1100 and 1200°C
- study of structural and mechanical properties of synthesized glasses
- study of thermal and optical properties of synthesized glasses
- study of dissolution and *in vitro* bioactivity properties of synthesized glasses
- the synthesis of 11Na<sub>2</sub>O-15BaO-29CaO-45P<sub>2</sub>O<sub>5</sub> glass coating on metallic implant materials such as stainless steel 316 L, duplex stainless steel (DSS) 2205 and Ti6Al4V by thermal enamelling technique
- study of structural properties of glass coated samples
- study of electrochemical corrosion and *in vitro* bioactivity properties of glass coated and uncoated samples

### 1.8 ORGANIZATION OF THE THESIS

The present thesis is organized as follows:

- **Chapter 1** gives brief introduction to glasses based on its historical origin and technological importance. An overview of principles of glass formation, classification of glass systems and synthesis methods of glass formation are also included in this chapter. This chapter also includes a brief review about the structure and properties of phosphate glasses along with the importance of present composition of glasses which are studied. An outline of glasses with special

properties i.e. bioactive glasses along with its technical capabilities are specified in this chapter. Other than this, it contains a brief description on glass coating and methods of synthesis of glass coating. In addition to that, scope and objectives of the present research work along with organization of the thesis are also included at the end of this chapter.

- **Chapter 2** describes the details of materials and synthesis techniques used for the preparation of glasses and glass coating in the present work. The various characterization techniques which were used to investigate the properties of glass and glass coating are included in this chapter. The principles and methods used for evaluating the properties are also explained briefly.
- **Chapter 3** illustrates the effect of BaO additions and melting temperature on structural and mechanical properties of Na<sub>2</sub>O-CaO-P<sub>2</sub>O<sub>5</sub> glasses. Some, structural parameters were calculated theoretically and tabulated along with experimental results. The changes in the properties were correlated with structure of glasses.
- **Chapter 4** refers to the effect of BaO on thermal and optical properties of Na<sub>2</sub>O-CaO-P<sub>2</sub>O<sub>5</sub> glasses. The trend of thermal properties was explained based on structure of glasses. Results mentioned in this chapter were used to select a particular composition of glass with better thermal stability for coating on metallic implant materials.
- **Chapter 5** describes the effect of BaO addition on the dissolution and *in vitro* bioactivity properties of Na<sub>2</sub>O-CaO-P<sub>2</sub>O<sub>5</sub> glasses. This study aimed to select a composition of glass with better chemical durability in deionized water and bioactivity in synthetic body fluids for coating.

- **Chapter 6** deals with the glass coated metallic bio-implants. The basic structural properties of glass-ceramic coating were evaluated with the *in vitro* bioactivity properties of coated substrates. Electrochemical corrosion studies of coated and uncoated implant materials were carried out to suggest a suitable material for biomedical implant applications.
- **Chapter 7** summarize the outcomes of the present research work. This chapter ends with the conclusion of major results of the study and suggestion of suitable material for future applications. Scope for the future research work is also included in this chapter.

## Chapter 2

### MATERIALS AND METHODS

In the present study, calcium sodium phosphate glasses with and without addition of BaO were prepared by melt-quenching technique. Glasses with composition  $(26-x)\text{Na}_2\text{O}-x\text{BaO}-29\text{CaO}-45\text{P}_2\text{O}_5$  were prepared by varying  $x$  as 0, 5, 10, 15 mol% to study the effect of BaO addition on their properties. These glasses were prepared at three different melting temperatures (1000, 1100 and 1200°C) to optimize a suitable melting temperature for getting homogeneous, bubble free glasses with better properties. Glasses prepared at 1200°C were selected for further thermal, optical, dissolution and bioactivity property studies based on their better mechanical properties. *In vitro* bioactivity studies of glasses were conducted in two different physiological solutions, Phosphate buffer saline (PBS) and Hank's balanced salt (HBS) solutions. Ammonium dihydrogen phosphate ( $\text{NH}_4\text{H}_2\text{PO}_4$ ) was used instead of phosphorous pentoxide ( $\text{P}_2\text{O}_5$ ) as a precursor material for glass preparation in the present work. This was done to avoid the loss of materials during preparation due to the hygroscopic and volatile nature of  $\text{P}_2\text{O}_5$ .

Among the four compositions of synthesized glasses, 11Na<sub>2</sub>O-15BaO-29CaO-45P<sub>2</sub>O<sub>5</sub> glass was selected for coating on biomedical metallic implant materials such as stainless steel 316 L, duplex stainless steel (DSS) 2205 and Ti6Al4V due to its better mechanical, thermal and bioactive properties. Thermal enamelling technique was adopted for coating since it was a simple and cheap method. A comparative study of *in vitro* bioactivity and electrochemical corrosion properties of all three coated and uncoated metallic implants were conducted to suggest a better implant material for biomedical applications. HBS solution was used for these studies due to its proximity to composition of human body plasma.

## 2.1 PREPARATION OF GLASSES

### 2.1.1 Materials used for glass preparation

Phosphate glasses in the system  $(26-x)\text{Na}_2\text{O}-x\text{BaO}-29\text{CaO}-45\text{P}_2\text{O}_5$  ( $x = 0, 5, 10, 15$  mol%) were prepared from high purity raw materials such as sodium carbonate ( $\text{Na}_2\text{CO}_3$  with purity 98%), barium carbonate ( $\text{BaCO}_3$  with 99%), calcium carbonate ( $\text{CaCO}_3$  with 98%) and ammonium dihydrogen phosphate ( $\text{NH}_4\text{H}_2\text{PO}_4$  with 98%) supplied by Alfa Aesar using melt-quenching technique. Batch composition of the synthesized glasses in the present study is given in Table 2.1.

Table 2.1: Batch composition of synthesized  $\text{Na}_2\text{O}-\text{BaO}-\text{CaO}-\text{P}_2\text{O}_5$  glasses

Sample code	Composition (mol%)				Melting temperature (°C)
	$\text{P}_2\text{O}_5$	CaO	$\text{Na}_2\text{O}$	BaO	
A 0	45	29	26	0	1000
A 5	45	29	21	5	
A 10	45	29	16	10	
A 15	45	29	11	15	
B 0	45	29	26	0	1100
B 5	45	29	21	5	
B 10	45	29	16	10	
B 15	45	29	11	15	
C 0	45	29	26	0	1200
C 5	45	29	21	5	
C 10	45	29	16	10	
C 15	45	29	11	15	

### **2.1.2 Methods used for glass preparation**

A batch of 25 gms of each composition was weighed and mixed thoroughly in an agate mortar. Finely mixed and powdered batch was placed in a silica crucible and calcined at 700°C for 1 hour in a muffle furnace to remove the water, NH<sub>3</sub> and CO<sub>2</sub> molecules from it. Calcined batch was melted in silica crucibles at three different temperatures 1000, 1100 and 1200°C for 1 hour in air by using PID controlled high temperature furnace. The melt was stirred for getting homogenized bubble free glasses during melting process. The homogenized melt was quenched to room temperature in air by pouring it on a stainless steel mold. As quenched glass samples were annealed at 350°C for 3 hours to remove any residual thermal stresses developed during quenching and then it was allowed to cool to room temperature in the furnace. Annealed glass samples were kept in a desiccator to prevent the atmosphere moisture attack. As quenched pulverized samples without annealing were used for DTA measurement. The annealed and polished glass samples were used for studying the mechanical, optical, dissolution and bioactivity properties. The process flow of glass preparation and characterization techniques are given in Figure 2.1. The image of synthesized glasses is given in Figure 2.2. Furnaces used for glass preparation are shown in Figure 2.3.

### **2.1.3 Surface polishing of the glass samples**

Synthesized glass samples were ground and polished on both sides using silicon carbide emery paper of different grit size and alumina powder suspension to obtain optically flat surfaces for mechanical and optical properties as well as to obtain samples with similar surface conditions for dissolution and bioactivity studies. Glasses were polished for 5 minutes per side with silicon carbide emery paper of grit size starting with 220 then 320, 400, 600, 800, 1000 and finally with 1200 using required quantity of distilled water as coolant. Finally velvet cloth polishing was done with alumina powder (0.05 µm) suspension. Grinding and polishing were carried out on motorized polishing machine (Chennai Metco, grinder-polishing machine). Samples were cleaned with

ethanol using ultrasonicator to remove the left over polishing agents and then dried gently with a hair dryer.

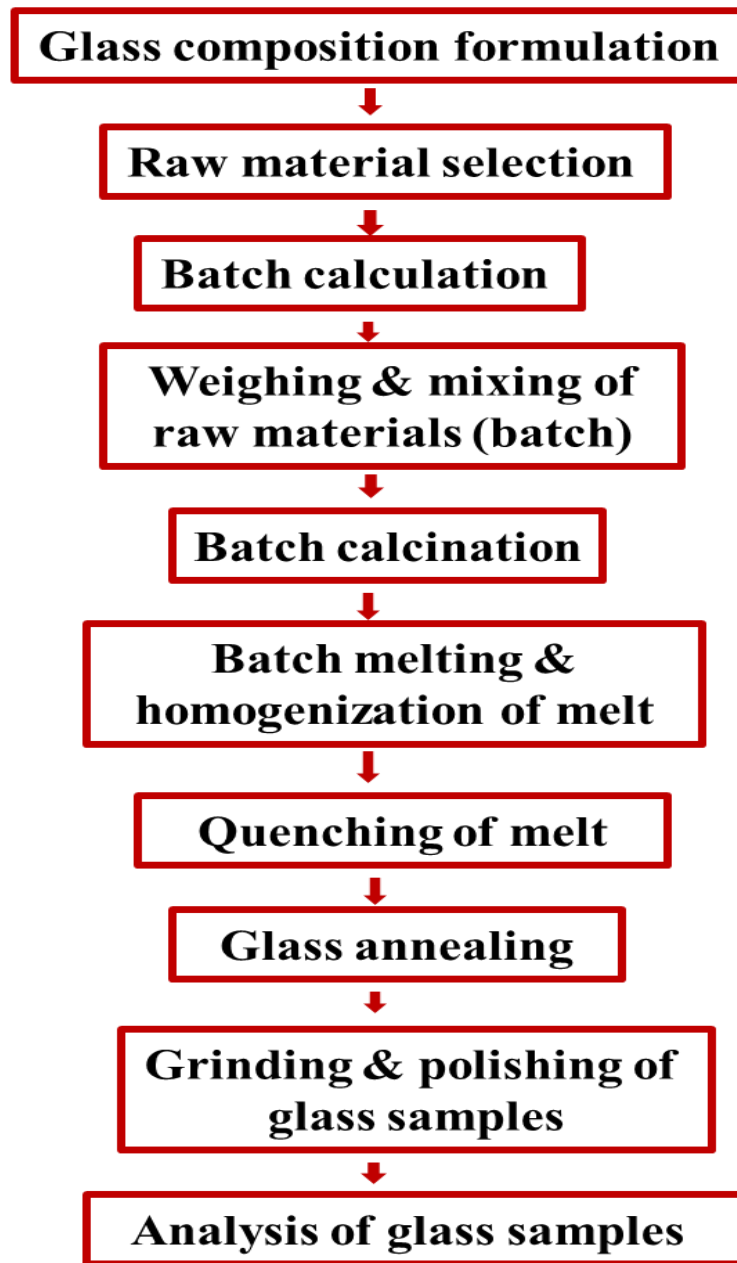


Figure 2.1: Flow chart of the steps involved in preparation and processing of glasses



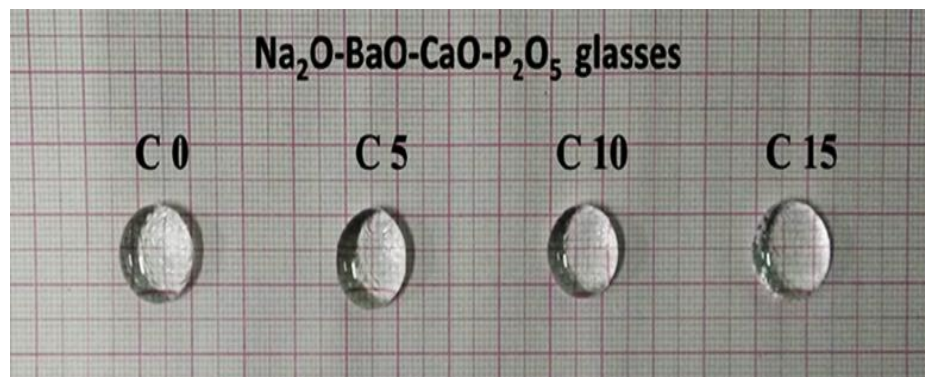


Figure 2.2: Images of synthesized glasses



Figure 2.3: Furnaces used for glass preparation

## 2.2 CHARACTERIZATION TECHNIQUES OF GLASSES

The structural studies of prepared glasses were carried out using X-ray Diffraction (XRD), Fourier Transform Infra-red (FTIR) Spectroscopy and Scanning Electron Microscopy (SEM). Elemental composition of the samples was analyzed using Energy

Dispersive X-ray Spectroscopy (EDS) attached with SEM. Micro-indentation techniques and SEM was used to evaluate mechanical properties of glasses. Physical properties of the glasses were studied by measuring density. Optical properties of the glass samples were studied with UV-Visible spectroscopy and Abbe Refractometer. Differential Thermal Analysis (DTA) of as quenched glass samples was performed to find out the thermal properties.

### **2.2.1 X-ray Diffraction (XRD) studies**

XRD is a non-destructive technique used to analyze crystal structure, geometry, identification of unknown substance and defects etc. The data obtained for a particular sample is compared with Joint Committee on Powder Diffraction Standards (JCPDS) and Inorganic Crystal Structure Database (ICSD) for analyzing its structure.

Crystalline materials having periodic arrangement of atoms in lattice planes show sharp intense X-ray diffraction peaks when X-rays are incident on them. In amorphous glasses where the atoms are arranged randomly, diffraction of incident X-ray beam results in a large hump distributed at an angle  $2\theta$ .

In the present work, XRD was carried out on glass samples using X-ray Diffractometer (Rigaku Miniflex 600) with an angular range of  $2\theta$  from  $10^\circ$  to  $70^\circ$  using Cu- $K_\alpha$  radiation at a voltage of 40kV and a current of 15mA. The scanning rate was kept as  $1^\circ/\text{min}$ . In case of glasses, XRD was carried out on glass samples which were taken out at regular intervals of dissolution and bioactivity tests and crystalline phases formed on sample surfaces after the tests were identified by PANalytical X'Pert Highscore Plus software, Version 2.1 (2.1.0) and JCPDS cards. XRD machine used for analysis is given in Figure 2.4.

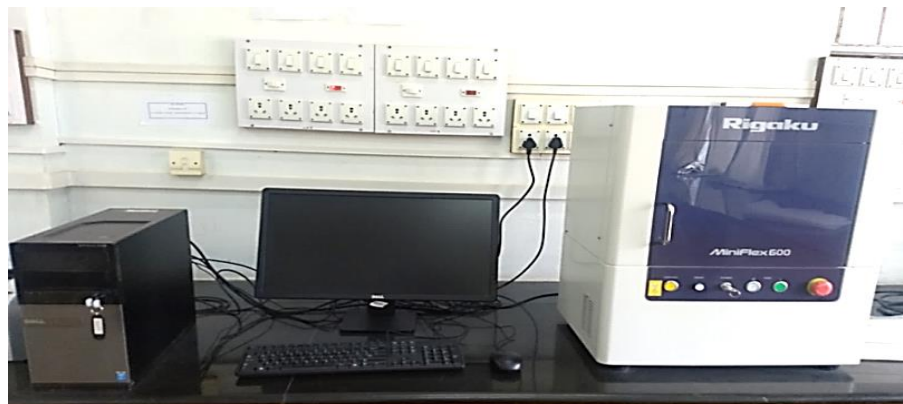


Figure 2.4: XRD machine used for analysis of synthesized glasses

### 2.2.2 Fourier Transform Infra-red (FTIR) spectroscopy

FTIR Spectroscopy is the study of interaction between matter and electromagnetic radiation in the IR region ( $\lambda = 7000-10^5 \text{ \AA}^\circ$ ). This vibrational spectroscopy is used to identify the structure of glasses. The radiation is strongly absorbed by the molecule if its photon energy is coinciding with the vibrational energy of that molecule. In case of IR active transitions, dipole moment of molecules changes during these vibrations. FTIR spectrometer work on principle called Fourier Transform. The recorded spectrum is intensity vs time and it is converted to intensity vs frequency spectrum by mathematical function called Fourier Transform.

FTIR analysis of oxide glasses is carried out by KBr pellet method where glass powder is mixed with Potassium Bromide (KBr) to form pellet by applying pressure of 10-15 tons in vacuum for five to ten minutes. KBr has large transmission region from UV to IR and no significant optical absorption lines in the high transmission region of the glass.

In the present work, Infra-Red (IR) spectra of synthesized glass samples were recorded by FTIR spectrometer (Thermo Nicolet Avatar 370) in the wave number range

of 400-4000  $\text{cm}^{-1}$  using KBr pellet method with scanning rate of 32 scans/min. The resolution of the spectrometer was 4  $\text{cm}^{-1}$ . In case of dissolution and bioactivity tests, FTIR studies were carried out on glass samples which were taken out after 28 days of immersion.

### **2.2.3 Scanning Electron Microscopy (SEM) and Energy Dispersive X-ray Spectroscopy (EDS)**

Scanning electron microscope generates focused beam of high energy electrons to generate variety of signals at the surface of solid samples. The signals formed from the electron-sample interactions give the information about surface morphology, chemical composition, crystalline structure and orientation. Electrons with high kinetic energy hit the samples and then decelerate. This dissipated energy is converted into various signals which contain secondary electrons (SE), back scattered electron (BSE) and diffracted back scattered electrons (EBSD), photons, visible light and heat. SE is used for making SEM images and BSE which is reflected from the sample used to analyze morphology as well as topography of samples. Electron beam generates X-rays in the specimen, which are directed towards X-ray detector for EDS analysis. Non-conductive samples should be coated with conductive materials such as carbon or metals in conventional SEM working in high vacuum mode to avoid the charging effect arising due to the accumulation of incident electrons on sample surfaces, which reduce the number of BSE and result in poor quality images.

In the present study, surface morphology and elemental composition of glasses samples were studied by Scanning Electron microscopy (SEM) attached with Energy Dispersive X-ray Spectrometer (EDS) using JEOL-JSM 6380LA. Prior to the SEM analysis, all the glass samples were polished and then gold sputtered in order to avoid the charging effect on non-conducting surfaces under electron beam. In case of dissolution and bioactivity studies, SEM/EDS were conducted on samples which were taken out after

28 days of immersion. In EDS analysis, both area and spot analysis were carried out on five different regions of sample surfaces and the error in EDS data was nearly 1-2 %.

#### 2.2.4 Density, molar volume and theoretical structural parameters

Density refers to the structural compactness of glasses. Liquids like xylene, kerosene can be used for density measurements due to its low reactive nature with glasses than water.

Density of the synthesized glasses was measured by Archimedes' principle using xylene as immersing liquid in room temperature. Glass samples were weighed using analytical weighing balance with an accuracy of 0.1 mg. They were weighed in air and in xylene. The buoyant force experienced on an immersing body is equal to the weight of the liquid that the body displaces. The photograph of apparatus used in the present work for density measurement is given in Figure 2.5.

Density of the solid was determined using equation,

$$\rho_{mes} = \frac{W_a - W_l}{W_a} \rho_l \quad (2.1)$$

where  $\rho_{mes}$  is the measured density,  $W_a$  and  $W_l$  is the weight of sample in air and xylene respectively.  $\rho_l$  is the density of xylene,  $0.86 \text{ gm/cm}^3$ , at room temperature. Measurements were carried out on three different glass samples of each composition and average value of density was considered as the density of the glass.

Molar volume ( $V_m$ ) was calculated from the measured values of density using the equation (Mandlule et al. 2014),

$$V_m = \frac{M_w}{\rho_{mes}} \quad (2.2)$$

where  $M_w$  is the molecular weight of glass calculated from batch composition (Hager and El-Mallawany 2010).

$$M_w = \sum X_i M_{w_i} \quad (2.3)$$

where  $X_i$  and  $M_{w_i}$  are the mole fraction and molecular weight of each component (i), in a batch composition respectively.

Number of moles of oxygen atoms present in one mole of glass,  $n(O)$  was given by an equation (Mandlule et al. 2014),

$$n(O) = \sum X_i n(O)_i \quad (2.4)$$

where  $n(O)$  is the number of oxygens present in each oxide.



Figure 2.5: Density measurement setup used for the synthesized glasses

Molar oxygen packing density ( $\rho_{ox}$ ) is the measure of the compactness of glass structure and it determines the packing of oxygen ions in a glass by the given formula (Mandlule et al. 2014),

$$\rho_{\text{ox}} = \frac{n(\text{O})}{V_m} \quad (2.5)$$

Molar volume that contains one mole of oxygen is oxygen molar volume ( $V_o$ ) (Çelikbilek et al. 2013) and was given as,

$$V_o = \frac{V_m}{n(\text{O})} \quad (2.6)$$

The ionic concentration  $n(\text{A})$  of atom 'A' for an oxide  $A_jO_k$  can be found out by the given equation (Hager and El-Mallawany 2010),

$$n(\text{A}) = \frac{j \times X_i \times N_{\text{avg}}}{100 \times V_m} \quad (2.7)$$

where  $N_{\text{avg}}$  is the Avogadro's number ( $6.02 \times 10^{23}/\text{mol}$ ), 'j', 'k' are the number of metal and oxygen atoms present in an oxide respectively.

The inter ionic distance  $R(\text{A})$  is the distance between ions in a glass and was given by the equation (Hager and El-Mallawany 2010),

$$R(\text{A}) = \sqrt[3]{\frac{1}{n(\text{A})}} \quad (2.8)$$

The average cross-link density (CLD) of glass was calculated by the following equation (Hager and El-Mallawany 2010),

$$\text{CLD} = (1/\eta) [ \sum (n_c N_c)_i ] \quad (2.9)$$

where,  $\eta = \sum (N_c)_i = \sum X_i n_i \cdot n_i$  is the number of cations of each component, (i).  $n_c = n_f - 2$ . The coordination numbers ( $n_f$ ) of  $\text{Na}^+$ ,  $\text{Ca}^{2+}$ ,  $\text{Ba}^{2+}$ ,  $\text{P}^{5+}$  are 6, 7, 8 and 4 respectively (Prison et al. 2008, Tang et al. 2010).

The number of bonds ( $N_b$ ) present in glasses were calculated by the formula (Çelikbilek et al. 2013),

$$N_b = \frac{N_{avg} \sum (n_f X)_i}{V_m} \quad (2.10)$$

The molar volume that contains one mole of phosphorous is called as phosphorous molar volume,  $V_m^P$  and was calculated by the equation (Kaur et al. 2015),

$$V_m^P = \frac{V_m}{2(1-X_n)} \quad (2.11)$$

where  $X_n$  is the mole fraction of  $P_2O_5$ .

The average distance between phosphorous ions,  $\langle d_{p-p} \rangle$  was given by the equation (Kaur et al. 2015),

$$\langle d_{p-p} \rangle = \sqrt[3]{\frac{V_m^P}{N_{avg}}} \quad (2.12)$$

### 2.2.5 Mechanical properties

Poor mechanical strength and brittle nature of glasses limit their wide usage in many technological fields especially in biomedical applications. So, the efforts were made to carry out mechanical property studies to tailor these properties by changing the appropriate composition.

In the present study elastic modulus and mechanical properties of the glasses were evaluated by Makishima Mackenzie model and also measured by microindentation studies.



### **Makishima and Mackenzie model**

Elastic moduli of oxide glasses were calculated by Makishima and Mackenzie (1973) model using dissociation energy of oxide per unit volume ( $G_i$ ) and packing density ( $V_i$ ). In the present study, young's modulus ( $E$ ) of synthesized glasses were theoretically calculated using formula,

$$E = 8.36 \times V_t \sum G_i X_i \quad (2.13)$$

where packing density,  $V_t = \frac{1}{V_m} \sum X_i V_i$  and packing factor,  $V_i$  of  $\text{Na}_2\text{O}$ ,  $\text{CaO}$ ,  $\text{BaO}$  and  $\text{P}_2\text{O}_5$  are 11.7, 9.9, 14.28 and 34.79  $\text{cm}^3/\text{mol}$  respectively (Makishima and Mackenzie 1973).  $G_i$  is the dissociation energy per unit volume of an oxide.  $G_i$  of  $\text{Na}_2\text{O}$ ,  $\text{CaO}$ ,  $\text{BaO}$  and  $\text{P}_2\text{O}_5$  are 8.9, 15.50, 9.7 and 15.0  $\text{kcal}/\text{cm}^3$  respectively (Makishima and Mackenzie 1973).

Poisson's ratio ( $\sigma$ ) was found out by the equation proposed by Makishima and Mackenzie (1975),

$$\sigma = 0.5 - \frac{1}{7.2 \times V_t} \quad (2.14)$$

Bulk modulus,  $K$  (in GPa) is the measure of resistance of a material to uniform compression and it was calculated by the formula (Makishima and Mackenzie 1975) given below,

$$K = 10 \times V_t^2 \sum G_i X_i \quad (2.15)$$

### **Microindentation studies**

Mechanical properties such as hardness, fracture toughness and brittleness were measured in the present work by simple indentation technique by applying a known load to the diamond tip. Length of generated crack was measured using optical microscope.

Four sided diamond pyramid indenter known as Vickers indenter was impressed into surface of sample by applied force or load of 1 to 1000 gf for prescribed dwell time in Vickers microindentation technique.

Vickers hardness ( $H_v$ ) was calculated using the formula,

$$H_v = 1.854 \times \frac{P}{d^2} \quad (2.16)$$

where ‘ $P$ ’ is the applied load (in N) and ‘ $d$ ’ is the half of the average of two diagonal lengths of indentation (in  $\mu\text{m}$ ). Hardness measures the resistance of a sample to permanent deformation by a compression load. Vickers hardness of a material depends on their bond strength, packing density of ions, presence of defects, surface features etc. Schematic diagram of residual impression formed on surface of sample by Vickers indentation is given in Figure 2.6.

Crack initiation and propagation results in mechanical failure of glasses and crack initiation is related to brittleness (Sehgal and Ito 1999). Radial-median crack is initiated around the indentation at a given indentation load by Vickers indenter. Schematic diagram of cracks propagating from four corners of Vickers indentation is given in Figure 2.7. Stress concentrated at the crack tip lead to the catastrophic failure of glass (Kato et al. 2010).

Crack propagation was evaluated by measuring fracture toughness ( $K_{IC}$ ) which was calculated using the formula developed by Anstis et al. (1981), with  $c/a \geq 2.5$ .

$$K_{IC} = 0.016 \times \left( \frac{E}{H_v} \right)^{\frac{1}{2}} \times \left( \frac{P}{c^{1.5}} \right) \quad (2.17)$$

where ‘ $c$ ’ is the half crack-length and ‘ $a$ ’ is the half of the average of two diagonal lengths of indentation (in  $\mu\text{m}$ ) and  $E$  is the Young’s modulus (in GPa).

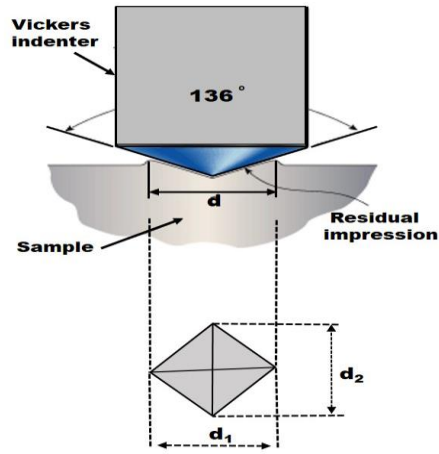


Figure 2.6: Schematic diagram of residual impression formed on surface of sample by Vickers indentation

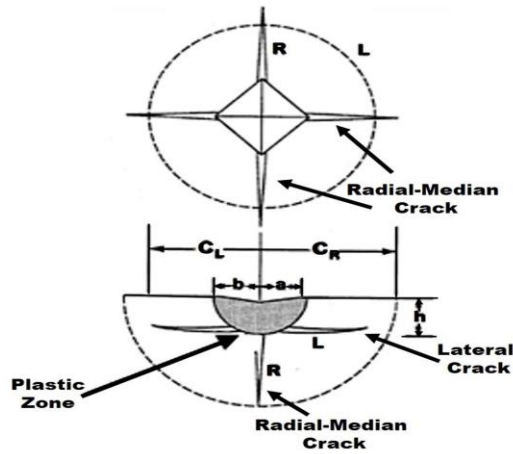


Figure 2.7: Schematic diagram of cracks propagating from four corners of Vickers indentation (Marshall 1990)

Brittleness or index of brittleness ( $\chi$ ) was calculated by a formula proposed by Lawn and Marshall (1979),

$$\chi = \frac{H_V}{K_{IC}} \quad (2.18)$$

Sehgal et al. (1995) used the brittleness to measure the degree of crack initiation in glasses.

Micro-hardness ( $H_v$ ) of the glass samples was measured with Vickers diamond pyramid indentation technique (Omni Tech MVH-S Auto, Quantimate V2.5) by applying a load of 0.98 N for 10 sec. Prior to the analysis, all the glass samples were finely polished as discussed earlier. The mean value of hardness was calculated as the mean of ten measurements taken on each sample. The fracture toughness ( $K_{IC}$ ) was calculated from the crack-length which was generated under an external load of 19.6 N for 10 sec. The crack-length was measured using optical microscope. The nature of indentations with cracks was also detected with SEM (JEOL-JSM 6380LA) after gold sputtering on samples.

Mechanical properties of the glasses synthesized at 1000, 1100 and 1200°C were studied and compared in the present work. Better mechanical properties such as lower brittleness and crack-length were obtained for glasses melted at 1200°C in comparison with samples melted at lower temperatures. So, these glasses were selected for further studies such as thermal, optical, dissolution and bioactivity properties.

### **2.2.6 Thermal analysis**

In Differential Thermal Analysis (DTA), differential thermal sensor is measuring the temperature difference between reference and sample which are kept inside furnace.

Three main thermal parameters such as glass transition ( $T_g$ ), onset of crystallization ( $T_x$ ) and melting ( $T_m$ ) temperatures were determined from Differential Thermal Analysis (EXSTAR TG/DTA 6300) of the synthesized glasses in the present work. The analysis was carried out from ambient to 1000°C in nitrogen atmosphere using powdered alumina as reference material. As quenched pulverized samples were used for DTA measurements and accuracy of temperature measurement was  $\pm 3^\circ\text{C}$ .

Thermal stability ( $\Delta T$ ) of glasses was calculated from  $T_g$  and  $T_x$  values as shown in equation (2.19). Thermal stability indicates the resistance against crystallization of samples and was given as,

$$\Delta T = T_x - T_g \quad (2.19)$$

Hruby's parameter ( $K_{gl}$ ) was calculated as follows, which indicates the glass forming ability of samples,

$$K_{gl} = \frac{(T_x - T_g)}{(T_m - T_x)} \quad (2.20)$$

## 2.2.7 Optical properties

### Refractive index measurements

Refractive index of glasses mainly depends on polarizability of ions coordinated with anion, field strength of ions, number of non-bridging ions etc. Refractive index of glass samples usually increases with increase in either polarizability of ions or electron density of atoms.

In the present work, refractive indices of glass samples were measured with Abbe (MAR-33) refractometer using light of wavelength 589.3 nm at room temperature. Mono-bromo naphthalene was used as the contact layer between the glass and refractometer prism. The reading was taken on three different glass samples of same composition which were fine polished as discussed earlier and the average was taken. The accuracy of measured refractive index was  $\pm 0.001$ .

### UV-Visible spectroscopy

UV-Visible spectroscopy is the measurement of attenuation in intensity of light with in a range of wavelength after it passes through sample or after it reflects from

sample. Transition of electron with in a molecule from a lower energy level to higher one after the absorbance of ultra-violet radiation of frequency,  $\nu$  results in UV-Visible absorption spectra. The plot between absorbance or transmittance versus wavelength or frequency of incident radiation gives absorption spectrum.

Due to lack of long range order, conduction and valence band in amorphous materials such as glasses do not have sharp cut off but have band tails and thus there are no sharp absorption edge existing for glasses.

The optical absorption spectra were evaluated to understand the electronic band structure, band tail and localized states of glasses. After obtaining UV-Visible absorption spectra of glasses at the higher photon energy or in the Tauc region, absorption coefficient  $\alpha(\nu)$  was related to the optical band gap energy ( $E_g$ ) using power law which was derived by Davis and Mott (1970) as shown below,

$$\alpha(\nu) = \frac{B(h\nu - E_g)^n}{h\nu} \quad (2.21)$$

where B is a constant,  $E_g$  is the optical band gap energy,  $h\nu$  is the incident photon energy. 'n' is an index related to the nature of inter-band electronic transitions and it takes values as 1/2, 3/2, 2 and 3 for allowed direct transitions, direct forbidden transitions, allowed indirect transitions and forbidden indirect transitions respectively. Tauc region is associated with the transition between extended valence band and the conduction band. The extrapolation of the linear region of the plots between  $(\alpha h\nu)^{1/2}$  and  $h\nu$  to the X-axis where  $(\alpha h\nu)^{1/2} = 0$  gave the optical band gap energy values.

At the lower photon energy or in the Urbach region,  $\alpha(\nu)$  is an exponential function of photon energy,  $h\nu$ , as derived by Urbach (1953),

$$\alpha(\nu) = \alpha_0 \exp\left(\frac{h\nu}{E_u}\right) \quad (2.22)$$

where  $\alpha_o$  is a constant and  $E_u$  is the Urbach energy which indicates the width of the localized states in the normally forbidden band gap i.e. band tailing.  $E_u$  is related to the optical electronic transition between a localized band tail and extended band. The inverse of the slope of the linear portion of plot between  $\ln(\alpha)$  versus  $h\nu$  gave the Urbach energy values.

### Optical basicity and oxide ion polarizability

Evaluation of polarizability nature of glasses is helpful to design new functional optical materials with high optical performance and non-linear optical properties. The molar electronic polarizability ( $\alpha_m$ ) of each glass was calculated from  $E_g$  and molar volume ( $V_m$ ) using the given equation (Dimitrov and Komatsu 2010) which was derived from familiar Lorentz-Lorentz equation,

$$\alpha_m = \frac{3V_m}{4\pi N_{avg}} \left( 1 - \sqrt{\frac{E_g}{20}} \right) \quad (2.23)$$

where  $N_{avg}$  is the Avogadro's number ( $6.02 \times 10^{23}$  /mol). Average anion or oxide ion polarizability ( $\alpha_o$ ) can be calculated from  $\alpha_m$  and cation polarizability ( $\alpha_i$ ) using the equation (Dimitrov and Komatsu 2010) given below,

$$\alpha_o = (\alpha_m - \sum \alpha_i) \left( \frac{1}{N_o} \right) \quad (2.24)$$

where  $N_o$  is the total number of oxygen ions per formula unit. Values of  $\alpha_i$  used for calculation of average anion polarizability were 0.021, 0.175, 0.469 and 1.595 for  $P^{5+}$ ,  $Na^+$ ,  $Ca^{2+}$  and  $Ba^{2+}$  respectively (Dimitrov and Komatsu 2010).

The molar refraction ( $R_m$ ) can be expressed as a function of molar polarizability ( $\alpha_m$ ) (Dimitrov and Komatsu 2010),

$$R_m = 2.52 \alpha_m \quad (2.25)$$

The metallization criteria ( $M_c$ ) indicates the insulating nature of prepared glasses by the formula (Dimitrov and Komatsu 2010),

$$M_c = 1 - \frac{R_m}{V_m} \quad (2.26)$$

Insulators are having large  $M_c$  close to one ( $R_m/V_m < 1$ ) whereas it is smaller values close to zero ( $R_m/V_m > 1$ ) for metallic solids.

Optical basicity is the ability of oxygen anions to transfer electron density to surrounding cations, which is related to acid or basic property of the glasses and depends on the degree of polarization of ions (Dimitrov and Komatsu 2010). The relation between average optical basicity ( $\lambda$ ) and oxide ion polarizability was derived by Duffy (2004) as follows,

$$\lambda = 0.755 \alpha_o - 0.631 \quad (2.27)$$

Optical absorption spectra of glass samples were recorded in the 200-850 nm wavelengths with fiber optic spectrometer USB4000 (Ocean Optics Inc., USA). Thickness of each sample was measured using micrometer with an accuracy of  $\pm 0.01$  mm and all the glass samples had the thickness in the range of 1.0-1.2 mm. In order to make optically flat surfaces, both the surfaces of the glass samples were fine polished as discussed earlier. The analysis was carried out on three different glass samples of the same composition to check the reproducibility of the results.

### 2.2.8 Dissolution studies

Dissolution studies of glasses are needed to design glasses for various technological applications since hygroscopic and poor chemical durability nature of phosphate glasses limit their broad usages. There are three types of dissolution studies such as static, dynamic and semi-dynamic tests based on solution flow. In static test,



solution is not replenished throughout the study period whereas in dynamic test, solution is flowing through the entire system. In case of semi-dynamic conditions solution is replenished at the particular intervals of study.

Dissolution tests of the polished glass samples were carried out in deionized water in static condition for 28 days at 37°C by immersing the samples in deionized water. Prior to the immersion tests, all the glass samples were polished as discussed earlier in order to keep the same surface conditions. The circular glass discs with dimensions of 10 mm (diameter) × 3 mm (thickness) were used for analysis. In order to keep the constant surface area to volume of solution ratio (0.1 cm<sup>2</sup>/ml) for all the samples based on Kokubo's criteria (Kokubo and Takadama 2006) and ISO 23317:2014(E) standard ("ISO 23317:2014 - Implants for surgery -- In vitro evaluation for apatite-forming ability of implant materials"), the mass of the each glass sample to be immersed in solution was found out from its density value and was nearly kept as 1 gm for all the compositions under study. Initial pH of deionized water was set as 7.4 using diluted HCl acid and NH<sub>4</sub>OH solution. The samples were taken out at the intervals of 1, 7, 14 and 28 days for analysis. Weight losses of glass samples were measured using analytical weighing balance (Contech, CA 234, accuracy ±0.10 mg). The immersed solutions were used for measuring the pH (micro controller pH meter, Equip Tronics, EQ-621) and ion concentrations. The cation (Na<sup>+</sup> and Ca<sup>2+</sup>) concentrations were measured by Flame photo meter (Elico CL 378) with below detectable limit of 0.1 ppm and the anion (PO<sub>4</sub><sup>3-</sup>) were measured by phospho-molybdenum blue method (Pradhan and Pokhrel 2013) using UV-Visible spectrometer (U-2000 spectrophotometer).

To calculate the dissolution rate, the weight loss per unit surface area of glass sample ( $W_L$ ) in deionized water was calculated by the following equation (Lee et al. 2013),

$$W_L = \frac{(W_0 - W_t)}{(W_0 \times S)} \quad (2.28)$$

where  $W_0$  is the measured initial weight of sample (in mg),  $W_t$  is the weight at time  $t$  (in mg),  $S$  is the surface area of sample (in  $\text{cm}^2$ ) and  $t$  is the time of immersion (in hr.). The dissolution rate was found out from the slope of the linear fit of weight loss ( $W_L$ ) vs time graph.

The concentrations of ions released into the solution were normalized in to initial composition of glass. The normalized elemental mass release or cumulative ion release (in  $\text{mg}/\text{cm}^2$ ) was calculated by the following equation (Ma 2014) as,

$$\text{Cumulative ion release} = \frac{(C \times V)}{(f_i \times S)} \quad (2.29)$$

where  $C$  is the measured concentration of ion in the solution (in ppm),  $V$  is the volume of solution (in L), and  $f_i$  is elemental concentration of glass sample (in wt%).

Dissolution nature of glasses was studied by XRD, SEM/EDS and FTIR analysis at the same conditions described earlier. XRD was carried out on glass samples at all the intervals of dissolution study, whereas SEM/EDS and FTIR were conducted on glass samples which were taken out after 28 days of immersion in solution.

### **2.2.9 *In vitro* bioactivity test of glasses**

In order to evaluate HAp (Hydroxyapatite) forming ability or bioactivity of glass samples, *in vitro* bioactivity test of polished glass samples were carried out in physiological solutions. The test of polished glass samples were carried out in sterile/cell culture tested Phosphate buffer saline (PBS, 1 $\times$ , pH 7.4, code-TL1101) and Hank's balanced salt (HBS, 1 $\times$ , pH 7.4, code-TL1010) solutions supplied by Himedia, India under the same conditions as discussed in the section 2.2.8. The ionic concentration and pH of immersed solution were measured as discussed in previous section 2.2.8. The cumulative ion release from glass surface was calculated using equation 2.29. The

bioactivity of glass samples were confirmed by XRD, SEM/EDS and FTIR analysis at the same conditions described earlier. XRD was carried out on samples at all the intervals of study, whereas SEM/EDS and FTIR were conducted on glass samples which were taken out after 28 days of immersion in solutions.

The ionic composition of human blood plasma is similar to physiological solutions such as commonly used SBF (simulated body fluid) and HBS solution etc. and it is given in Table 2.2 for comparison purpose.

Table 2.2: Ionic composition of human blood plasma and simulated body fluids

Composition (in mM/L)	Na <sup>+</sup>	K <sup>+</sup>	Mg <sup>2+</sup>	Ca <sup>2+</sup>	Cl <sup>-</sup>	HCO <sub>3</sub> <sup>-</sup>	HPO <sub>4</sub> <sup>2-</sup>	H <sub>2</sub> PO <sub>4</sub> <sup>2-</sup>	SO <sub>4</sub> <sup>2-</sup>	Glucose
Human blood plasma	142.0	3.6- 5.5	1	2.1- 2.6	95.0- 107.0	27.0	0.65- 1.45	-	1	< 6.9 (3.88- 5.55)
SBF	142.0	6.5	1.5	2.5	148.0	4.2	1.0	-	-	-
HBS	141.7	5.7	0.8	1.7	145.0	4.2	0.7	-	0.8	5.55
PBS	157.0	4.10	-	-	140.0	-	11.98	2.06	-	-

Glass with composition 45P<sub>2</sub>O<sub>5</sub>-29CaO-11Na<sub>2</sub>O-15BaO possesses better mechanical properties (lower brittleness), thermal properties (higher thermal stability and crystallization temperature) and lower dissolution rate in deionized water in comparison with other prepared samples. It showed better bioactivity in physiological solutions such

as Hank's balanced salt (HBS) and Phosphate buffer saline (PBS) solutions. So, this particular composition of glass was selected for coating on metallic biomedical implant materials in order to evaluate its corrosion resistance and bioactivity properties.

### **2.3 PREPARATION OF GLASS COATINGS**

Stainless steel 316 L, duplex stainless steel (DSS) 2205 and Ti6Al4V alloy were used as substrates for glass coatings. The metallic substrates were cut into small pieces of required dimension (10×10×3 mm) and polished using emery paper of grit size from 80 to 1500 for constant duration followed by subsequent cleaning and ultrasonication using acetone.

Thermal enamelling technique (Sola et al. 2014) and glass with composition 45P<sub>2</sub>O<sub>5</sub>-29CaO-11Na<sub>2</sub>O-15BaO were selected for coatings. Glass was ground until it became powder. 0.3 gm of sieved glass powder with particle size less than 45 µm was used for making suspension in 2 ml. iso-propanol. The amount of glass powder and solution volume was optimized after several experimental trials in order to get a homogeneous crack free glass coatings. The substrates were put in this suspension and then heat treated at 60°C for 1 hour for the evaporation of iso-propanol resulting in proper sedimentation of glass powder on substrates. After that, this sample was heat treated at a temperature selected between glass transition (T<sub>g</sub>) and onset of crystallization temperature (T<sub>x</sub>) of glass (Sola et al. 2014). It was placed in the preheated furnace at 500°C and heat treated up to 560°C with heating rate of 10°C/min. in air. The coated specimen was held at 560°C for 20 min. and was allowed to cool to room temperature.

The sample code for coated substrates was given as 316 L/Glass, DSS/Glass and Ti6Al4V/Glass. The flow chart of processes involved in glass coating method is given in Figure 2.8.

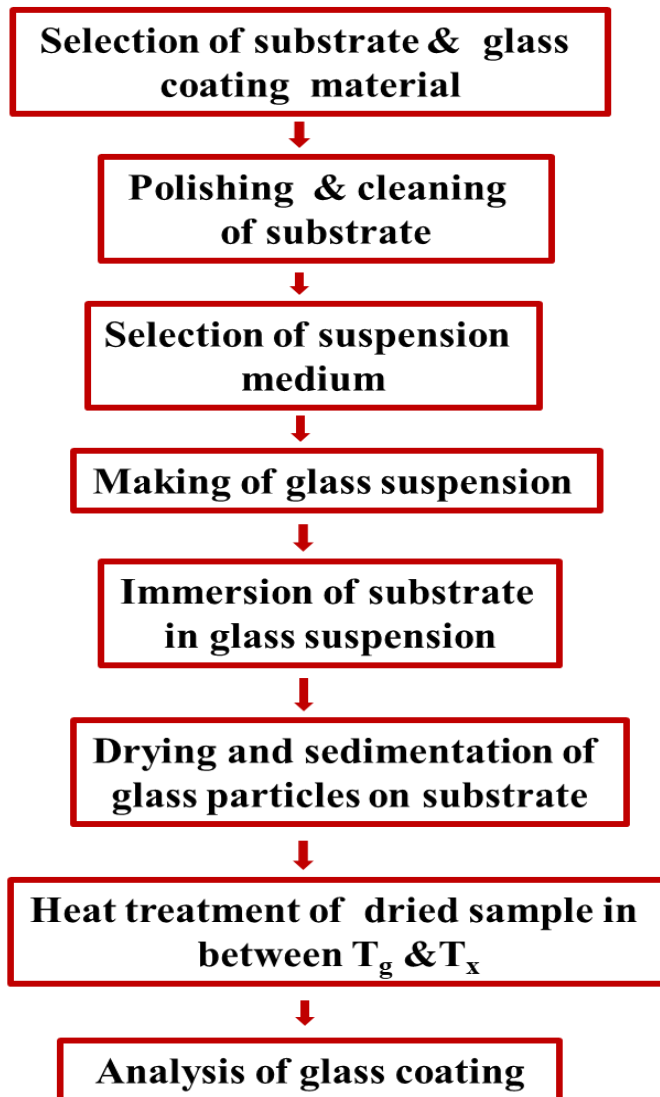


Figure 2.8: Flow chart of process involved in glass coating synthesis and processing

## 2.4 CHARACTERIZATION TECHNIQUES OF GLASS COATINGS

### 2.4.1 Structural and compositional studies

The structure of coated and uncoated substrates was studied by using XRD. The conditions and diffractometer used for XRD analysis were same as reported in section

2.2.1. The surface morphology and elemental composition of coated substrates have been studied with Scanning Electron Microscope (SEM) attached with Energy Dispersive Electron Spectroscopy (EDS) using Zeiss, EVO 18. Prior to the SEM analysis, all the glass coated samples were gold sputtered in order to avoid the charging effect on non-conducting surfaces of glasses under electron beam. The conditions used for EDS analysis were same as reported in section 2.2.3 and error in EDS data was nearly 1-2 %.

#### **2.4.2 Electrochemical corrosion study**

Corrosion is an electrochemical process of oxidation and reduction reactions. In a corrosion process, electrons are released from a metal (oxidation) and gained by elements in the solution (reduction). The electrons or current passing through the corrosion media or electrolyte is measured and controlled electronically. Corrosion characteristics are unique for a particular material.

The schematic diagram of polarization cell setup is given in Figure 2.9 (b). In a corrosion experimental set up, reference electrode, counter electrode and working electrode or sample are placed in an electrolyte which is selected based on application of testing sample. Electrodes are connected to a potentiostat and electrochemical potential or voltage is created between electrodes in an electrolyte solution. Potentiostat is used to measure the corrosion potential ( $E_{COR}$ ) as an energy difference between working and reference electrodes. A potential is imposed on a working electrode for a given period and the resulting current is measured. In potentiodynamic experiments, applied potential is increased with time and the current is monitored constantly. The current or current density is plotted against the potential as shown in Figure 2.9 (a).

The general technique used for corrosion tests of coatings are DC polarization (DCP) and Electrochemical Impedance Spectroscopy (EIS). DCP test is the potentiodynamic corrosion testing technique. When an electrode is polarized, it can cause current to flow via electrochemical reactions that occur at electrode surface. The amount of current

generation is controlled by the kinetics of the reactions and the diffusion of reactants both towards and away from the electrode. In a cell where an electrode undergoes uniform corrosion at open circuit, the open circuit potential is controlled by the equilibrium between two different electrochemical reactions. One of the reactions generates anodic current and the other cathodic current. The potential at which the anodic and cathodic currents are equal is called open circuit potential ( $E_{oc}$ ). The value of the current for either of the reactions is called corrosion current ( $I_{COR}$ ).

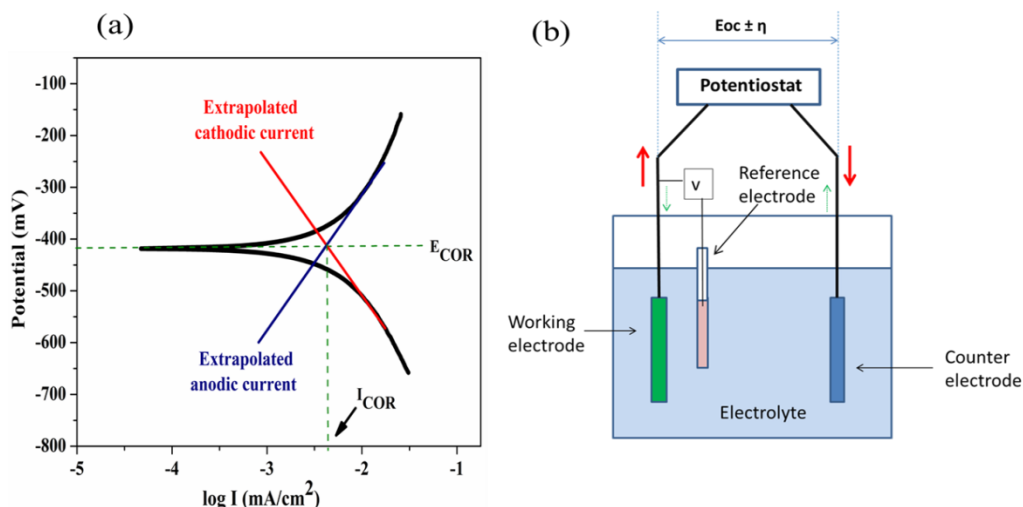


Figure 2.9: (a) Potentiodynamic polarization curve or tafel plot and (b) schematic diagram of electrochemical polarization cell

The electrochemical corrosion studies of all the three uncoated and coated substrates were conducted in a synthetic body fluid such as Hanks's balanced salt (HBS, 1 $\times$ , pH 7.4, code-TL1010, supplied by Himedia, India) solution at 37°C using ACM instruments, Gill AC (serial No.1480). The sample surface area was kept as 1 cm<sup>2</sup> and the solution volume as 200 ml. The potentiodynamic polarization tests were carried out at the scanning rate of 1 mV/sec. by using three electrode system (platinum electrode, saturated calomel electrode and glass coated/uncoated substrate as working electrode).

Before starting the polarization test, the working electrode was immersed in HBS solution nearly for 10 min. to achieve a stable open circuit potential ( $E_{oc}$ ).

The polarization resistance ( $R_p$ ) was calculated using the Stern-Geary equation (Stern and Geary 1957) according to ASTM G102-89 (Reapproved 2015) standard (“ASTM G102 - 89(2015)E1 - Standard Practice for Calculation of Corrosion Rates and Related Information from Electrochemical Measurements”),

$$R_p = \frac{\beta_a \beta_c}{2.303 I_{COR}(\beta_a + \beta_c)} \quad (2.30)$$

where  $\beta_a$  and  $\beta_c$  are the Tafel proportionality constants for the anodic and cathodic reactions respectively.

XRD and SEM/EDS analysis were carried out on uncoated and coated samples to evaluate the electrochemical corrosion behavior.

#### **2.4.3 *In vitro* bioactivity test of glass coatings**

*In vitro* bioactivity test of coated substrates were carried out to evaluate HAp forming ability or bioactivity of samples. The test was carried out in Hanks’s balanced salt (HBS, 1×, pH 7.4, code-TL1010, supplied by Himedia, India) solution. The surface area of sample to volume of solution ratio was kept constant (0.1 cm<sup>2</sup>/ml) based on Kokubo’s criteria (Kokubo and Takadama 2006) and ISO 23317:2014(E) standard (“ISO 23317:2014 - Implants for surgery -- *In vitro* evaluation for apatite-forming ability of implant materials”). The samples were kept in HBS solution in an incubator at 37°C and the tests were carried out under static conditions for 14 days. The samples were taken out at the intervals of 3, 7 and 14 days for measuring the pH of solution (micro controller pH



meter, Equip Tronics, EQ-621) and ion release rate. The concentration of  $\text{PO}_4^{3-}$ ,  $\text{Ca}^{2+}$  and  $\text{Na}^+$  ions released from the coated substrates were measured using the methods as discussed earlier. The XRD and SEM/EDS analysis were carried out after bioactivity tests in order to evaluate bioactivity behavior of coated samples. XRD was conducted on all the samples taken out from the solution at regular intervals and SEM/EDS were carried out on samples which were taken out after 14 days of HBS solution immersion.

To verify the electrochemical corrosion nature of uncoated substrates, the *in vitro* bioactivity test was also conducted to find out the weight loss of uncoated samples in HBS solution at the same conditions as mentioned above. The weight losses of uncoated substrates and pH of immersed solution were measured at the intervals of 3, 7 and 14 days by using analytical weighing balance (Contech, CA 234, accuracy  $\pm 0.10$  mg) and pH meter respectively. The weight loss per unit surface area of sample ( $W_L$ ) was calculated by the equation 2.28.

The synthesized glasses showed better bioactivity in HBS solution in comparison with PBS solution as observed from the *in vitro* bioactivity studies of glasses. So, HBS solution was used for *in vitro* corrosion and bioactivity studies of coated substrates. The samples were rinsed with deionized water after electrochemical corrosion and *in vitro* bioactivity tests and gently dried at room temperature for further analysis.

## **2.5 ERROR ANALYSIS**

Uncertainties are a part of experimental measurements so, error analysis is necessary to keep the error in measured readings as small as possible. Error in the measured quantities was estimated by taking the standard deviation of mean (SDOM) (Taylor 1997) of all measured readings in the present experimental methods. Error in the calculated quantities was estimated using the quadrature sum of uncertainty rule of error propagation.

### 2.5.1 Standard Deviation of Mean (SDOM)

Average of N measurements ( $\bar{x}$ ) such as  $x_1, x_2, \dots, x_N$  which were taken by using same apparatus was calculated as follows,

$$\bar{x} = \frac{x_1 + x_2 + \dots + x_N}{N} \quad (2.31)$$

Standard deviation ( $\sigma_x$ ) was calculated as,

$$\sigma_x = \sqrt{\frac{1}{N-1} \sum_i (x_i - \bar{x})^2} \quad (2.32)$$

Standard deviation of mean (SDOM) or error of the N measurements ( $\sigma_{\bar{x}}$ ) was calculated as,

$$\sigma_{\bar{x}} = \frac{\sigma_x}{\sqrt{N}} \quad (2.33)$$

Final result (X) of N measurements was represented as,

$$X = \bar{x} \pm \sigma_{\bar{x}} = \bar{x} \pm \frac{\sigma_x}{\sqrt{N}} \quad (2.34)$$

### 2.5.2 Quadrature sum of uncertainty

Some quantities can not be measured directly, which was calculated from the measured quantities. In such cases, error also propagates through calculations and the final result contains propagated errors. Uncertainty in calculated quantity was obtained by adding uncertainty in quadrature as given below (Taylor 1997).

If 'x' was calculated from measured quantities  $m, \dots, r$  with uncertainties  $\delta m, \dots, \delta r$  as,

$$x = \frac{m \times \dots \times o}{q \times \dots \times r} \quad (2.35)$$

then the fractional uncertainty in 'x' was obtained by summing quadrature of fractional uncertainties of measured quantities,

$$\frac{\delta x}{|x|} = \sqrt{\left(\frac{\delta m}{m}\right)^2 + \dots + \left(\frac{\delta o}{o}\right)^2 + \left(\frac{\delta q}{q}\right)^2 + \dots + \left(\frac{\delta r}{r}\right)^2} \quad (2.36)$$

$\delta x$  was obtained by multiplying  $|x|$  with quadrature of fractional uncertainties with measured quantities.

In the present work, error in measured quantities was calculated by SDOM method. Error in calculated quantities was obtained by quadrature sum of uncertainty rule of error propagation. Errors were not given for theoretically calculated parameters and all the errors were rounded to one significant digit.

## Chapter 3

### **EFFECT OF BaO ADDITION ON THE STRUCTURAL AND MECHANICAL PROPERTIES OF Na<sub>2</sub>O-CaO-P<sub>2</sub>O<sub>5</sub> GLASSES**

*Phosphate glasses of composition (26-x)Na<sub>2</sub>O-xBaO-29CaO-45P<sub>2</sub>O<sub>5</sub> (x = 0, 5, 10, 15 mol%) were prepared with and without the addition of BaO by melt-quenching technique at three different melting temperatures such as 1000, 1100 and 1200°C. Effect of BaO addition and melting temperature on the structural and mechanical properties of glasses has been studied. XRD patterns indicated the amorphous nature of samples. Q<sup>1</sup> and Q<sup>2</sup> phosphate tetrahedra was observed to be the main structural unit of these glasses and the vibrational frequency associated with P-O-P band remained constant with BaO substitution as per FTIR analysis. Density of glasses increased with BaO content, whereas molar volume hardly showed any compositional effect for glasses prepared at different temperatures. The microhardness was measured using Vickers indentation method and nature of crack formation was studied by SEM. The hardness and fracture toughness of glasses have not shown any compositional effect. The changes in the brittleness and measured crack-length were associated with plastic flow of deformation in the glass materials. Lower density and higher molar volume have obtained for glasses prepared at higher melting temperature. Lower brittleness and crack-length was found in glasses prepared at higher melting temperature.*

#### **3.1 RESULTS AND DISCUSSION**

Na<sub>2</sub>O-BaO-CaO-P<sub>2</sub>O<sub>5</sub> glasses with composition mentioned in Table 2.1 were synthesized and subjected to the following investigations.

### 3.1.1 Structural investigations of synthesized glasses

#### X-ray Diffraction (XRD) studies of synthesized glasses

Figure 3.1 shows the X-ray diffractograms of glasses synthesized at different melting temperatures. Presence of broad hump in between Bragg angle, 20-40° and the absence of sharp reflections in the XRD spectra indicated the amorphous nature of all the synthesised samples.

The shift of the amorphous hump towards the higher angular side with BaO content indicated the lower spacing between atoms and thus increases in the compactness of the glass structure.

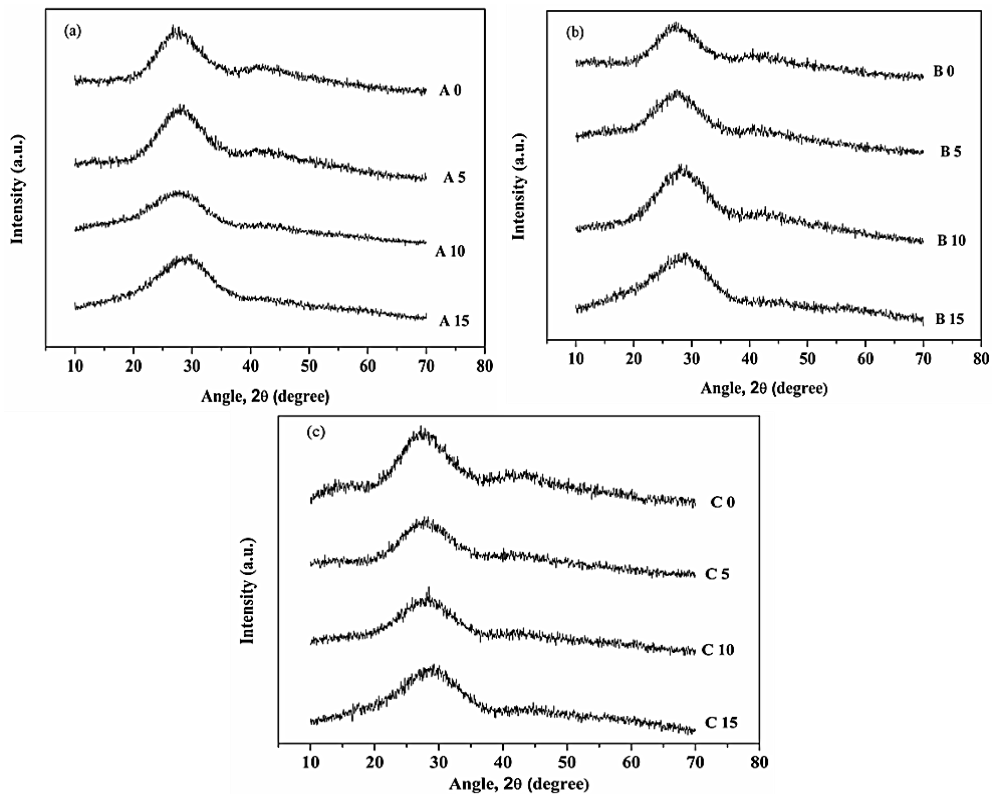


Figure 3.1: XRD pattern of glasses prepared at (a) 1000°C, (b) 1100°C and (c) 1200°C

## Fourier Transform Infra-red Spectroscopy (FTIR) studies of synthesized glasses

FTIR spectra of  $\text{Na}_2\text{O}-\text{BaO}-\text{CaO}-\text{P}_2\text{O}_5$  glasses recorded up to  $2000\text{ cm}^{-1}$  are shown in Figure 3.2. The different vibrational bands present in the glasses are tabulated in Table 3.1.

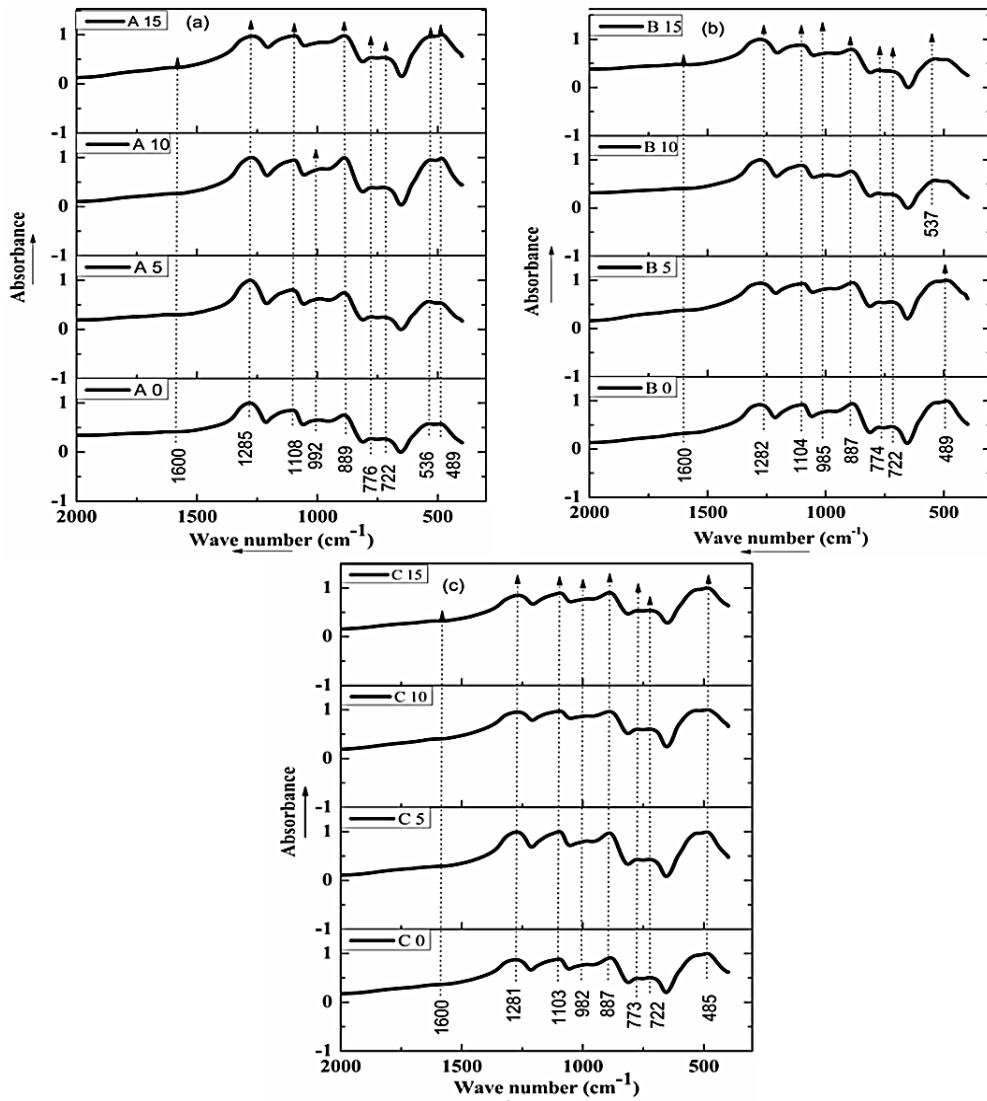


Figure 3.2: FTIR spectrum of glasses prepared at (a)  $1000^{\circ}\text{C}$ , (b)  $1100^{\circ}\text{C}$  and (c)  $1200^{\circ}\text{C}$

Table 3.1: Assigned vibrational bands in FTIR spectra of Na<sub>2</sub>O-BaO-CaO-P<sub>2</sub>O<sub>5</sub> glasses

Vibrational modes (in cm <sup>-1</sup> )	A 0	A 5	A 10	A 15	B 0	B 5	B 10	B 15	C 0	C 5	C10	C 15
V <sub>as</sub> (PO <sub>2</sub> )	1285	1283	1278	1273	1282	1279	1281	1280	1281	1276	1276	1272
V <sub>as</sub> (PO <sub>3</sub> )	1108	1110	1102	1100	1104	1103	1110	1108	1103	1103	1101	1099
V <sub>s</sub> (PO <sub>3</sub> )/ P-O-Na	992	988	979	-	985	982	991	988	982	983	979	-
V <sub>as</sub> (POP)	889	889	888	888	887	888	893	892	887	891	891	890
V <sub>s</sub> (POP)	776	775	774	773	774	773	777	777	773	775	773	771
V <sub>s</sub> (POP)	722	728	727	726	722	724	731	737	722	725	726	725
V(PO <sub>4</sub> <sup>3-</sup> )	536	537	529	526	-	-	537	535	-	-	-	-
δ(PO <sub>2</sub> )	489	492	484	481	489	486	-	-	485	490	485	487

The data shows Q<sup>2</sup> and Q<sup>1</sup> to be the main tetrahedral structural units present in the synthesized phosphate glasses. Bending vibration of H<sub>2</sub>O was associated with the bands

observed in the region of  $1600\text{ cm}^{-1}$  (Rai et al. 2014, Jastrzębski et al. 2011). The stretching frequency of asymmetric  $\text{PO}_2$  group of  $\text{Q}^2$  units or asymmetric  $\text{P}=\text{O}$  groups were obtained in between  $1285\text{-}1272\text{ cm}^{-1}$  (Byun et al. 1995, Kiani et al. 2012). The vibrational frequencies of asymmetric and symmetric  $\text{PO}_3$  group of  $\text{Q}^1$  units were observed in between  $1099\text{-}1108\text{ cm}^{-1}$ . Band associated with symmetric  $\text{PO}_3$  group of  $\text{Q}^1$  units or  $\text{P-O-Na}$  linkages were observed between  $979\text{-}992\text{ cm}^{-1}$ . The bands present at  $887\text{-}893\text{ cm}^{-1}$  were attributed to the stretching frequency of asymmetric  $\text{P-O-P}$  linkages of  $\text{Q}^2$  units (Kiani et al. 2012). The bands present in wavenumber region of  $771\text{-}777\text{ cm}^{-1}$  were obtained due to the symmetric  $\text{P-O-P}$  linkages of  $\text{Q}^1$  units. The vibrational frequencies of  $\text{P-O-P}$  linkages formed between  $\text{Q}^1$  and  $\text{Q}^2$  groups were present at  $722\text{-}737\text{ cm}^{-1}$  (Jha et al. 2015). Bands associated with the fundamental frequency of  $\text{PO}_4^{3-}$  groups or harmonics of  $\text{P}=\text{O}$  bending vibrations and bending mode of  $\text{PO}_2$  group,  $\delta(\text{PO}_2)$  were obtained between  $526\text{-}537\text{ cm}^{-1}$  and  $481\text{-}492\text{ cm}^{-1}$  respectively (Ivascu et al. 2011).

The observed shift in the various band positions was not uniform with added  $\text{BaO}$  composition. Asymmetric  $\text{PO}_2$  and  $\text{PO}_3$  groups associated with glasses prepared at  $1000$  and  $1200^\circ\text{C}$  were shifted towards the lower frequency with  $\text{BaO}$  content due to the decrease in  $\text{O-P-O}$  bond angle resulting from the larger size of Barium ions ( $149\text{ pm}$ ) than Sodium ( $116\text{ pm}$ ) (Byun et al. 1995). This was not observed in the glasses prepared at  $1100^\circ\text{C}$ , in which shift in the band position of  $\text{P-O-P}$  linkages formed between  $\text{Q}^1$  and  $\text{Q}^2$  tetrahedra towards the higher frequency region was observed along with the increase in the intensity of symmetric  $\text{PO}_3$  ( $\text{Q}^1$ ) end groups. This indicated the formation of  $\text{Q}^1$  end groups and thus more number of linkages between  $\text{Q}^1$  and  $\text{Q}^2$  tetrahedra.

### **Scanning Electron Microscopy (SEM) and Energy Dispersive X-ray Spectroscopy (EDS) of synthesized glasses**

The representative images of SEM and EDS spectra of synthesised glasses with and without  $\text{BaO}$  are given in Figures 3.3 and 3.4 respectively. The homogeneous nature of synthesized glasses was observed in SEM analysis and there was no evidence of phase separation as observed from XRD data. The representative EDS data of glasses prepared



at 1200°C is given in Table 3.2. Elemental composition of the glasses analysed from EDS was in a reasonable agreement with the calculated values of the batch composition and the contamination from silica crucibles used for melting was less ( $\text{Si} \leq 1\%$ ).

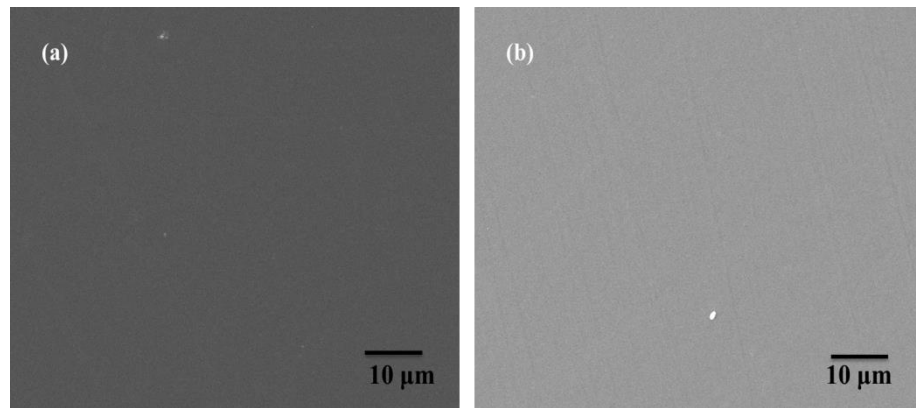


Figure 3.3: SEM images of synthesized glasses (a) C0 and (b) C15

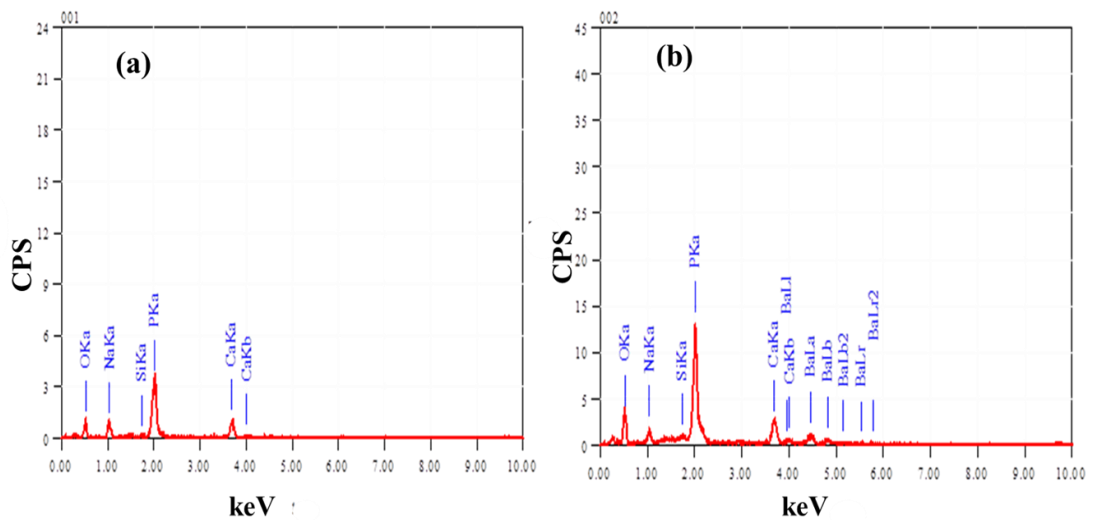


Figure 3.4: EDS spectra of synthesized glasses (a) C0 and (b) C15

Table 3.2: Mass % of elements calculated from batch composition and obtained from EDS analysis for glasses prepared at 1200°C. Minimum and maximum values are reported

Sample code		C 0	C 5	C 10	C 15
Oxygen (O)	Batch	46.54	44.43	42.51	40.74
	EDS	44.70 - 45.68	42.43 - 43.12	40.87 - 41.26	38.73 - 39.46
Phosphorous (P)	Batch	28.96	27.65	26.45	25.35
	EDS	29.37 - 31.14	28.21 - 29.99	27.76 - 29.92	26.69 - 27.78
Calcium (Ca)	Batch	12.08	11.53	11.03	10.57
	EDS	13.57 - 14.27	11.08 - 12.43	11.00 - 10.74	11.33 - 12.25
Sodium (Na)	Batch	12.42	9.58	6.98	4.60
	EDS	11.07 - 13.26	7.59 - 8.46	6.17 - 6.31	5.68 - 6.10
Barium (Ba)	Batch	-	6.81	13.03	18.73
	EDS	-	7.47 - 8.11	14.82 - 15.31	19.16 - 19.73

### Density measurement of synthesized glasses

Measured density, molar volume and other calculated structural properties are listed in Tables 3.3 and 3.4. The density of glasses was observed to increase with BaO addition in all the samples prepared at three melting temperatures, owing to the higher molecular weight of BaO (153.33 gm/mol) in comparison with Na<sub>2</sub>O (61.98 gm/mol). The strength of cross-linking in the glass structure increased with BaO additions due to the higher field strength of Ba<sup>2+</sup> ( $0.24 \times 10^{-20} \text{ m}^{-2}$ ) ion which can strongly attract non-

bridging oxygen than that of  $\text{Na}^+$  ( $0.19 \times 10^{-20} \text{ m}^{-2}$ ). A divalent ( $\text{Ba}^{2+}$ ) ion can bond with two non-bridging oxygens, whereas a monovalent ( $\text{Na}^+$ ) ion is bond with only one. This resulted in the effective cross-linking of the glass structure with BaO content (Shelby 2007). Molar volume of glasses was not varying much with BaO content due to nearly equal molar volume of BaO ( $26.80 \text{ cm}^3/\text{mol}$ ) and  $\text{Na}_2\text{O}$  ( $27.30 \text{ cm}^3/\text{mol}$ ) (Hafid et al. 2002).

Table 3.3: Density ( $\rho_{\text{mes}}$ ), molar volume ( $V_{\text{m}}$ ), oxygen packing density ( $\rho_{\text{ox}}$ ), oxygen molar volume ( $V_{\text{o}}$ ) and cross-link density (CLD) values of  $\text{Na}_2\text{O}$ -BaO-CaO- $\text{P}_2\text{O}_5$  glasses

Sample Code	$\rho_{\text{mes}}$ ( $\text{gm}/\text{cm}^3$ )	$V_{\text{m}}$ ( $\text{cm}^3/\text{mol}$ )	$\rho_{\text{ox}}$ ( $\text{mol}/\text{L}$ )	$V_{\text{o}}$ ( $\text{cm}^3/\text{mol}$ )	CLD
A 0	$2.594 \pm 0.002$	$37.11 \pm 0.03$	75.46	13.25	3.11
A 5	$2.716 \pm 0.003$	$37.12 \pm 0.04$	75.44	13.26	3.15
A 10	$2.846 \pm 0.007$	$37.03 \pm 0.09$	75.61	13.23	3.18
A 15	$2.966 \pm 0.004$	$37.07 \pm 0.07$	75.53	13.24	3.22
B 0	$2.592 \pm 0.002$	$37.13 \pm 0.08$	75.41	13.26	3.11
B 5	$2.715 \pm 0.003$	$37.14 \pm 0.05$	75.40	13.26	3.15
B 10	$2.833 \pm 0.005$	$37.20 \pm 0.04$	75.28	13.28	3.18
B 15	$2.953 \pm 0.002$	$37.24 \pm 0.06$	75.20	13.30	3.22
C 0	$2.588 \pm 0.003$	$37.19 \pm 0.05$	75.30	13.28	3.11
C 5	$2.710 \pm 0.002$	$37.21 \pm 0.07$	75.26	13.29	3.15
C 10	$2.823 \pm 0.004$	$37.33 \pm 0.03$	75.01	13.33	3.18
C 15	$2.950 \pm 0.006$	$37.28 \pm 0.06$	75.10	13.32	3.22

Table 3.4: Number of bonds ( $N_b$ ), inter ionic distance between  $Ba^{2+}[R(Ba^{2+})]$  and  $Na^+[R(Na^+)]$  ions, phosphorous molar volume ( $V_m^P$ ), average phosphorous-phosphorous distance ( $\langle d_{p-p} \rangle$ ) values of  $Na_2O-BaO-CaO-P_2O_5$  glasses

Sample code	$N_b (\times 10^{20})$ ( $cm^3$ )	$R(Ba^{2+})$ (nm)	$R(Na^+)$ (nm)	$V_m^P$ ( $cm^3/mol$ )	$\langle d_{p-p} \rangle$ (nm)
A 0	874	-	0.62	33.73	0.824
A 5	890	1.07	0.66	33.74	0.825
A 10	909	0.85	0.73	33.66	0.824
A 15	924	0.73	0.82	33.70	0.824
B 0	873	-	0.62	33.76	0.825
B 5	890	1.07	0.66	33.76	0.825
B 10	905	0.85	0.73	33.81	0.825
B 15	920	0.74	0.83	33.85	0.825
C 0	873	-	0.62	33.81	0.825
C 5	888	1.07	0.67	33.82	0.825
C 10	902	0.85	0.73	33.93	0.826
C 15	919	0.75	0.83	33.89	0.826

### 3.1.2 Mechanical properties of synthesized glasses

There are three types of deformation processes which affect the hardness of a material such as densification, elastic and plastic (shear) deformation (Kjeldsen et al.

2015, Rouxel et al. 2010). Hardness is the resistance to deformation of a body while applying a certain load and fracture toughness is the resistance to fracture under certain load or the maximum energy that can be absorbed before fracture happens (Rocha-Rangel 2011).

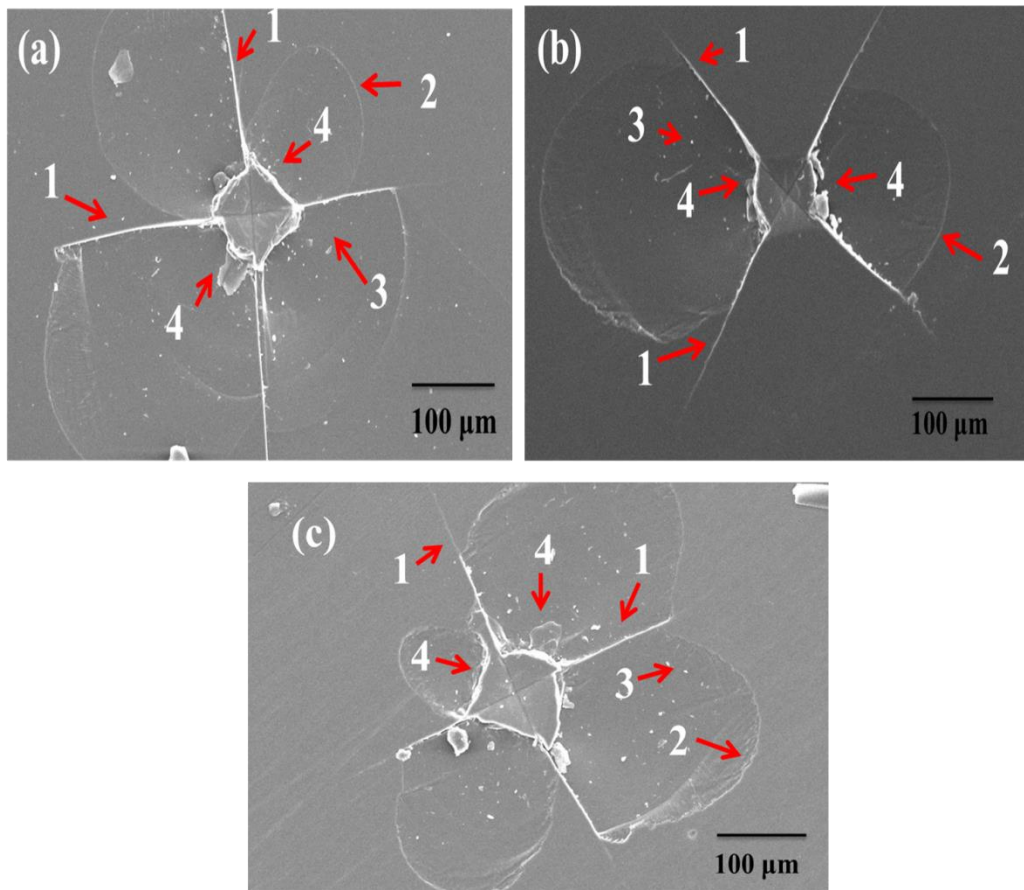


Figure 3.5: SEM images of synthesized glasses after indentation (a) A5, (b) A15 and (c) C15

Some representative images of nature of Vickers indentation on the glass surfaces observed from SEM micrographs after applying 19.6 N is shown in Figure 3.5. Radial/median cracks are seen to extend from the four corners of indentation pattern as indicated

by arrow 1 and the lateral cracks are represented by arrow 2. The white reflections of the bright region obtained by the lifting of small amount of material from glass surface are shown by arrow 3. Chipping of material from the closely spaced shear faults indicating the presence of plastic flow of deformation is indicated by arrow 4.

Table 3.5: Measured microhardness ( $H_v$ ), calculated brittleness ( $\chi$ ), fracture toughness ( $K_{IC}$ ) and measured half crack-length ( $c$ ) of  $\text{Na}_2\text{O}$ - $\text{BaO}$ - $\text{CaO}$ - $\text{P}_2\text{O}_5$  glasses

Sample code	$H_v$ (GPa)	$\chi$ ( $\mu\text{m}^{-1/2}$ )	$K_{IC}$ ( $\text{MPam}^{1/2}$ )	$C$ ( $\mu\text{m}$ )
A 0	3.90 $\pm$ 0.14	11.85 $\pm$ 0.13	0.33 $\pm$ 0.04	247 $\pm$ 5
A 5	3.79 $\pm$ 0.31	10.68 $\pm$ 0.29	0.36 $\pm$ 0.05	238 $\pm$ 8
A 10	4.09 $\pm$ 0.24	13.42 $\pm$ 0.21	0.31 $\pm$ 0.05	258 $\pm$ 7
A 15	3.97 $\pm$ 0.13	12.41 $\pm$ 0.10	0.32 $\pm$ 0.04	253 $\pm$ 4
B 0	3.76 $\pm$ 0.20	10.83 $\pm$ 0.15	0.35 $\pm$ 0.04	235 $\pm$ 6
B 5	3.66 $\pm$ 0.27	9.82 $\pm$ 0.21	0.37 $\pm$ 0.05	233 $\pm$ 8
B 10	3.56 $\pm$ 0.25	8.84 $\pm$ 0.17	0.40 $\pm$ 0.05	224 $\pm$ 7
B 15	3.47 $\pm$ 0.14	7.76 $\pm$ 0.12	0.45 $\pm$ 0.04	211 $\pm$ 6
C 0	3.60 $\pm$ 0.20	9.40 $\pm$ 0.17	0.38 $\pm$ 0.05	229 $\pm$ 7
C 5	3.42 $\pm$ 0.24	8.04 $\pm$ 0.22	0.43 $\pm$ 0.05	218 $\pm$ 9
C 10	3.35 $\pm$ 0.22	6.99 $\pm$ 0.18	0.48 $\pm$ 0.06	203 $\pm$ 7
C 15	3.39 $\pm$ 0.15	7.28 $\pm$ 0.12	0.47 $\pm$ 0.04	207 $\pm$ 6
40BaO-10CaF <sub>2</sub> -50P <sub>2</sub> O <sub>5</sub> glass (Narayanan and Shashikala 2015)	2.78 $\pm$ 0.04	8.33 $\pm$ 0.03	0.33 $\pm$ 0.01	146 $\pm$ 2
20BaO-5La <sub>2</sub> O <sub>3</sub> -50P <sub>2</sub> O <sub>5</sub> glass (Kurkjian 2000)	4.00	-	0.48	-
20Na <sub>2</sub> O-10Al <sub>2</sub> O <sub>3</sub> -50P <sub>2</sub> O <sub>5</sub> glass (Kurkjian 2000)	4.10	-	0.50	-

Vickers hardness ( $H_v$ ), fracture toughness ( $K_{IC}$ ) and brittleness ( $\chi$ ) values of synthesized glasses are given in Table 3.5. The theoretically calculated values of modulus were increased with BaO content as shown in Table 3.6. There was no change observed for the measured  $H_v$  and  $K_{IC}$  with the substitution of BaO in all the glasses prepared at different temperatures and the values were come within the error limit, which was associated with the trend in molar volume as the molar volume is the measure of rigidity of the glass network. The structural back bone of phosphate glasses is P-O-P linkages (Shelby 2007) and thus the strength of glass is mainly correlated to these linkages. The observed shift in the P-O-P band position was negligible with BaO content as per IR spectra, which indicated that P-O-P linkages was not strengthened with BaO additions and it might be a reason for insignificant changes in hardness and fracture toughness.

The trend observed in the brittleness and crack length with BaO addition was similar. Densification and plastic flow of modes of deformation can change the brittleness of glasses (Sehgal and Ito 1999) and plastic flow initiates cracks in the structure under a certain load (Hermansen et al. 2013). The chances of densification under a certain load is difficult in glasses with density greater than  $2.4 \text{ gm/cm}^3$  and so plastic flow was having significant role in the brittleness and crack-length of synthesised glasses rather than densification (Sehgal and Ito 1999). The variations in the brittleness and crack length were different in glasses prepared at different melting temperature as shown in Table 3.5. The reduction in plastic flow with BaO content in the glasses prepared at  $1000^\circ\text{C}$  as indicated by the arrow 4 in Figure 3.5 (a) & (b) was the reason for increase in these properties, whereas it has decreased due to higher amount of plastic flow in the glasses prepared at  $1100$  and  $1200^\circ\text{C}$  as shown in representative image, Figure 3.5 (c). The large amount of cross-linking in the glass network was indicated by the calculated values of Poisson's ratios of 0.25-0.26 (Abd El-Moneim 2001).

The present results were compared with the work of other researchers, which has given in Table 3.5.

Table 3.6: Theoretically calculated mechanical properties of Na<sub>2</sub>O-BaO-CaO-P<sub>2</sub>O<sub>5</sub> glasses

Sample Code	Young's modulus (GPa)	Bulk modulus (GPa)	Poisson's ratio	Packing density
A 0	64.648	44.382	0.258	0.574
A 5	65.317	45.157	0.260	0.578
A 10	66.163	46.180	0.262	0.584
A 15	66.792	46.904	0.263	0.587
B 0	64.600	44.320	0.258	0.574
B 5	65.286	45.114	0.260	0.578
B 10	65.872	45.774	0.261	0.581
B 15	66.496	46.489	0.262	0.584
C 0	64.507	44.193	0.257	0.573
C 5	65.162	44.943	0.259	0.577
C 10	65.640	45.452	0.260	0.579
C 15	66.411	46.370	0.262	0.584

### 3.1.3 Effect of melting temperature on the properties of synthesized glasses

Density of synthesized glasses of a particular composition was decreased, whereas molar volume was increased for glasses prepared at higher melting temperature. This was due to the higher cooling rate of melt at fixed quenching time and lower viscosity of melt at higher melting temperature which resulted in lesser structural rearrangement of atoms (Shelby 2007).

While considering a particular composition of glass with fixed BaO content, glasses prepared at higher melting temperatures have lower brittleness and crack-length, which was attributed to their slightly lower density values. As the density of glasses



decreased, compactness of structure also decreased and thus ease of densification and plastic flow in glasses was more, which decreased the brittleness (Sehgal and Ito 1999). Arrow 4 in Figure 3.5 (b) & (c) indicates higher amount of chipping of material for the same composition of glasses (A15 & C15) which were prepared at higher melting temperature and this indicated the presence of more amount of plastic flow of deformation.

### 3.2 SUMMARY

BaO added Na<sub>2</sub>O-CaO-P<sub>2</sub>O<sub>5</sub> glasses were prepared at three different melting temperatures 1000, 1100 and 1200°C. Effect of BaO addition and melting temperatures on the structural and mechanical properties of these glasses was subjected to study. All the synthesized samples were amorphous in nature as shown by XRD pattern. Glass structure was mainly constituted with Q<sup>1</sup> and Q<sup>2</sup> structural units according to FTIR spectra. All the glass samples were homogeneous in nature. Density of the glasses has increased with BaO addition, whereas molar volume did not show any compositional effect. Hardness and fracture toughness were independent of composition in all the glasses prepared at different melting temperatures. The brittleness and crack-length have increased with BaO content in glasses prepared at 1000°C, whereas it has decreased in glasses prepared at 1100 and 1200°C, which are mainly due to the plastic flow of deformation.

Lower density and higher molar volume was found for glass samples prepared at higher melting temperature. Lower brittleness and crack-length have been obtained for glasses melted at higher melting temperature and these were attributed to the changes in density and plastic flow of deformation of glasses.

The glasses prepared at 1200°C were selected for further studies due to their better mechanical properties (lower brittleness and crack-length) in comparison with other synthesized samples.

## Chapter 4

### EFFECT OF BaO ADDITION ON THE THERMAL AND OPTICAL PROPERTIES OF Na<sub>2</sub>O-CaO-P<sub>2</sub>O<sub>5</sub> GLASSES

*Effect of BaO addition on the thermal and optical properties of phosphate glasses with composition (26-x)Na<sub>2</sub>O-xBaO-29CaO-45P<sub>2</sub>O<sub>5</sub> (x = 0,5,10,15 mol %) melted at 1200°C have been studied. The glass transition and onset of crystallization temperature have increased with BaO content, which can be attributed to the higher field strength of Ba<sup>2+</sup> ions. The thermal stability of the glasses has increased with BaO addition. The thermal stability values of all the synthesized glasses were greater than 100°C indicating their fiber drawing capability. The glass forming ability has increased with initial addition of BaO. The observed increase in refractive index values was ascribed to the higher electron density of Ba<sup>2+</sup> ions. The optical band gap energy has increased due to the formation of stronger ionic cross-links and more covalent P—O—Ba bonds. The additions of BaO above 5 mol % did not make any changes in the band gap energy values. The changes observed in the optical band gap energy values were related to the calculated optical basicity and metallization criteria of glasses. No uniform variation was observed in the Urbach energy values of BaO added glasses. However, the decrease in Urbach energy with initial BaO additions can be attributed to the reduction in the formation of defects and/or interstitial bonds.*

#### 4.1 RESULTS AND DISCUSSION

(26-x)Na<sub>2</sub>O-xBaO-29CaO-45P<sub>2</sub>O<sub>5</sub> (x = 0, 5, 10, 15 mol%) glasses prepared at 1200°C were selected for studying the effect of BaO addition on the thermal and optical properties. This glass system was selected based on their better mechanical properties mentioned in chapter 3.

#### 4.1.1 Thermal properties of synthesized glasses

DTA data of as quenched glasses are given in Figure 4.1 and the thermal properties derived from these patterns are given in Table 4.1. The first inflection in the DTA thermogram corresponds to the glass transition temperature ( $T_g$ ). The exothermic and endothermic peaks correspond to peak crystallization ( $T_c$ ) and melting ( $T_m$ ) temperatures of glasses respectively (Tulyaganov et al. 2006). The onset of crystallization temperature ( $T_x$ ) is found out as shown in Figure 4.1.

Table 4.1: Thermal properties obtained from DTA analysis and density of Na<sub>2</sub>O-BaO-CaO-P<sub>2</sub>O<sub>5</sub> glasses

Sample Code	$T_g$ °C, (±3)	$T_x$ °C, (±3)	$T_m$ °C, (±3)	Thermal stability ( $\Delta T$ ), °C	Hruby's parameter ( $K_{gl}$ )	Density gm/cm <sup>3</sup>
C 0	374	528	726	154	0.777	2.588
C 5	384	570	695	186	1.488	2.710
C 10	390	584	794	194	0.923	2.823
C 15	418	626	826	208	1.040	2.950
48BaO-2CaF <sub>2</sub> - 50P <sub>2</sub> O <sub>5</sub> (Narayanan and Shashikala 2015)	428	543	831	115	0.399	3.508
28CaO-27Na <sub>2</sub> O- 45P <sub>2</sub> O <sub>5</sub> glass (Franks et al. 2001)	~ 365	~ 490	~ 730	-	-	-

The data of samples without (C0) and with BaO (C5) are given in Figure 4.1 for comparison purpose as representative graphs and the baseline fit has been carried out to find out the deviations from the thermogram. The thermal properties of phosphate glasses prepared by other researchers are given in Table 4.1 for comparison purpose.

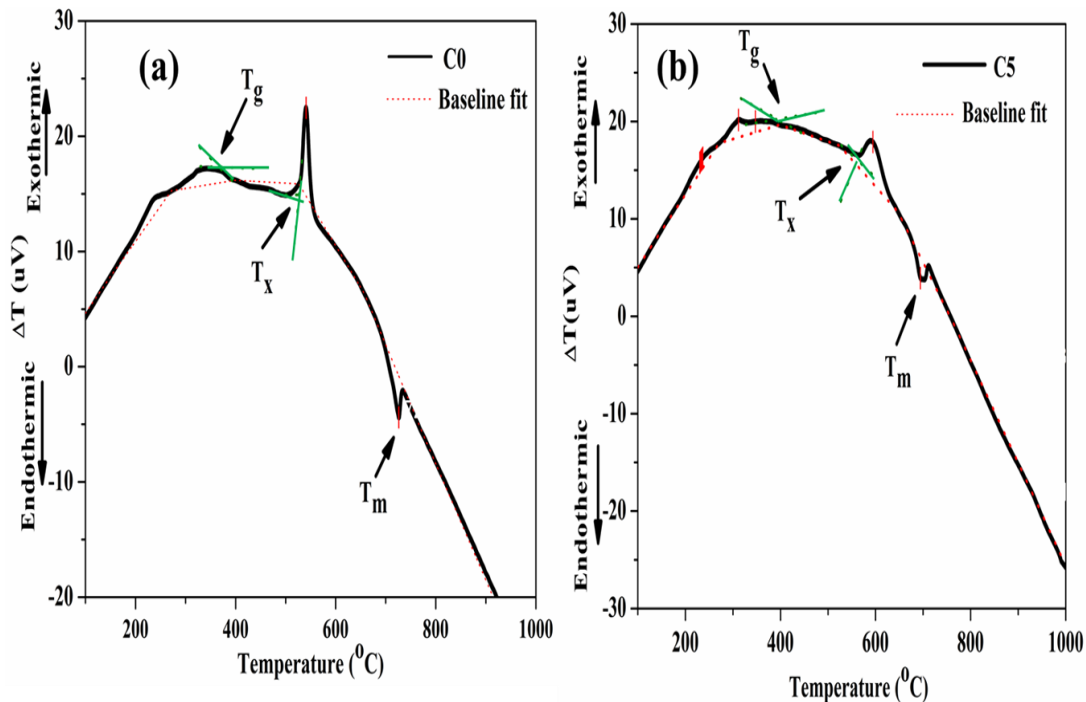


Figure 4.1: DTA thermograms of glass samples (a) without (C0) and (b) with BaO (C5)

The observed results can be explained as following. The temperature required to activate rotational motion of a molecule while it undergoes heating is called as glass transition temperature,  $T_g$  (Ma 2014). Density of covalent cross-links and strength of ionic cross-links formed between cations and Oxygen anions in the glass structure can control  $T_g$ . Close packing of the atoms and/or increase in the cross-link density results in higher  $T_g$  of glasses. The measured density of the glasses was mainly correlated to the cross-link density as mentioned in chapter 3 (B Edathazhe and Shashikala 2016). The

density of glass has increased with BaO content indicating the increase in cross-link density thereby increase in  $T_g$ .

The addition of  $Ba^{2+}$  ( $0.24 \times 10^{-20} \text{ m}^{-2}$ ) ions with higher field strength by replacing  $Na^+$  ( $0.19 \times 10^{-20} \text{ m}^{-2}$ ) increased the strength of ionic cross-links formed between  $Ba^{2+}$  and non-bridging oxygen ions resulting in higher  $T_g$  values (Hafid et al. 2002). The slightly higher ionic nature of Ba-O bond resulting from lower electronegativity values of  $Ba^{2+}$  (0.89) ions in comparison with  $Na^+$  (0.93) increase the covalent nature of P-O-Ba bond in comparison with P-O-Na as the covalent nature of a bond is directly related to its strength (Jermoumi et al. 2003). It has been reported that increase in the valency of cations and covalent character of bond linkages of the phosphate chains resulting from the presence of higher field strength cations can increase  $T_g$  (Ma 2014). The observed shift to the lower frequency side and final disappearance of symmetric stretching vibration of  $PO_3$  group of  $Q^1$  tetrahedra ( $982\text{-}979 \text{ cm}^{-1}$ ) with BaO content in the FTIR spectra of the present system of glasses (B Edathazhe and Shashikala 2016) indicated the reduction in the end group ( $Q^1$ ) formation and increase in  $T_g$  as reported in case of Hafid et al. (2002). So, the increase in  $T_g$  of present system of glasses was mainly attributed to the formation of stronger ionic cross-links with BaO content. The bond formed between the metal polyhedra and phosphate anions can regulate the compositional dependence on the thermal properties such as  $T_g$  of glasses with same O/P ratios and different modifying oxides (Ma 2014).

The stability of glasses against crystallization on reheating process is referred as their thermal stability ( $\Delta T$ ). The increase in the onset of crystallization temperature ( $T_x$ ) as shown in Table 4.1 indicated the suppression of crystallization with BaO additions.  $Ba^{2+}$  ions can hinder the mobility of phosphate chains in the melt due to their higher field strength in comparison with  $Na^+$  ions, which can result in increase of  $T_x$  and  $T_g$  values (Groh et al. 2014). Glasses with  $\Delta T > 100^\circ\text{C}$  are suitable for fiber drawing (Rasool et al. 2013) and so all the synthesized glasses are stable enough to draw fibers. The ability of sintering and resistance towards crystallization is higher in glasses with higher thermal

stability which is an important factor when coating glasses using thermal methods such as thermal enamelling technique. Since, the sintering viscous flow and dissolution/bioactivity of glasses can be adversely affected with crystallization (Al-Noaman et al. 2012), it is better to select a glass with higher thermal stability for coating. The heat of crystallization attributed to the area of crystallization peak in DTA thermogram was reduced with BaO content, which was also an indication of the improvement in the thermal stability of glasses. Crystalline phases containing Barium may be formed at slower rate rather than Barium-free crystalline phases formed in glasses without BaO. This can also be one of the reasons for reduction in the intensity of crystallization peak with the addition of BaO (Massera et al. 2014) as observed in the present work.

The incorporation of nucleating agents in to glasses enhances the crystalline phase formation in the glass matrix, which obviously reduces their crystallization temperature,  $T_x$  (Massera et al. 2014).  $T_x$  has increased with 5 mol% of BaO addition in the present study, indicating the entering of  $Ba^{2+}$  ions into the crystal structure and thus altering of crystalline phase composition/structure which was formed in the glasses during heating process rather than acting as a nucleating agent. The reduction in the melting temperature,  $T_m$  with 5 mol % of BaO addition also substantiated this result (Massera et al. 2014). The increase in  $T_m$  with the addition of BaO from 5 to 15 mol % was attributed to the formation of stronger P—O—Ba bonds and replacing of weaker P—O—Na bonds. Since P—O—Ba bonds are stronger, more energy was required to break the stronger bonds during melting and thus increase in  $T_m$  was observed.

Glass forming ability or ease of vitrification when cooling a melt towards  $T_g$  is denoted with Hruby's parameter ( $K_{gl}$ ) (Ma 2014). Hruby's parameter was found to increase when comparing the end members of composition such as C0 and C15. Ma et al. (2014) have reported that addition of higher field strength ions can increase the glass forming ability of melt.

## 4.1.2 Optical properties of synthesized glasses

### Refractive index of glasses

The measured refractive index of the glasses is given in Table 4.2 and it increased with the BaO addition. Refractive index of glass mainly depends on electron density and polarizability of ions present in it. Electron density of the Ba<sup>2+</sup> ions is higher than that of Na<sup>+</sup> because of which passage of light through glass matrix with Ba<sup>2+</sup> ions was hindered and thus increasing the refractive index (Dimitrov and Komatsu 2010). Based on Lorentz-Lorentz equation (Lorentz 1880) refractive index and density of glasses are having correlation to each other. Increase in the compactness of glass structure (or density) can prevent the movement of light through glasses and thereby increasing the refractive index. This was substantiated by the measured density (B Edathazhe and Shashikala 2016) of present system of synthesized glasses as shown in Table 4.2.

### UV-Visible absorption spectra and band gap studies of glasses

The optical band gap energy ( $E_g$ ) of glasses derived from Figure 4.2 (a) is given in Table 4.2. Not much variation in the band gap energy values was observed with 5 to 15 mol % of BaO content, however initial addition of 5 mol % increased the band gap energy. Ionic cross-links were formed in the glass structure with the addition of divalent ions such as Ba<sup>2+</sup> and Oxygen bond strength also increased due to the formation of such P—O—Ba—O—P linkages resulting in the requirement of higher amount of energy for optical transitions by excitation of electrons. Ionicity of Oxygen ions reduced by the formation of such cross-links which lowered the top of the valence band and thus increased the band gap energy according to Khor et al. (2013). Also the addition of higher field strength ions, Ba<sup>2+</sup> improved the strength of bonding and thus reduction in the number of electrons of Oxygen ions contributing in the electronic transitions resulted in higher band gap energy values (Khor et al. 2013).

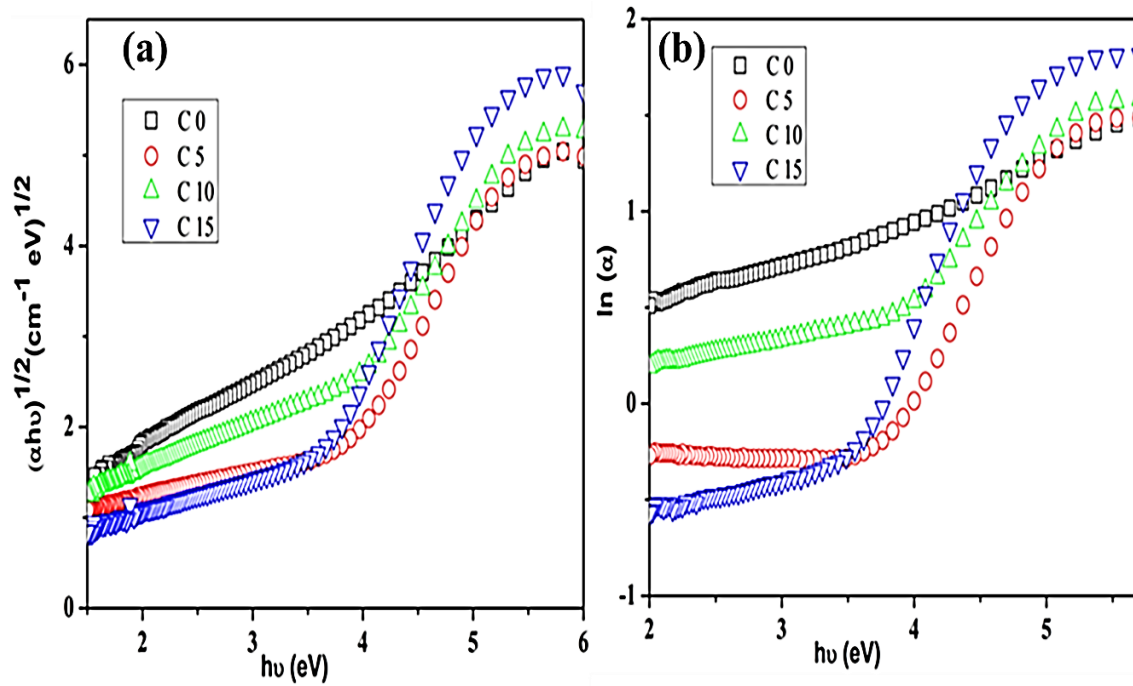


Figure 4.2: (a)  $(\alpha h\nu)^{1/2}$  and (b)  $\ln(\alpha)$  as a function of photon energy,  $h\nu$  of Na<sub>2</sub>O-BaO-CaO-P<sub>2</sub>O<sub>5</sub> glasses

The optical basicity ( $\lambda$ ) of the glasses which is given in Table 4.3 indicates the electron donating power of the glass matrix. The addition of BaO to BaO-free base glass (C0), reduced the optical basicity which indicated the reduction in the number of electrons taking part in the optical transitions and thus substantiating the rise in band gap energy values. The increase in the metallization criteria ( $M_C$ ) or the insulating nature of glasses as shown in Table 4.3 also supported the increase in the band gap energy values (Dimitrov and Komatsu 2010).

The measured optical properties of the present glasses were compared with the work of other researchers, which is given in Table 4.2.



Table 4.2: Density, refractive index, optical band gap energy and Urbach energy of Na<sub>2</sub>O-BaO-CaO-P<sub>2</sub>O<sub>5</sub> glasses

Sample code	Density gm/cm <sup>3</sup>	Refractive index (n) ± 0.001	Band gap Energy (E <sub>g</sub> ), ±0.1 eV	Urbach Energy (E <sub>u</sub> ), ±0.05 eV
C 0	2.588	1.522	1.76	2.46
C 5	2.710	1.535	3.29	0.70
C 10	2.823	1.551	2.98	1.06
C 15	2.950	1.557	3.23	0.52
48 BaO-2CaF <sub>2</sub> -50P <sub>2</sub> O <sub>5</sub> glass (Narayanan and Shashikala 2015)	3.508	1.576	3.04	0.68
50CaO-50P <sub>2</sub> O <sub>5</sub> glass (Venkateswara Rao and Shashikala 2014)	2.589	1.547	3.44	0.390

Urbach energy (E<sub>u</sub>) of glasses found out from Figure 4.2 (b) is given in Table 4.2. Urbach energy is the direct measure of extent of band tailing in the glass structure. The addition of BaO, increased the band gap energy values and lowered the Urbach energy or density of localized states in the band structure of the glasses. According to the Davis and Mott (1970), higher the states of disorder in the non-crystalline materials, greater the density and tail of the localized states present in the energy gap. Presence of defects, impurities and broken as well as dangling bonds result in the formation of localized states within the energy gap. Davis and Mott (1970) proposed that the presence of high density of localized states lowers the band gap energy of glasses. The decreasing trend of Urbach energy with BaO content might also be attributed to the reduction in the defects

formation. The presence of interstitial bonds resulted in the formation of localized states and increased the Urbach energy of glasses (Altaf et al. 2005). As the  $Ba^{2+}$  ions were unlikely to move into the interstitial position due to their higher ionic radii (149 pm) than that of  $Na^+$  (116 pm), the addition of BaO was expected to reduce the Urbach energy as observed

Table 4.3: Optical properties of  $Na_2O$ -BaO-CaO- $P_2O_5$  glasses calculated from molar volume and optical band gap energy values

Sample code	Calculated molar volume $cm^3/mol$	Molar polarizability $(\alpha_m)$ $\text{\AA}^3$	Oxide ion polarizability $(\alpha_o)$ $\text{\AA}^3$	Metallization criteria ( $M_C$ )	Optical basicity ( $\lambda$ )
C0	37.19	10.378	3.61	0.296	2.101
C5	37.21	8.775	3.02	0.405	1.652
C10	37.33	9.094	3.11	0.386	1.721
C15	37.28	8.847	3.00	0.402	1.638

## 4.2 SUMMARY

The effect of BaO addition on the thermal and optical properties of  $Na_2O$ -CaO- $P_2O_5$  glasses has been studied. The increase in the glass transition temperature of glasses with BaO content was attributed to the formation of stronger ionic cross-linking in the glass structure. The crystallization tendency of glasses has decreased with increase in BaO content. The glass forming ability of glasses was found to increase with initial addition of BaO. All the synthesized glasses were suitable for fiber drawing due to their higher thermal stability values greater than  $100^\circ C$ . The refractive indices of glasses have

increased with BaO content in accordance with the measured density values resulting from their higher electron densities. The initial addition of BaO increased the optical band gap energy of glasses, whereas the increase in BaO content has negligible effect on it. The changes in the optical basicity and metallization criteria of glasses substantiated the observed trends of band gap energy values. The decrease in the Urbach energy values was due to the reduction in the formation of defects and/or interstitial bonds in the glass structure.

## Chapter 5

### EFFECT OF BaO ADDITION ON THE DISSOLUTION AND *IN VITRO* BIOACTIVITY PROPERTIES OF Na<sub>2</sub>O-CaO-P<sub>2</sub>O<sub>5</sub> GLASSES

*The phosphate glasses with composition (26-x)Na<sub>2</sub>O-xBaO-29CaO-45P<sub>2</sub>O<sub>5</sub> (x = 0, 5, 10, 15 mol %) were subjected to the dissolution test in deionized water and *in vitro* bioactivity test in Phosphate buffer saline (PBS) as well as Hank's balanced salt (HBS) solutions. The effect of BaO on the dissolution and bioactivity properties of Na<sub>2</sub>O-CaO-P<sub>2</sub>O<sub>5</sub> glasses has been studied under static dissolution conditions for 28 days and the dissolution nature of glasses was analyzed by XRD, SEM/EDS, FTIR and ions release rate measurements. The dissolution rate of glasses in deionized water has increased with time and decreased with BaO content. The glasses without BaO and with 15 mol % of BaO showed the formation of crystalline hydroxyapatite (HAp) phases within 14 days of immersion in PBS, whereas the glasses with 5 and 10 mol % BaO showed the formation of amorphous calcium-phosphate (ACP) and/or poorly crystallized HAp phases. Crystalline hydroxyapatite phases were formed on all the glass samples within 7 days of immersion in HBS solution and the bioactivity of glasses was found to improve with BaO content.*

#### 5.1. RESULTS AND DISCUSSION

(26-x)Na<sub>2</sub>O-xBaO-29CaO-45P<sub>2</sub>O<sub>5</sub> (x = 0, 5, 10, 15 mol %) glasses prepared at 1200°C were selected for the dissolution and *in vitro* bioactivity studies.

### 5.1.1 Dissolution studies of synthesized glasses

Glasses were immersed in deionized water for 28 days to find out their dissolution rates. Weight loss of glasses has been measured using sensitive weighing balance. The increase in the weight losses was observed in all the compositions of glasses as the time of immersion increases, whereas addition of BaO decreased it drastically as indicated in Table 5.1.

Table 5.1: Weight losses and dissolution rates of Na<sub>2</sub>O-BaO-CaO-P<sub>2</sub>O<sub>5</sub> glasses in deionized water

Days	Weight losses (in mg/cm <sup>2</sup> )			
	C 0	C 5	C 10	C 15
1	10.64 ±1	0.68 ±0.2	0.48 ±0.07	0.41 ±0.05
7	19.32 ±2	1.92 ±0.5	0.51 ±0.06	0.43 ±0.04
14	31.03 ±2	6.28 ±1	0.74 ±0.05	0.45 ±0.04
28	50.71 ±3	16.90 ±2	1.46 ±0.06	0.47 ±0.02
Dissolution rate (mg/cm <sup>2</sup> /hr)	6.2 × 10 <sup>-2</sup>	2.6 × 10 <sup>-2</sup>	1.5 × 10 <sup>-3</sup>	8.9 × 10 <sup>-5</sup>

The reduction in the dissolution rate of glasses by three orders of magnitude with increase in BaO content upto 15 mol % is an interesting factor to note. Addition of BaO formed stronger ionic cross-links and more compact glass structure which resulted in the decrease in the dissolution rate as indicated in Table 5.1. As mentioned in the chapter 4, the formation of stronger P—O—Ba linkages at the expense of slightly weaker P—O—Na increased the strength of the glass network (Hafid et al. 2002), which was attributed to

the higher field strength of  $\text{Ba}^{2+}$  ions ( $0.24 \times 10^{-20} \text{ m}^{-2}$ ) than that of  $\text{Na}^+$  ( $0.19 \times 10^{-20} \text{ m}^{-2}$ ). In general, higher dissolution rates of BaO-free phosphate glasses were mainly due to the hygroscopic nature of covalent P—O—P linkages which was comparatively sensitive to moisture attack or less chemically durable than P—O—M (M – Modifier cation) linkages and the modifying oxides such as BaO can convert the bridging P—O—P bonds into the non-bridging P—O—Ba. These factors are supported by our previous work (B Edathazhe and Shashikala 2016) which was given in chapter 3 as follows. The observed increase in density and shift in the amorphous halo of XRD spectra towards the higher angular value with BaO content indicated the increase in compactness of glass structure. The reduction in the intensity and final disappearance of the IR vibrational bands associated with P—O—Na linkages ( $982\text{-}979 \text{ cm}^{-1}$ ) substantiated the replacement of P—O—Na with P—O—Ba.

Acid/base catalysis, hydration and hydrolysis reactions are the three major processes leading to the dissolution of phosphate glasses in aqueous solutions. Penetration of water molecules into the bulk glass forms a hydrated layer on its surface at the initial stages of dissolution. Cations present in such a layer get detached from  $\text{PO}_4$  tetrahedra and exchange with  $\text{H}^+$  ions in the solutions.  $\text{H}^+$  ions in the hydrated layer attack P—O—P linkages of glass structure followed by breakage of those linkages and finally the dissolution of entire phosphate chains. As the time of immersion proceeds, more number of ions were released due to these reactions resulting in the higher dissolution rate of glasses (Tošić et al. 2013, Bunker et al. 1984). According to Döhler et al. (2015), hydration and hydrolysis are having the primary and secondary effect on the dissolution process of glasses respectively. They made this conclusion based on the study of dissolution of polyphosphate glasses containing 45 mol % of  $\text{P}_2\text{O}_5$  in Tris-buffer solution.

The measured anion ( $\text{PO}_4^{3-}$ ) and cation ( $\text{Na}^+$  and  $\text{Ca}^{2+}$ ) concentrations for 28 days of immersion are given in Figure 5.1. They increased up to 14 days and reached a steady state beyond that. Dissolution was more in the initial days due to the fast release of

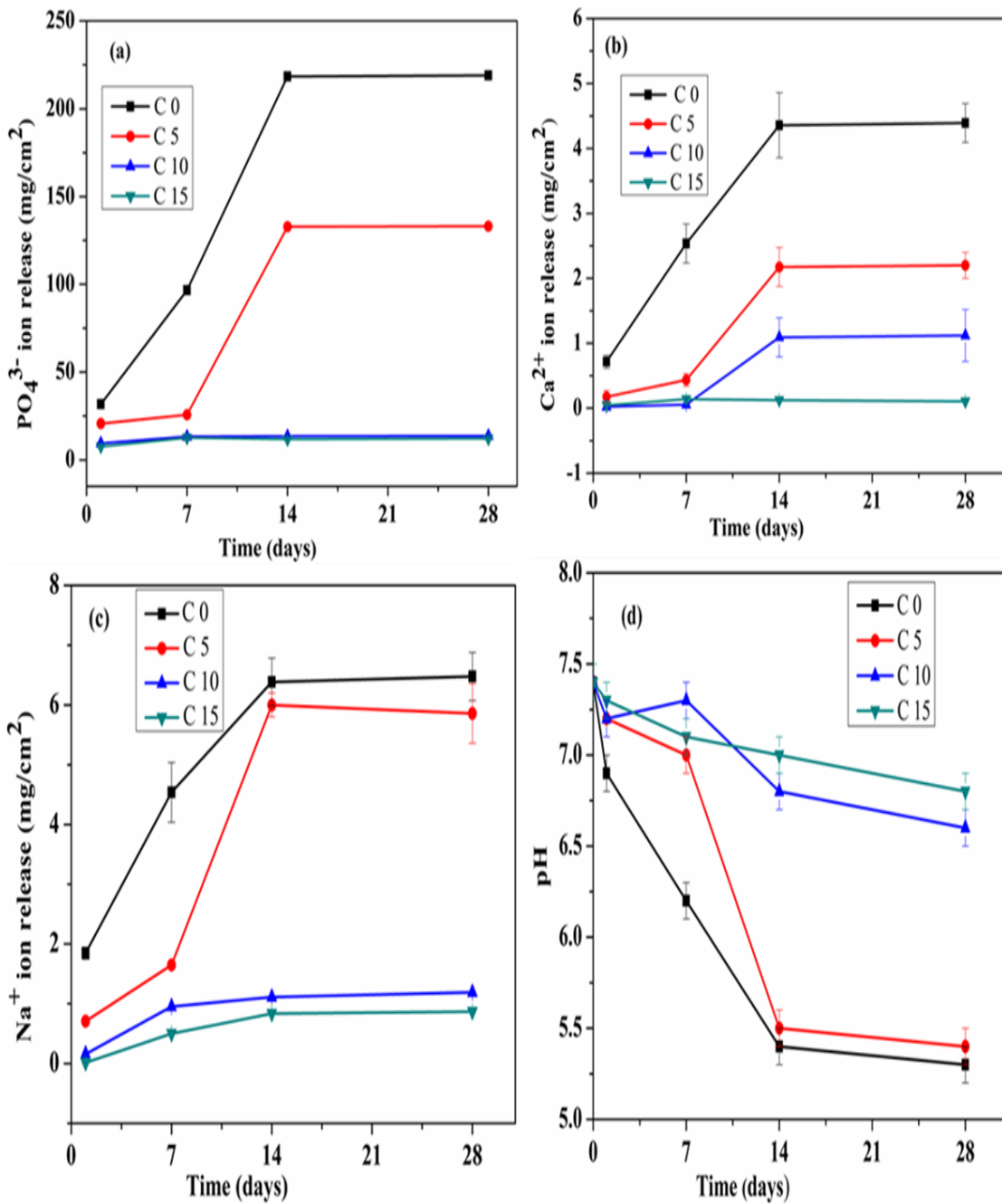


Figure 5.1: Ionic concentration of (a)  $\text{PO}_4^{3-}$ , (b)  $\text{Ca}^{2+}$ , (c)  $\text{Na}^+$  and (d) pH in deionized water

cations which increased the ionic strength of solution and further release of ions was prevented by the electrostatic interactions. The decrease in the ion release rate in glasses

with BaO content substantiated the weight loss data/dissolution rate in which the lowest value was observed for glasses with higher BaO content as discussed earlier. The higher amount of anions were released from glasses with less BaO content (C0 & C5), whereas nearly same rate of both anion and cations were released from glasses containing higher amount of BaO (C10 & C15) indicating the reduction in the dissolution of  $\text{PO}_4^{3-}$  ions with BaO additions due to the formation of stronger P—O—Ba—O—P linkages as discussed in chapter 4. P—O—P bonds are susceptible to moisture attack, whereas the P—O—M linkages are stable towards moisture and solution attacks (Lee et al. 2013).

The amount of phosphate anions in the original glass structure (45%  $\text{P}_2\text{O}_5$ ) is more than that of  $\text{Na}^+$  and  $\text{Ca}^{2+}$  and so it was expected to obtain higher rate of  $\text{PO}_4^{3-}$  release rather than cations as shown in Figure 5.1 (a), similar to observations made in another study of MgO added  $\text{P}_2\text{O}_5$ - $\text{Na}_2\text{O}$ - $\text{CaO}$  glasses by Lee et al. (2013).  $\text{H}^+$  ions in the solution were exchanged with cations ( $\text{Na}^+$  and  $\text{Ca}^{2+}$ ) of glasses leading to an increase in pH or basic nature, whereas the release of  $\text{PO}_4^{3-}$  ions due to the breakage/dissolution of P—O—P chains and exchange of these ions with  $\text{OH}^-$  ions in the solution resulted in the reduction in pH or acidic nature of solution. The initial decrease in pH followed with time independent variations after 14 days in all the samples as shown in Figure 5.1 (d) was attributed to the ions release rate. The initial stages of dissolution process of phosphate glasses in deionized water was controlled by the hydration reaction in which the outer hydrated layer was formed on glass surfaces according to the study of Bunker et al. (1984). The observed initial decrease in pH and increase in weight losses confirmed the consumption of  $\text{OH}^-$  ions from the solution and thus the formation of hydrated layer.

The increase in pH with BaO content was attributed to the lower rate of anions release and amount of anion release was significant or higher than that of cations. The release of more number of  $\text{PO}_4^{3-}$  anions (~220 & 125  $\text{mg}/\text{cm}^2$  respectively) in comparison with cations made the immersed solution of C0 and C5 acidic (~5.5), whereas the release of nearly same rate of both anion and cations resulted almost steady and neutral pH (7.4-6.9) of C10 and C15. Variation in pH and weight losses was more prominent in glasses



containing less BaO (C0 & C5) when compared to C10 and C15 which supported the reduction in the dissolution rate of glasses with BaO content. However, changes in pH were negligible or within error limit for all the samples in the final days due to the steady rate of ions release. The observed ion release rates, pH and weight loss profiles of samples in deionized water were correlated with each other and no such remarkable differences was observed in these properties between C10 and C15 glasses.

Figure 5.1 indicates that time dependence of various ions release rate to be different, which indicates the selective (or incongruent) dissolution of all the constituents of glasses in deionized water (Tošić et al. 2013).

The changes in the surface morphology of glass samples after the immersion in deionized water for 28 days were analyzed with SEM. Some representative SEM images are given in Figure 5.2 and surface of unimmersed C15 is shown in Figure 5.2 (a) for comparison purpose which shows a clear and homogeneous surface. Figure 5.2 (b) and (c) indicate a white layer formation on the surface of C0 and C5. The magnified image of grain structure of this formed layer on C5 is given in Figure 5.2 (f) and the grains are uniform with varying diameter of 600-850 nm. Lesser amount of white layer was formed on the cracked surface of C10 as indicated in Figure 5.2 (d). Merging of pits to form honey-comb like structure was observed in C15 as shown in Figure 5.2 (e) and these pits were having varying diameter of 0.6-4.0  $\mu\text{m}$ . Tošić et al. (2013) have reported that pits were formed on the surface of polyphosphate glasses in the initial days of immersion and white layer was formed on prolonged duration of immersion. It is worthy to note that the addition of 15 mol % of BaO enabled  $\text{Na}_2\text{O-CaO-P}_2\text{O}_5$  glasses to survive without any layer and crack formation and only pits were formed on its surface which indicates the initial stages of dissolution even after 28 days of immersion in deionized water and reduction in the dissolution rate of glasses with increase in BaO content.

EDS analysis recorded on the surface of immersed samples is given in Table 5.2. The amount of Phosphorous and Sodium have decreased in all the samples, whereas the amount of divalent ions such as Calcium (only in case of C0 & C5) and Barium (in C5 &

C10) have increased after immersion in deionized water for 28 days. Such changes were due to the difference in the rates of release of various cations.

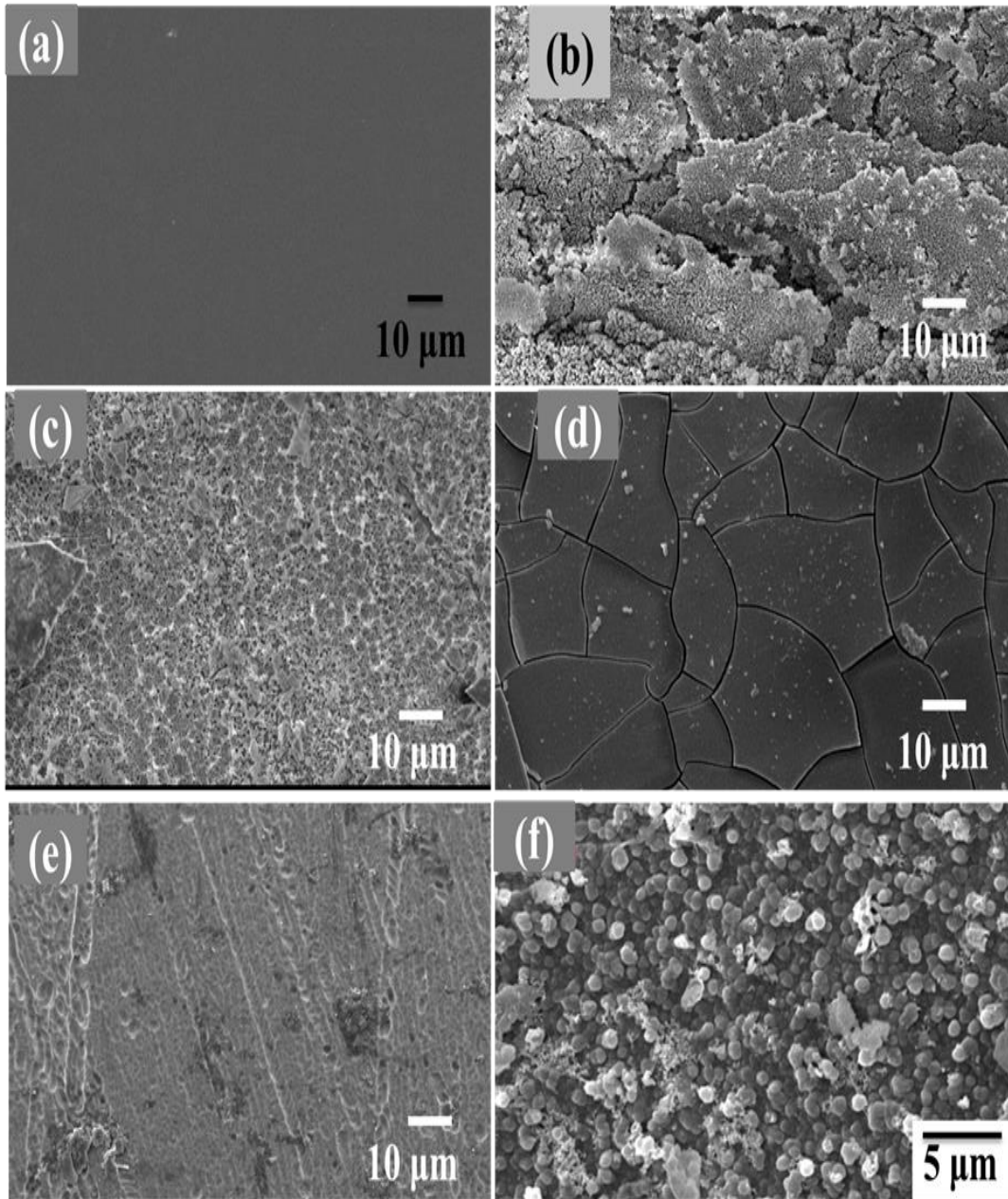


Figure 5.2: SEM images of (a) untreated C15 and treated (b) C0, (c) C5, (d) C10, (e) C15 in deionized water for 28 days and (f) grain structure of white layer formed on C5

According to Tošić et al. (2013), divalent ions ( $Ba^{2+}$  and  $Ca^{2+}$ ) were released slowly in comparison with monovalent ions ( $Na^+$ ). The decrease in the concentration of divalent ions along with no clear evidence of surface layer formation observed in C15 indicated the relatively lesser amount of white layer formation on their surface. Thus EDS also supported selective dissolution of ions from all the glasses which was due to the observed difference in the release rate of various ions (Tošić et al. 2013).

Table 5.2: Mass % of elements on  $Na_2O$ - $BaO$ - $CaO$ - $P_2O_5$  glasses before and after the immersion in deionized water for 28 days

Sample code		C 0	C 5	C 10	C 15
Oxygen (O)	Before	45.19	42.77	41.06	39.09
	After	51.67	45.95	49.88	55.29
Phosphorous (P)	Before	30.25	29.10	28.84	27.24
	After	28.82	23.86	21.90	22.50
Calcium (Ca)	Before	13.92	11.76	10.87	11.79
	After	16.45	13.67	9.17	4.69
Sodium (Na)	Before	12.17	8.03	6.24	5.89
	After	3.06	0.90	0.97	4.32
Barium (Ba)	Before	-	7.79	15.07	19.45
	After	-	15.61	18.16	13.20

All the synthesized glasses were in amorphous state as per XRD studies mentioned in chapter 3 (B Edathazhe and Shashikala 2016). Absence of sharp reflections

and retaining of amorphous nature of all the immersed samples as shown in Figure 5.3 indicated the formed white layer might be the surface layer of glass with changed ratios of oxides and confirmed the absence of precipitation during the dissolution in deionized water under the given experimental conditions as reported in case of Tošić et al. (2013). Amorphous hump present in the BaO-free samples (C0) was slightly shifted towards lower angular side specifying the depletion of ions from these glasses (Brauer et al. 2010), whereas no such shift was observed in BaO added samples supporting their lower ion release and dissolution rate.

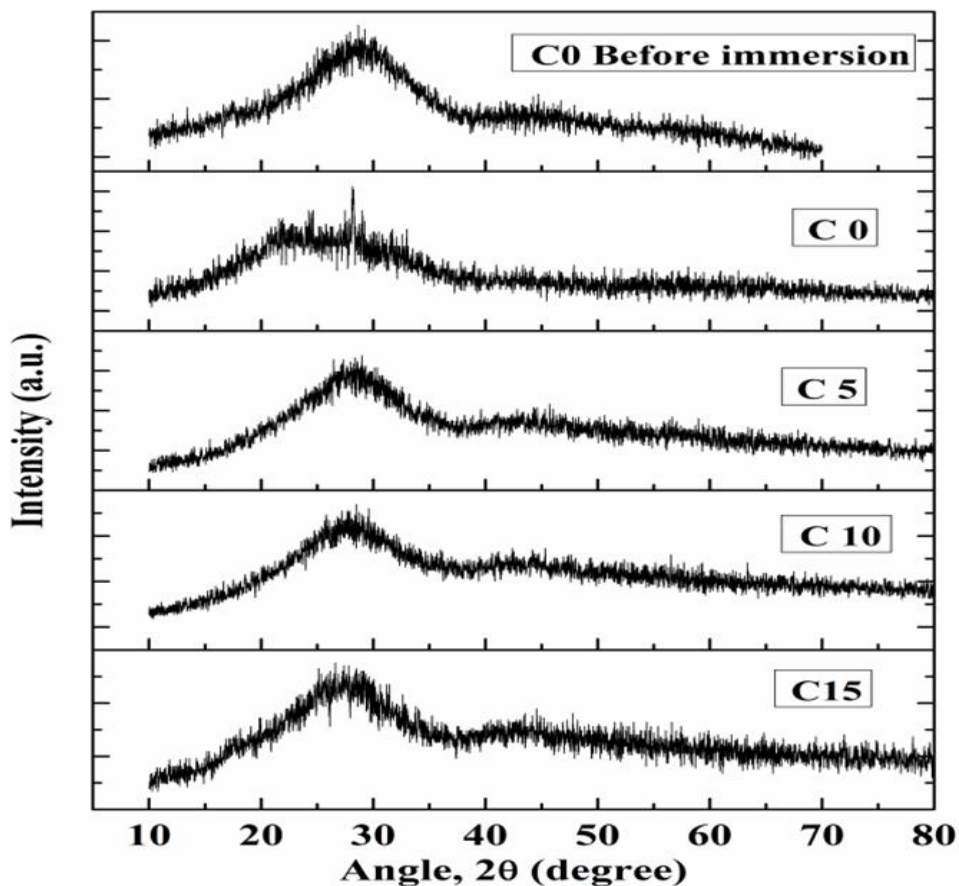


Figure 5.3: XRD spectra of  $\text{Na}_2\text{O}$ - $\text{BaO}$ - $\text{CaO}$ - $\text{P}_2\text{O}_5$  glasses after the immersion in deionized water for 28 days

Selective (or incongruent) type of dissolution was observed in all the compositions of glasses according to XRD, SEM, EDS and ions release data.

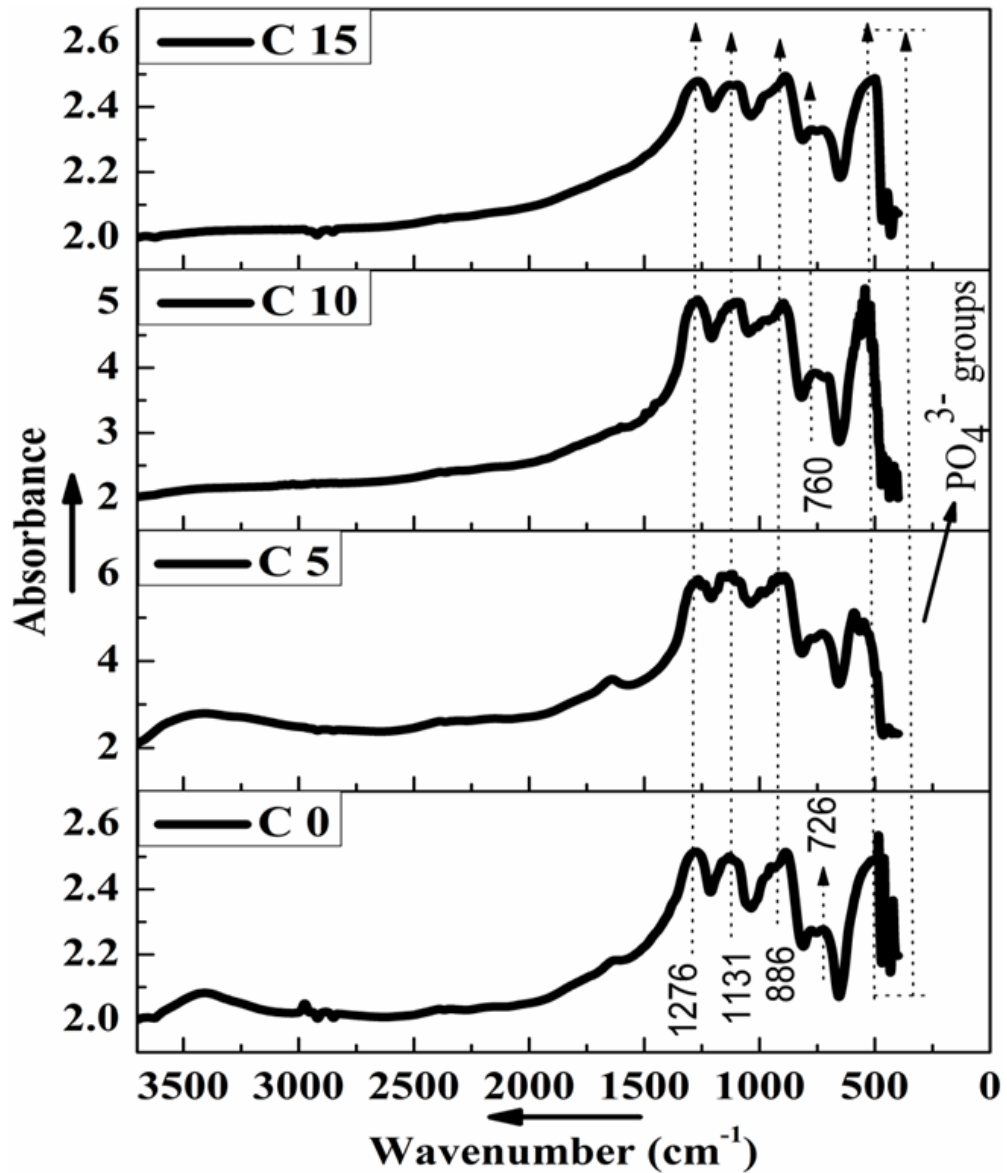


Figure 5.4: FTIR spectra of Na<sub>2</sub>O-BaO-CaO-P<sub>2</sub>O<sub>5</sub> glasses after immersion in deionized water for 28 days

Dissolution of glass samples led to the depolymerization of glass network, which can be verified by comparing FTIR spectra of samples before (B Edathazhe and Shashikala 2016) and after immersion in deionized water. The results were consolidated and given in Figure 5.4 and Table 5.3. The characteristic vibrational modes present in between 722 and 1281  $\text{cm}^{-1}$  were reported in chapter 3 (B Edathazhe and Shashikala 2016). The bands associated with  $Q^2$  (meta) chains and  $Q^1$  (pyro) phosphate groups became less prominent, whereas new orthophosphate ( $\text{PO}_4^{3-}$ ,  $Q^0$ ) groups have appeared between 415 and 438  $\text{cm}^{-1}$  indicating the depolymerization of glass matrix i.e. the breakage of longer phosphate chains and conversion into smaller phosphate groups.

( $Q^1$ - $Q^2$ ) bands were shifted towards the higher wavenumber side due to increase and decrease in non-bridging O—P—O and bridging P—O—P bond lengths respectively. The attack of solutions on bulk glasses and thus breakage/dissolution of P—O—P linkages led to the conversion of bridging oxygens into the non-bridging ones which resulted in the depolymerization of glass network by the conversion of longer  $Q^2$  chains to smaller pyrophosphate ( $Q^1$ ) to orthophosphate ( $Q^0$ ) groups. The shift in  $\text{PO}_3$  ( $Q^1$ ) band position was more prominent in C0 and C5 than other samples which might be due to the conversion of more  $Q^2$  chains into  $Q^1$  groups and it supported the higher dissolution of glasses with less BaO content. Bands associated with P—O—P linkages between  $Q^1$ - $Q^2$  (722  $\text{cm}^{-1}$ ) were slightly shifted towards the higher wavenumber side in BaO-free sample (C0), whereas these bands have disappeared along with the appearance of P—O—P linkages of  $Q^1$  at 760-775  $\text{cm}^{-1}$  in BaO added samples, which can be attributed to faster dissolution of  $Q^2$  chains than  $Q^1$ . Longer phosphate chains ( $Q^2$ ) are more susceptible for dissolution rather than smaller groups ( $Q^1$ ) (Döhler et al. 2015). All these points were ascribed to the reduction in the depolymerization of  $\text{Na}_2\text{O}$ - $\text{CaO}$ - $\text{P}_2\text{O}_5$  glasses with BaO content.

Vanishing of vibrational bands attributed to P—O—Na linkages (982-979  $\text{cm}^{-1}$ ) from glasses containing up to 10 mol% BaO were due to the leaching of  $\text{Na}^+$  ions. Intensity of O-H bands (3000-3500  $\text{cm}^{-1}$ ) (Arepalli et al. 2015) has decreased with

increase in BaO content, which supported the reduction in the dissolution rate of glasses. The bands present in between 2300-2400  $\text{cm}^{-1}$  might be due to the adsorption of  $\text{CO}_2$  from air (Raouf et al. 2015) at the time of pellet formation for analysis and these were present in all the samples before and after the immersion in deionized water.

Table 5.3: Assigned vibrational bands in FTIR spectra of  $\text{Na}_2\text{O-BaO-CaO-P}_2\text{O}_5$  glasses before and after the immersion in deionized water for 28 days

Characteristic vibrational modes (in $\text{cm}^{-1}$ )	Before immersion				After immersion			
	C0	C5	C10	C15	C0	C5	C10	C15
$\nu_{\text{as}}\text{PO}_2$ of $\text{Q}^2$ units	1281	1276	1276	1272	1276	1269	1266	1266
$\nu_{\text{as}}\text{PO}_3$ of $\text{Q}^1$ units	1103	1103	1103	1099	1131	1121	1098	1095
$\nu_s\text{PO}_3$ of $\text{Q}^1$ units/ P—O—Na linkages	982	983	979	-	-	-	-	-
$\nu_{\text{as}}\text{POP}$ of $\text{Q}^2$ units	887	891	891	890	886	889	887	888
$\nu_s\text{POP}$ of $\text{Q}^1\text{-Q}^2$ linkages	722	725	725	725	726	-	-	-
$\nu_s\text{POP}$ of $\text{Q}^1$ units	-	-	-	-	-	-	760	775
$\nu\text{POP}$ mode (Jha et al. 2015)	-	-	-	-	589	-	-	-
$\delta\text{O=P-O}^{(*)}/\delta\text{P=O}^{(*)}$ (Jha et al. 2015)	-	-	-	-	-	-	543 <sup>(*)</sup>	500 <sup>(*)</sup>
$\delta\text{PO}_2$ of $\text{PO}_4^{3-}$	485	490	485	487	484	-	-	-
$\delta\text{PO}_2$ (Spevak et al. 2013)	-	-	-	-	460	441	456, 447	447
Crystalline $\delta\text{PO}_4^{3-}$ (Al-Noaman et al. 2012)	-	-	-	-	438, 422	418	429, 418	415

### 5.1.2 *In vitro* bioactivity tests of synthesized glasses

The glasses (C0, C5, C10 & C15) were immersed in PBS and HBS solutions for 28 days. At the intervals of 1, 7, 14 and 28 days, the immersed samples were taken out and subjected to further studies.

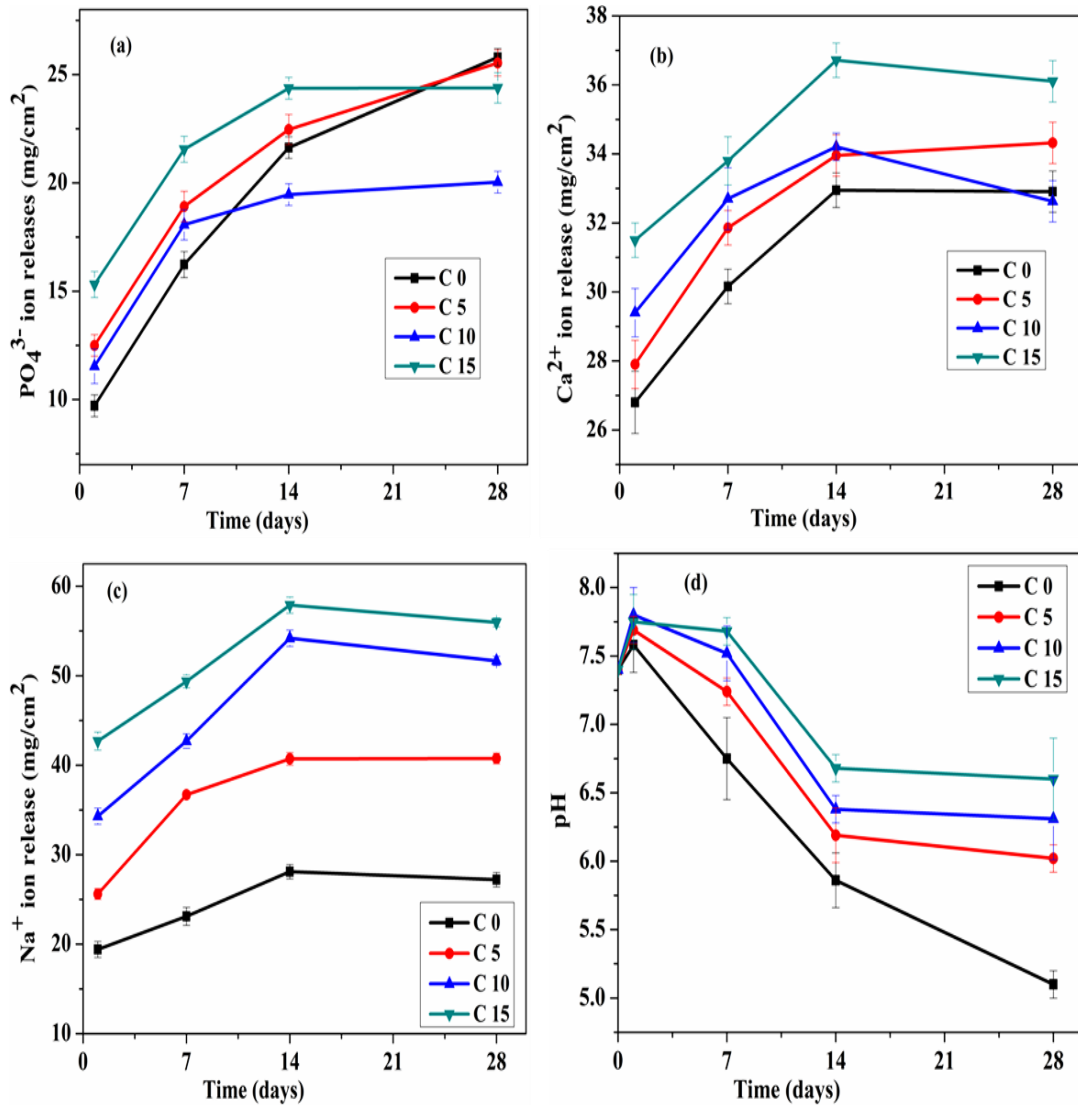


Figure 5.5: Ionic concentration of (a)  $PO_4^{3-}$ , (b)  $Ca^{2+}$ , (c)  $Na^+$  and (d) pH measurements in PBS solution



The variations in the release rate of anion and cations of PBS and HBS immersed glass samples are shown in Figures 5.5 and 5.6 respectively. The release rates of both anion ( $\text{PO}_4^{3-}$ ) and cation ( $\text{Na}^+$  &  $\text{Ca}^{2+}$ ) in to PBS have increased up to 7 days followed with negligible variations up to 28 days. The steady rate of  $\text{Ca}^{2+}$  and  $\text{Na}^+$  ions releases in to HBS were observed from 14<sup>th</sup> day onwards. The constant rate of ion release obtained for all the glasses in the final days of PBS and HBS immersion was ascribed to the accumulation of these released ions on the glass surfaces and also substantiated the calcium-phosphate (Ca-P) layer/HAp formation.

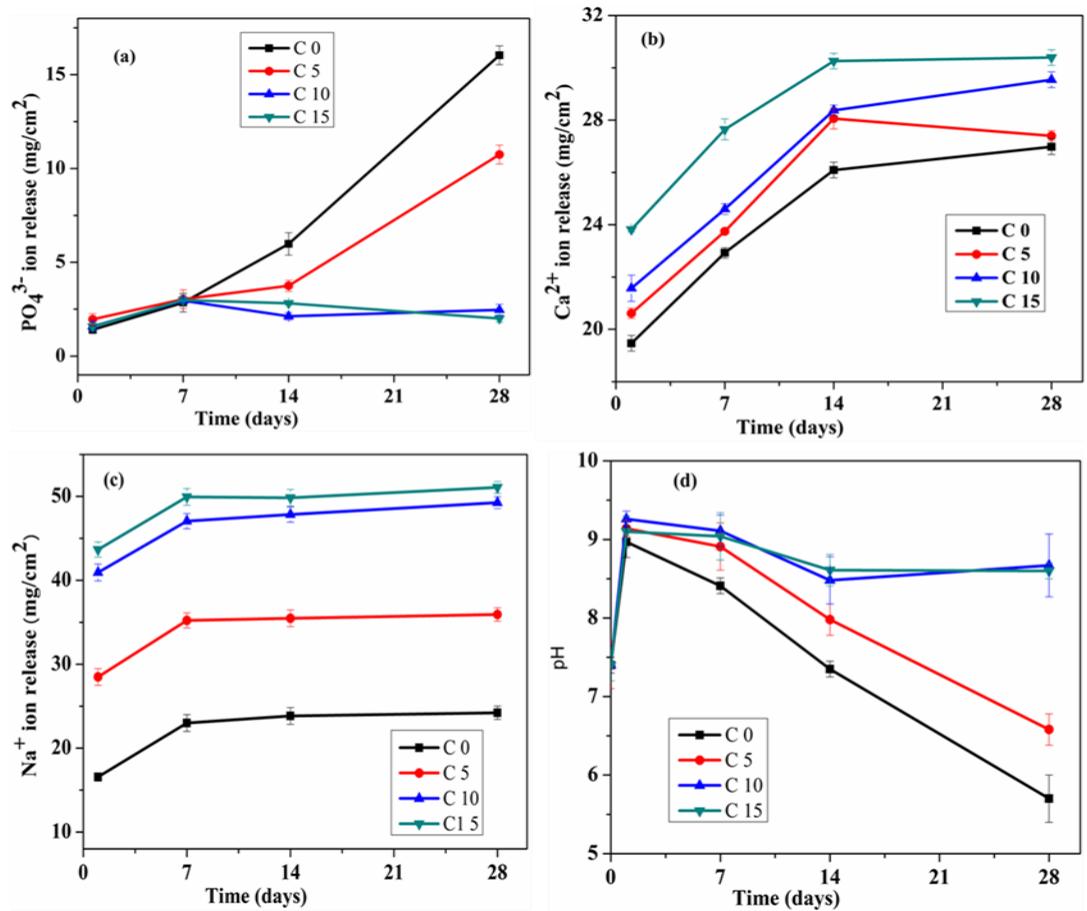


Figure 5.6: Ionic concentration of (a)  $\text{PO}_4^{3-}$ , (b)  $\text{Ca}^{2+}$ , (c)  $\text{Na}^+$  and (d) pH measurements in HBS solution

Comparing the Figures 5.1, 5.5 and 5.6, it can be seen that rate of cation release in to deionized water has decreased with increase in BaO content, whereas, it has increased in PBS and HBS solutions along with reduction in anion release. This can be attributed to higher ionic strength of PBS and HBS solutions than that of deionized water. Cations were usually released during the initial stages of dissolution which increased the ionic strength of solution and thus decreased the dissolution rate of glasses by preventing the release of phosphate anions due to electrostatic interactions in the hydrated layer (Burling 2006). The amount of release of  $\text{Na}^+$  was more than that of  $\text{Ca}^{2+}$  in both solutions, which was due to the higher mobility rate of monovalent  $\text{Na}^+$  ions rather than divalent  $\text{Ca}^{2+}$  with larger atomic size.

pH of both solutions has slightly increased on the first day for all the glasses due to the dissolution of more number of cations. As shown in Figure 5.5 (d), pH of PBS decreased up to 14<sup>th</sup> days due to increase in the anion release rate in comparison with cations in all the samples. It attained almost a steady state in BaO added samples from 14<sup>th</sup> days onwards which can be related to their constant ion release rate. As shown in Figure 5.6 (d), pH of HBS has decreased from 1<sup>st</sup> day onwards in samples containing below 10 mol % of BaO, whereas it remained almost same after 14 days of immersion for samples containing 10 and 15 mol % of BaO which can be correlated to anion release rate rather than cations. As the BaO content increases, pH of PBS solution reached nearly neutral level (~6.7) at the final days, whereas it became basic (~8.5) in case of HBS.

However, pH of both solutions has increased with BaO content due to the higher amount of cation release rather than anions. It is reported that acidic pH hinders the bioactivity and biocompatibility of glasses due to the cytotoxic effects and also it increases the dissolution rate of glasses (Uo et al. 1998). The lowest phosphate ( $\text{PO}_4^{3-}$ ) concentration in physiological solution can lead to the fastest HAp formation and higher exchange of cations initiates bone mineralization mechanism (Brauer et al. 2010). So it can be expected to achieve better bioactivity and biocompatibility properties along with the lower dissolution rate (or lower  $\text{PO}_4^{3-}$  ion release) and fastest HAp formations as can

be observed from increase in the cation release rates and pH variation with BaO addition in Na<sub>2</sub>O-CaO-P<sub>2</sub>O<sub>5</sub> glasses.

While comparing the PO<sub>4</sub><sup>3-</sup>, Na<sup>+</sup> and Ca<sup>2+</sup> ions release rate in to PBS and HBS solutions which is given in Figures 5.5 and 5.6 respectively, it can be seen that lesser amount of ions were released into HBS solution in comparison with PBS due to higher ionic strength of HBS solution which might prevent further ionic release by electrostatic interactions. Delahaye et al. (1998) have reported that dissolution rate decreases as the ionic strength of solution increases due to increase in electrostatic interactions occurring in the hydrated layer (Ahmed et al. 2004). Franks et al. (2000) have reported that higher ionic strength of solutions can slow down the dissolution process or decrease the dissolution rate by preventing the diffusion of ions from the glasses. Franks et al. (2000) have also reported that formation of surface layer during immersion hinders further diffusion and exchange of ions from the glasses. Comparison of constant ion release rate after 7 days in HBS and after 14 days in PBS solution gave the information that Ca-P layer formation was faster in HBS solution than in PBS. This was further confirmed by XRD data. Faster Ca-P layer formation hindered the further ion release and thus rate of ion release in to HBS was less than that of PBS solution (Franks et al. 2000).

XRD crystalline reflections obtained for C0 and C15 were same, whereas amorphous nature was observed in C5 and C10 even after the immersion in PBS for 28 days. The representative XRD spectra of C0 and C5 are given in Figure 5.7 and the crystalline phases are marked in the figure. The crystalline reflections corresponding to (211) plane of HAp (Ca<sub>10</sub>(PO<sub>4</sub>)<sub>6</sub>(OH)<sub>2</sub>) [JCPDS Card No. 01-072-1243] were observed at ~31.74° in C0 and C15 within 14 days of immersion in PBS. An extra broad hump (42-52°) has appeared in all PBS immersed samples due to an amorphous calcium-phosphate (ACP) layer formation (“Measurement of Crystallinity and Phase Composition of Hydroxyapatite by XRD - Hitpages” 2016), which became more prominent or intense due to the higher amount of formation of such layer as the days of immersion increased. R. L. and Alshathly (2014) suggested that the appearance of an amorphous halo in

between 32-40° in SBF immersed boro-phosphate glasses was due to the formation of amorphous HAp or poorly crystallized HAp or combination of both.

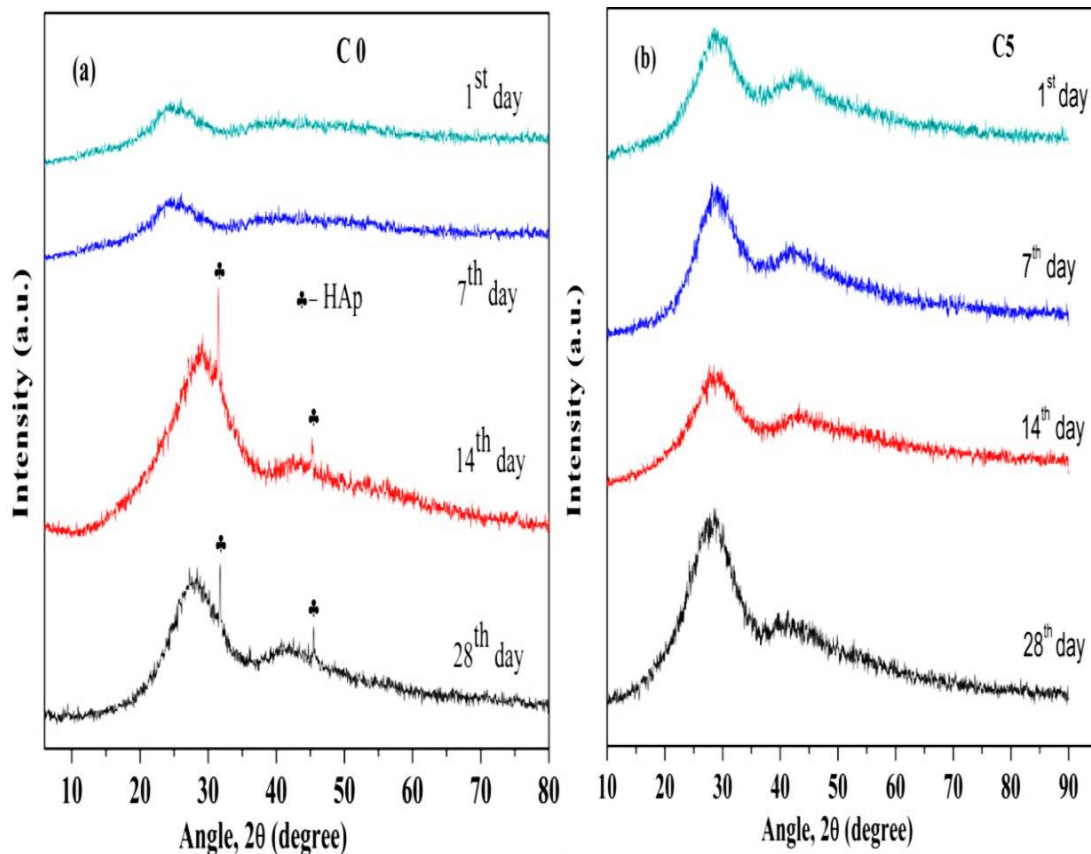


Figure 5.7: XRD pattern of (a) C0 and (b) C5 after immersion in PBS for 28 days

XRD pattern of HBS immersed C0 and C15 are only given in Figure 5.8 for comparing the BaO-free and BaO added glasses. The crystalline bioactive phases such as hydroxyapatite (HAp) and  $\text{Ca}_2\text{P}_2\text{O}_7$  were formed in all the samples after the immersion in HBS solution for 7 days. The sharp HAp reflections at  $\sim 31.93^\circ$  corresponding to (211) planes was observed in all glass samples except in C5 where (300) plane of HAp was observed [JCPDS Card No. 01-072-1243]. The reflections present at  $\sim 45.65^\circ$  was

attributed to the (232) plane of  $\text{Ca}_2\text{P}_2\text{O}_7$  [JCPDS Card No. 00-033-0297]. In additions to this, less intense HAp reflections were also observed in all samples at an angle of  $56.56^\circ$ ,  $65.51^\circ$ ,  $75.52^\circ$  and  $84.34^\circ$  (JCPDS Card No's 01-074-0565, 01-089-6437 and 01-074-0566).

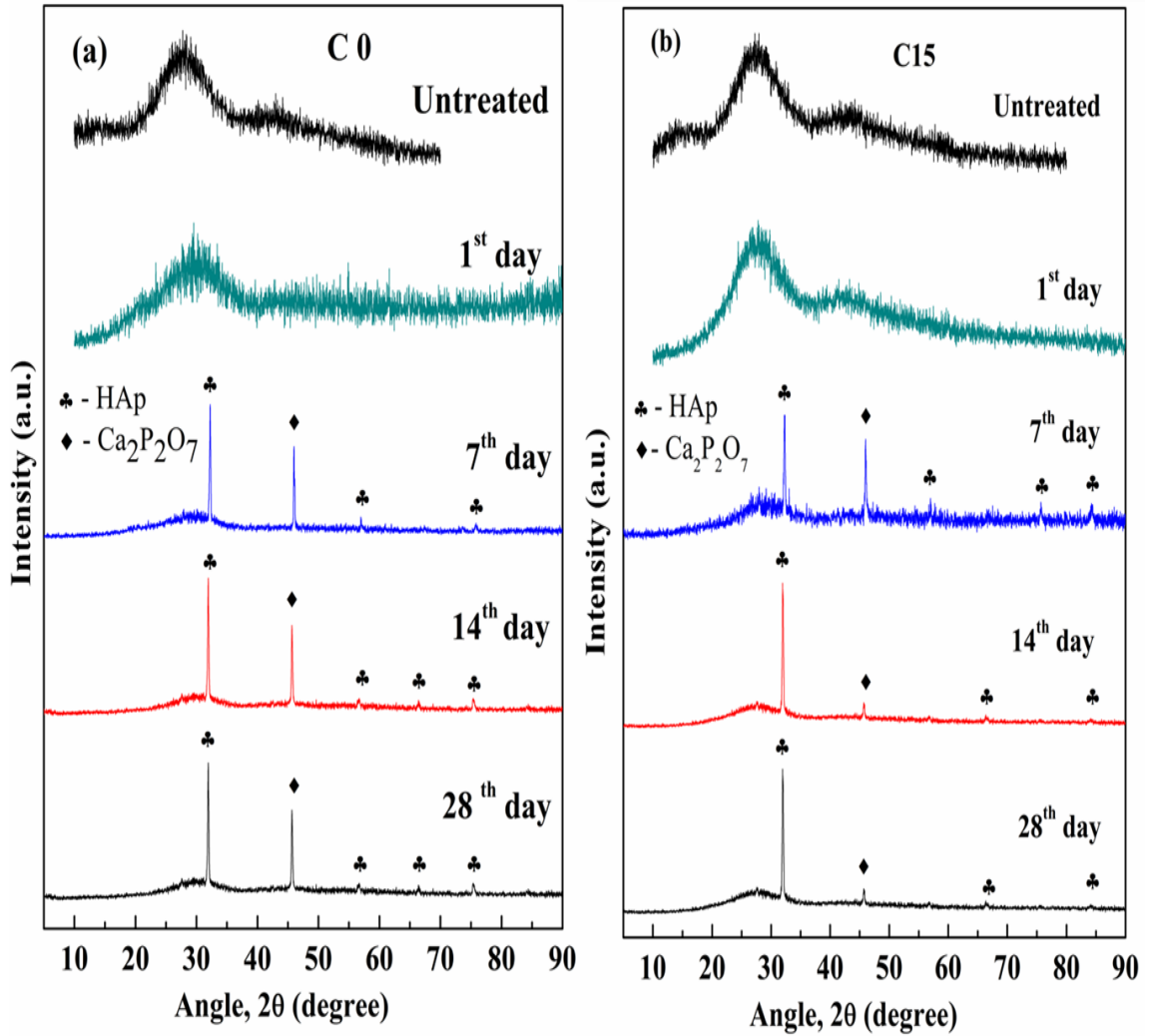


Figure 5.8: XRD pattern of (a) C0 and (b) C15 after immersion in HBS for 28 days

The shift in the position of amorphous hump was not observed in PBS and HBS immersed samples after the 1<sup>st</sup> day of immersion, whereas it was observed in case of

deionized water indicates the lower dissolution rates of glasses in PBS and HBS solutions due to their higher ionic strength in comparison with deionized water.

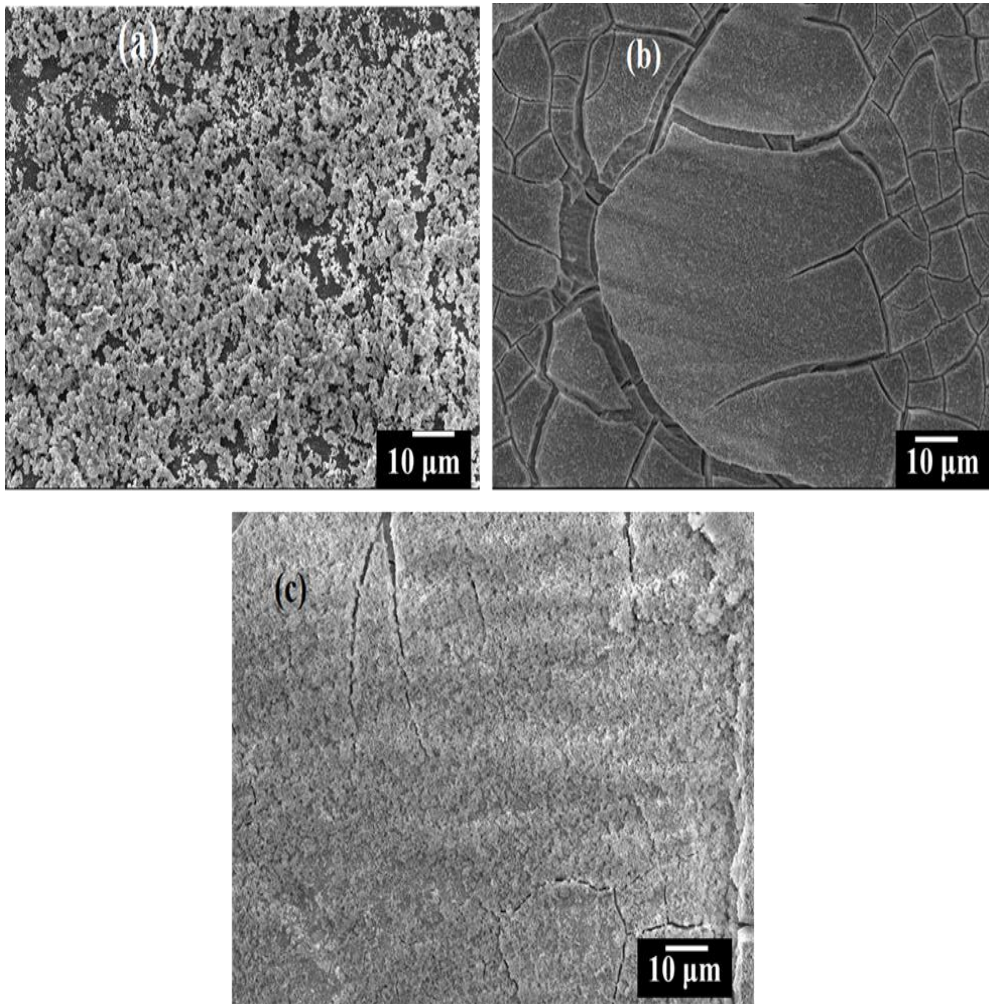


Figure 5.9: SEM images of (a) C0, (b) C10 and (c) C15 after immersion in PBS for 28 days

White layer formation was observed in the micrographs of all PBS immersed samples and some representative images are shown in Figure 5.9. Less dense white precipitate was observed on C5 and C10 in comparison with other samples, which

substantiated absence of sharp XRD reflections and thus amorphous calcium-phosphate (ACP) formation on these samples.

White layer formation was observed in the micrographs of all HBS immersed samples and some representative images are shown in Figure 5.10, which supported the additional HAp reflections appearing in XRD spectra. As the BaO content increases, the formed layer became denser and it contained almost spherical shaped particles as shown in Figure 5.10 (c). It is worth to note that Barium substituted phosphate glasses can be bioactive.

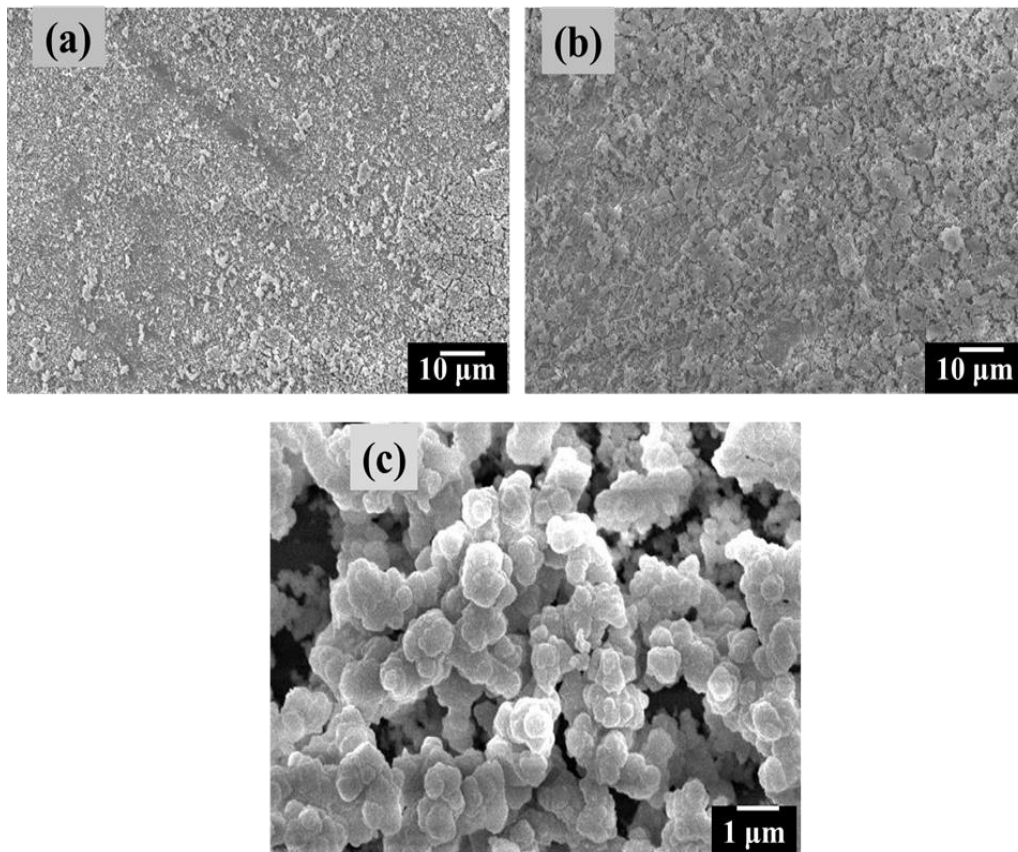


Figure 5.10: SEM images of (a) C0, (b) C15 and (c) grain structure of layer formed on C15 after the immersion in HBS for 28 days

Ca/P molar ratio was calculated from the elemental compositions of glasses and the data obtained from EDS spectra of PBS and HBS immersed samples is given in Table 5.4. Presence of Sodium and Barium obtained in the EDS indicates the incorporation of such ions into the formed Ca-P layer on both PBS and HBS immersed samples. (Ca+Na+Ba)/P ratio was varied between 0.65-0.75 and 0.71-0.99 in case of PBS and HBS immersed samples respectively. These ratios were matching with the Ca-P phases such as  $\text{Ca}_4\text{H}_2\text{P}_6\text{O}_{20}$  (Tetra calcium dihydrogen phosphate, Ca/P=0.67),  $\text{Ca}_7(\text{P}_5\text{O}_{16})_2$  (Hepta calcium phosphate, Ca/P=0.7),  $\text{Ca}_2\text{P}_2\text{O}_7$  (Calcium pyrophosphate,  $\text{Ca}_2\text{P}_2\text{O}_7$ , Ca/P=1) and  $\text{CaHPO}_4 \cdot 2\text{H}_2\text{O}$  (Dicalcium phosphate dehydrate or brushite, Ca/P =1) rather than HAp (Ca/P=1.67) (Laeny 2008). However these are the initial phases of HAp formation.

Table 5.4: Mass% of elements on glass samples after immersion in PBS and HBS solutions for 28 days

Composition	PBS				HBS			
	C0	C5	C10	C15	C0	C5	C10	C15
Oxygen (O)	61.53	52.16	54.12	53.37	52.16	48.73	47.92	45.34
Phosphorous (P)	20.35	28.07	19.18	19.75	28.07	25.61	22.09	20.23
Calcium (Ca)	12.54	12.73	9.88	7.20	12.73	10.84	9.58	15.21
Sodium (Na)	3.62	6.83	2.27	3.58	6.83	6.01	4.65	3.74
Barium (Ba)	-	8.02	15.62	16.09	-	8.07	11.63	14.07
Ca/P	0.48	0.35	0.40	0.28	0.35	0.33	0.34	0.58
(Ca+Na)/P	0.72	0.68	0.56	0.53	0.68	0.64	0.62	0.83
(Ca+Na+Ba)/P	-	0.65	0.74	0.71	-	0.71	0.74	0.99



The rate of increase of Calcium content on the surface of BaO added glasses was higher than that of BaO-free samples (C0) after PBS immersion, which supports formation of more quantity of Ca-P layer on the surface of BaO added samples. No such remarkable decrease in the quantity of Calcium was observed on the surface of HBS immersed glasses containing up to 10 mol % of BaO even after the release of  $\text{Ca}^{2+}$  ions indicating the reaccumulation of these ions and Ca-P layer formation on glass surfaces. The relevant variations in Ca/P molar ratio between end members of composition (C0 and C15) indicate the enhanced formation of Ca-P layer on HBS immersed samples with the addition of 15 mol % of BaO. The noticeable decrease in the mass % of P might be one of the reasons to increase Ca/P ratio. Thus EDS data supported the formation of Ca-P layer on the surface of  $\text{Na}_2\text{O-CaO-P}_2\text{O}_5$  glasses with additions of BaO in both PBS and HBS solutions and amorphous Ca-P getting converted in to crystalline HAp on prolonged duration of immersion by consuming  $\text{Ca}^{2+}$  and  $\text{PO}_4^{3-}$  ions from solutions.

FTIR spectra of PBS immersed glass samples are given in Figure 5.11 (a) and Table 5.5.  $\text{PO}_4^{3-}$  modes of HAp and non-apatite  $\text{HPO}_4^{2-}$  vibrations have appeared ~ at  $1016\text{-}1018\text{ cm}^{-1}$  and  $531\text{-}534\text{ cm}^{-1}$  respectively after PBS immersion. R. L. and Alshathly (2014) have reported a band at  $525\text{ cm}^{-1}$  in SBF immersed boro-phosphate glasses, which corresponds to the extremely small size HAp crystallites. So, amorphous calcium-phosphate or poorly crystallized HAp or HAp crystallites of extremely small size or combination of all these were present in all PBS immersed glass samples according to XRD and FTIR spectra. Presence of doublet was observed in C0 and C15 at  $3438$  and  $3472\text{ cm}^{-1}$  due to the vibrations of loosely bound water in brushite ( $\text{CaHPO}_4 \cdot 2\text{H}_2\text{O}$ ) (Suguna and Sekar 2011).

FTIR spectra of HBS immersed samples are given in Figure 5.11 (b) and Table 5.5. The various bands associated with HAp and  $\text{Ca}_2\text{P}_2\text{O}_7$  phases have appeared in the range of  $432\text{-}496\text{ cm}^{-1}$  after HBS immersion. Bands present at  $1628\text{-}1636\text{ cm}^{-1}$  was either attributed to the vibrations of surface adsorbed  $\text{H}_2\text{O}$  of HAp lattice (Jha et al. 2015) or C-O bending vibration of  $\text{CO}_3^{2-}$  (Rajkumar et al. 2012). Presence of broad O—H bands at

3650-3700  $\text{cm}^{-1}$  in all the samples might be due to the reduction of O-H groups and substitution of  $\text{CO}_3^{2-}$  in the HAp lattice (A-type substitution) (Müller and Müller 2006).

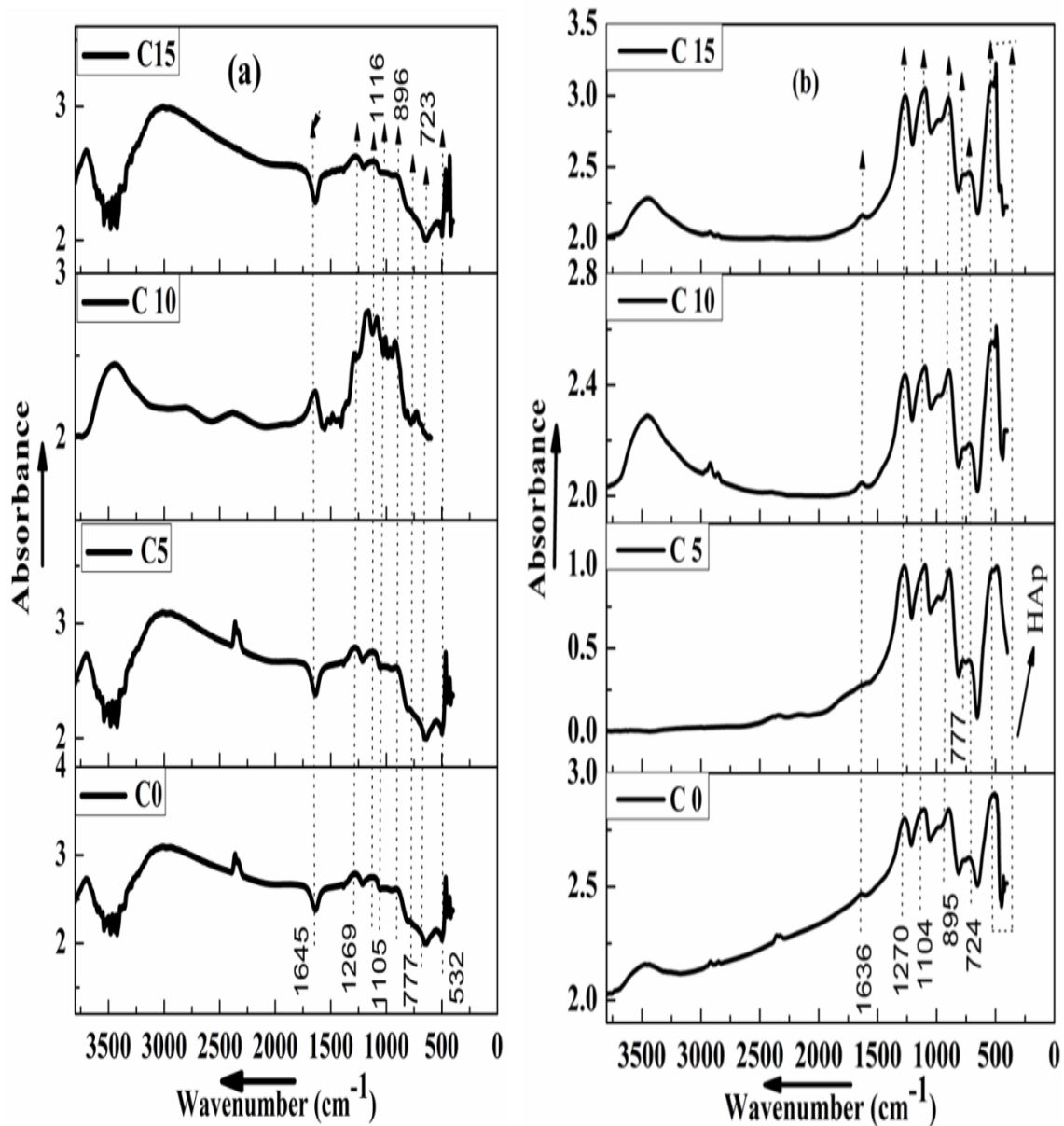


Figure 5.11: FTIR spectra of  $\text{Na}_2\text{O-BaO-CaO-P}_2\text{O}_5$  glasses after immersion in (a) PBS and (b) HBS solutions for 28 days

Table 5.5: Assigned vibrational bands in FTIR spectra of Na<sub>2</sub>O-BaO-CaO-P<sub>2</sub>O<sub>5</sub> glasses after the immersion in PBS and HBS solutions for 28 days

Characteristic vibrational modes (in cm <sup>-1</sup> )	PBS				HBS			
	C0	C5	C10	C15	C0	C5	C10	C15
Surface adsorbed H <sub>2</sub> O/ bending mode of HCO <sub>3</sub> <sup>2-</sup>	-	-	-	-	1636	-	1631	1628
$\nu_{as}PO_2 (Q^2)$	1269	1269	1267	1265	1270	1269	1266	1264
$\nu_{as}PO_3 (Q^1)$	1105	1100	1097	1097	1104	1101	1097	1097
$\nu PO_4^{3-}$ mode of HAp (Raouf et al. 2015)	1016	1017	1018	1018	-	-	-	-
$\nu_s PO_3(Q^1)/P-O-Na$	-	-	-	-	-	984	980	-
$\nu_{as}POP (Q^2)$	896	896	896	895	895	897	895	897
$\nu_s POP (Q^1)$	777	778	779	779	-	777	768	769
$\nu_s POP (Q^1-Q^2)$	723	726	725	724	724	732	722	723
$\nu_4 PO_4^{3-}$ mode of HAp (Radev et al. 2009)	-	-	-	-	520, 505	507	512	523
Non-apatite HPO <sub>4</sub> <sup>2-</sup> (Spevak et al. 2013)	532	531	532	534	-	-	-	-
Symmetric bending mode of $\beta$ -Ca <sub>2</sub> P <sub>2</sub> O <sub>7</sub> (Rajkumar et al. 2012)	-	-	-	-	493	-	493	496
$\delta PO_2$	-	-	-	-	487	487	-	-
PO <sub>4</sub> <sup>3-</sup> group of HAp/ $\delta(PO_2)$ of PO <sub>4</sub> <sup>3-</sup> (Spevak et al. 2013)	-	-	-	-	456	455, 473	446	452, 465
Calcium deficient HAp/crystalline $\delta PO_4^{3-}$ (Al- Noaman et al. 2012)	-	-	-	-	432	432	-	433

The slight increase in the intensity of O-H vibrational modes (3400- 3600  $\text{cm}^{-1}$ ) and also sharpening of phosphate bands (700-1300  $\text{cm}^{-1}$ ) with BaO content might be due to the decrease in the HAp lattice disorder caused by the substitution of  $\text{PO}_4^{3-}$  and  $\text{HPO}_4^{2-}$  (Ahmad et al. 2017). Sheha (2007) has reported that replacement of  $\text{Ca}^{2+}$  in the HAp crystal lattice with  $\text{Ba}^{2+}$  ions increased the intensity of O-H bands due to the different electronegativity and polarizing power of both ions. Asymmetric stretching vibration of  $\text{PO}_2$  and  $\text{PO}_3$  groups was red shifted from 1270 to 1264 and 1105 to 1097  $\text{cm}^{-1}$  as well as symmetric  $\text{PO}_3$  and POP groups were red shifted from 985 to 977 and 777 to 769  $\text{cm}^{-1}$  respectively as BaO content increases from 5 mol % to 15 mol %. This observed red shift to the low wavenumber side might be due to the replacement of  $\text{Ca}^{2+}$  ions in HAp crystal lattice with  $\text{Ba}^{2+}$  ions (R. L. and Alshathly 2014).

The various stretching modes of phosphate groups present in between 1265-977  $\text{cm}^{-1}$  have become more intense after the HBS treatments and their intensity has also increased with BaO content. O'Donnell et al. (2009) have reported that HAp formation increased the intensity of phosphate (P—O) stretching mode. It can be concluded from FTIR spectra of HBS immersed samples that bioactivity of  $\text{Na}_2\text{O-CaO-P}_2\text{O}_5$  glasses has improved with BaO addition and some amount of  $\text{Ba}^{2+}$  ions was incorporated into HAp crystal lattice. Vibrational bands present in between 1265-777  $\text{cm}^{-1}$  can be attributed to the different phosphate groups which were more intense in PBS immersed samples in comparison with HBS immersed ones. This was due to the accumulation of phosphate ions on PBS immersed samples being more due to the presence of higher concentration of  $\text{PO}_4^{3-}$  ions in PBS.

Formation of HAp was confirmed by XRD and FTIR, whereas the observed molar ratios from EDS were not consistent with it. The freshly formed layer accumulated on the top surface of glasses in the final days of immersion needed still more time to nucleate. The layer which was formed during the initial days of immersion accumulated beneath these fresh layers, which can be analyzed well with FTIR and XRD having larger penetration depth ( $>10\mu\text{m}$ ) rather than EDS with small penetration depth ( $\sim 1-2\mu\text{m}$ ).

Moreover, Ca/P ratio obtained from EDS was not representative for the formed layer composition and if the thickness of layer was less, the signal coming from several microns below the surface could be influenced substantially by the composition of original glasses.

## 5.2 SUMMARY

Effect of BaO addition on the dissolution and *in vitro* bioactivity properties of Na<sub>2</sub>O-CaO-P<sub>2</sub>O<sub>5</sub> glasses was studied for 28 days under static dissolution conditions. Dissolution rate of glasses in deionized water increased with time, whereas it decreased by three orders of magnitude with BaO content. All the glass samples retained their amorphous nature even after 28 days of immersion in deionized water and they have dissolved selectively or incongruently. Depolymerization of glass network and appearance of new orthophosphate (Q<sup>0</sup>) groups after immersion in deionized water was confirmed by FTIR. Bioactive nature of all PBS and HBS immersed glass samples were confirmed by ion release, XRD, SEM/EDS and FTIR analysis. The steady rate of Ca<sup>2+</sup> and PO<sub>4</sub><sup>3-</sup> ions release in to PBS and HBS solutions in the final days of immersion, increase in Calcium content on the surface of glass samples observed from EDS and white layer formation shown in the micrographs supported the accumulation of these ions and calcium-phosphate layer formation on the surface of all glasses. Not much influence of BaO addition was found on the bioactivity of Na<sub>2</sub>O-CaO-P<sub>2</sub>O<sub>5</sub> glasses in PBS, in which amorphous calcium-phosphate (ACP) and/or poorly crystallized HAp with extremely small size crystals was formed in glasses containing 5 and 10 mol % of BaO, whereas crystalline HAp was formed with the addition of 15 mol % of BaO. Bioactivity of glasses in HBS solution has improved by the formation of crystalline HAp with BaO content. Based on ion release rate and XRD studies, faster HAp formation was found to take place in HBS solution when compared to PBS. The higher cation release rate and lower phosphate dissolution observed in HBS solution with BaO content supported the enhancement of bioactive nature and lowest dissolution rate of glasses respectively. The

increase in pH of both PBS and HBS solutions with increase in BaO content might improve the biocompatibility by reducing the cytotoxicity of glasses.

## Chapter 6

### **ELECTROCHEMICAL CORROSION AND *IN VITRO* BIOACTIVITY PROPERTIES OF BaO CONTAINING Na<sub>2</sub>O-CaO-P<sub>2</sub>O<sub>5</sub> PHOSPHATE GLASS-CERAMIC COATING ON 316 L, DUPLEX STAINLESS STEEL 2205 AND Ti6Al4V**

*Phosphate glass with composition 11Na<sub>2</sub>O-15BaO-29CaO-45P<sub>2</sub>O<sub>5</sub> was coated on biomedical implant materials such as stainless steel 316 L, duplex stainless steel (DSS) 2205 and Ti6Al4V alloy by thermal enamelling method. The structural and compositional properties of glass coated substrates were studied by X-ray diffraction (XRD), Scanning electron microscopy (SEM) and Energy dispersive X-ray spectroscopy (EDS) analysis. The coatings were partially crystalline in nature with porous structure and pore size varied from micro to nanometer ranges. Electrochemical corrosion and in vitro bioactivity tests of coated and uncoated samples were carried out in Hank's balanced salt (HBS) solution at 37°C. Polarization resistance ( $R_p$ ) was derived from potentiodynamic polarization curves and it has increased for 316 L substrate, whereas it has decreased for DSS 2205 and Ti6Al4V after coating. The formation of crystalline hydroxyapatite (HAp) layer on the surface of all coated samples was observed after electrochemical corrosion test, which improved the corrosion resistance. The observed electrochemical corrosion behavior can be explained based on protective HAp layer formation, composition and diffusion of ions of glass coated surfaces. pH and ion release rate measurements obtained from in vitro bioactivity test of coated samples substantiate their electrochemical corrosion resistance ( $R_p$ ). The lower rate of Na<sup>+</sup> and Ca<sup>2+</sup> release from coated 316 L supports its higher electrochemical corrosion resistance among other coated samples. DSS is having higher electrochemical corrosion resistance among other uncoated samples. Formation of amorphous calcium-phosphate (ACP) layer on the surface of all coated samples after in-vitro bioactivity test was confirmed by XRD, SEM/EDS and ion release measurements. It was a comparative study of corrosion*

*resistance and bioactivity of glass coated and uncoated biomedical implants such as 316 L, DSS 2205 and Ti6Al4V.*

## **6.1 RESULTS AND DISCUSSION**

Synthesized glass with composition  $11\text{Na}_2\text{O}-15\text{BaO}-29\text{CaO}-45\text{P}_2\text{O}_5$  is having better mechanical (lower brittleness), thermal (higher thermal stability), dissolution and in-vitro bioactivity properties in comparison with other compositions. So, it was selected for coating on three different metallic implant materials such as 316 L, duplex stainless steel (DSS) 2205 and Ti6Al4V using thermal enamelling technique and the following characterizations have been carried out on coated samples.

### **6.1.1 Structural and compositional studies of coatings**

X-ray diffraction (XRD) analysis has been carried out on coated and uncoated substrates and these patterns are given in Figure 6.1. The crystalline phases obtained in all the coatings were  $\text{NaPO}_3$  (JCPDS card No. 00-011-0650),  $\text{Ba}(\text{PO}_3)_2$  (01-070-1214),  $\text{Ca}(\text{PO}_3)_2$  (00-009-0363),  $\text{CaP}_2\text{O}_7$  (00-009-0346) and NaBaP (01-085-0214) as marked in the respective XRD spectra. Absence of various crystalline reflections of substrate in the spectra of coated samples indicated the uniform distribution of coating on the surface of substrates. Presence of broad hump at  $20-30^\circ$  and appearance of new crystalline reflections in the coated samples indicated the partially amorphous/crystalline nature of coatings.

Some representative micrographs of coated Ti6Al4V are given in Figure 6.2 (a) and (b) and all the coatings were uniformly distributed on the surface of substrates as substantiated by XRD. All the coatings have porous morphology with varying pore diameter of micro to nanometer ranges and these pores were distributed non-uniformly.



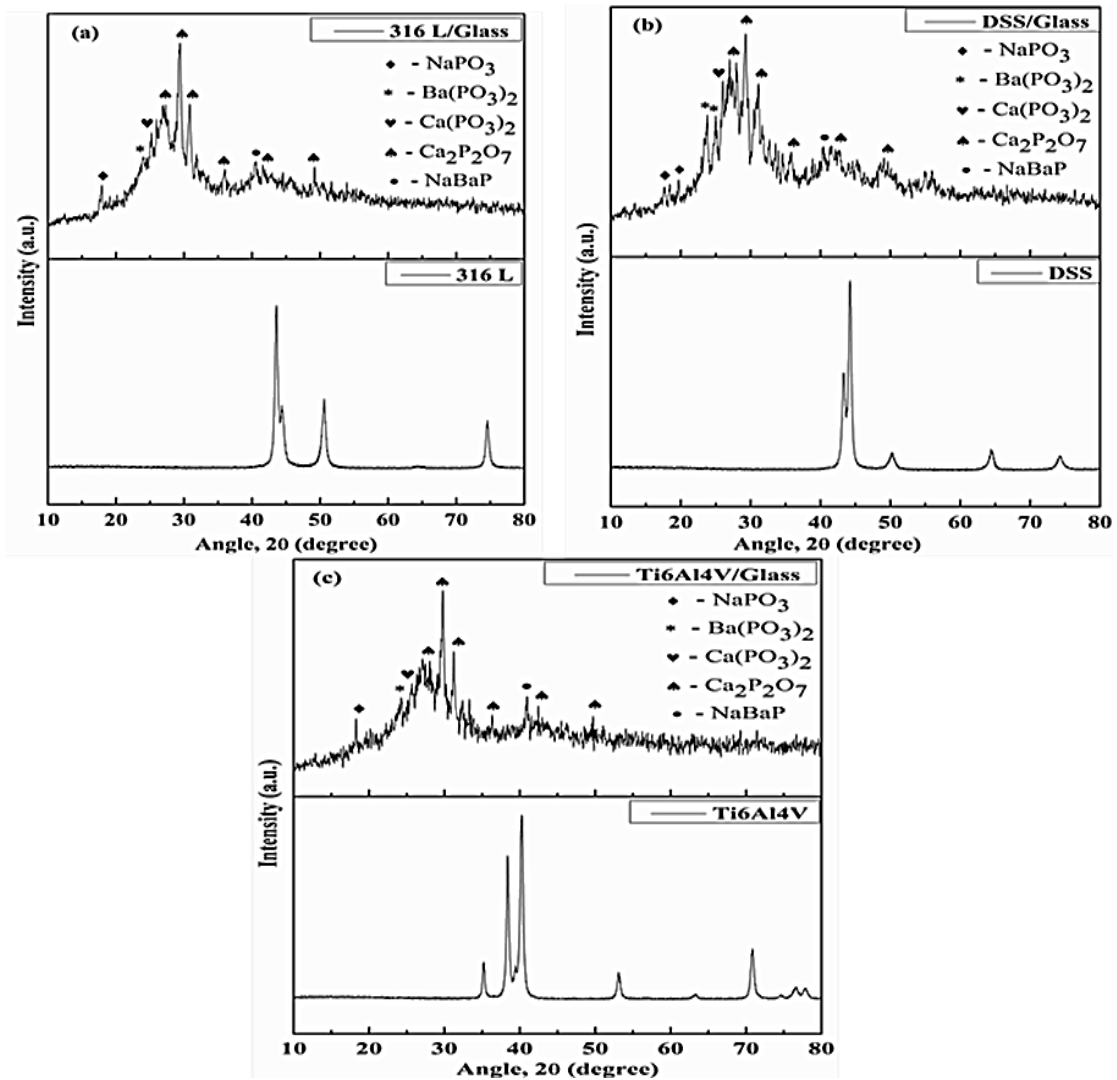


Figure 6.1: XRD spectra of glass coated and uncoated (a) 316 L, (b) DSS 2205 and (c) Ti6Al4V

There were no cracks observed on the surface of the coatings. Absence of cracks or delamination of coating from substrates can be observed from the cross sectional view of coated Ti6Al4V as shown in Figure 6.2 (c), which indicated the proper adherence of coating on to substrates without any discontinuity in between them. The measured thickness of coatings was ~158, ~179 and ~230  $\mu\text{m}$  for coated 316 L, DSS and Ti6Al4V

samples respectively. The lower thickness was observed for coated 316 L and higher for coated Ti6Al4V for the same duration of synthesizing conditions.

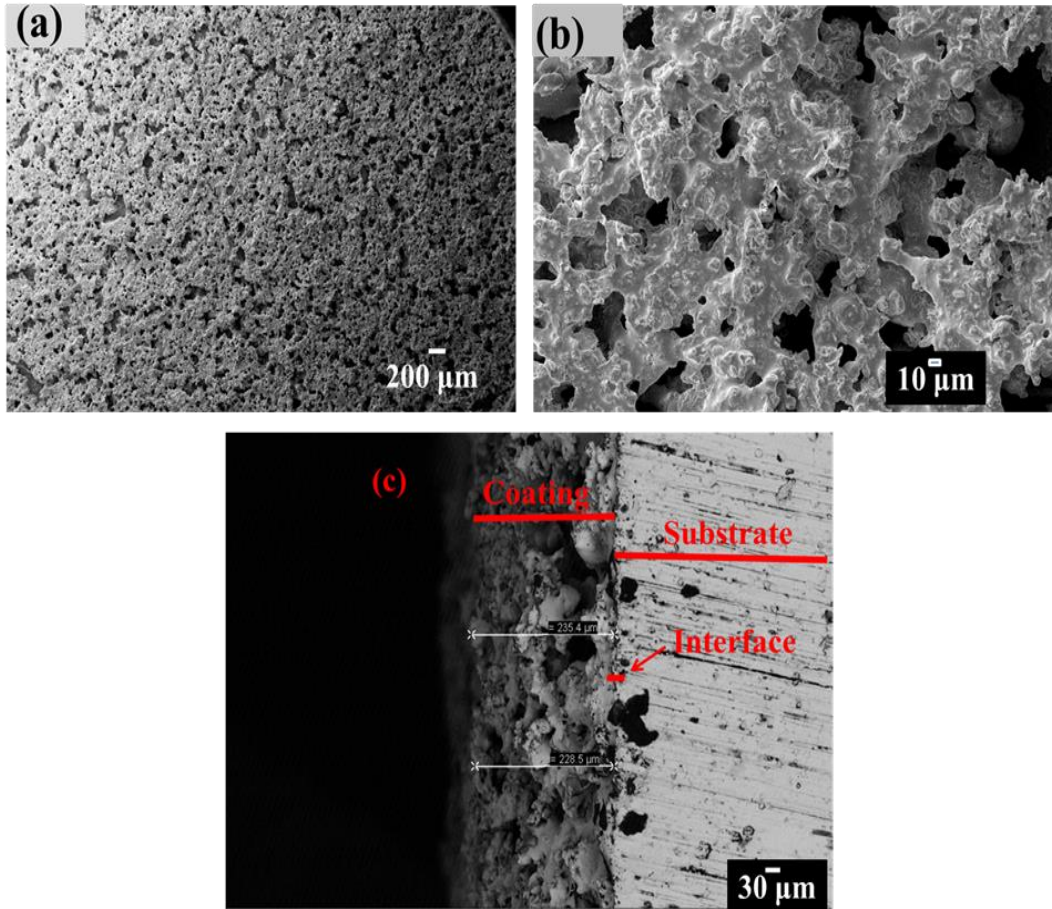


Figure 6.2: SEM images of glass coated Ti6Al4V (a) & (b) at different magnifications and (c) cross-sectional view of coating

The elemental composition of the glass and coated substrates at the top surface, interface and substrate as indicated by EDS are given in Table 6.1. Interface was referred to as region ~ 20-30 μm between coating and substrate as marked in Figure 6.2 (c). The concentration of Phosphorous, Barium, Sodium and Calcium slightly decreased from surface to interface of coatings as observed from EDS analysis carried out on the cross-

sectional images of coated samples which indicated the diffusion of these elements from coating to substrate. Variation in the diffusion was the reason for obtaining the different thickness for coatings which were prepared under similar experimental conditions. The diffusion may increase or decrease the coating thickness, which again depends on imperfections in the coating and porosity. Better adherence of coating due to the formation of chemical bonds near the interface area by the diffusion of elements may reduce the coating thickness (Azeem et al. 2016). Since the chemical bonding formed by diffusion may offer better adherence of coating material to substrate, it can reduce the peeling of glass coating from substrate during corrosion (Toma et al. 2013).

Table 6.1: Mass % of elements present on coated substrates and glass. Column I, II and III indicate top surface, interface (~ 20-30  $\mu\text{m}$  between coating & substrate) and substrate respectively

Sample code	316L/Glass			DSS/Glass			Ti6Al4V/Glass			Glass
	I	II	III	I	II	III	I	II	III	
Oxygen (O)	47.0	37.2	21.0	45.9	40.0	7.2	46.9	31.3	11.8	39.5
Phosphorous (P)	28.3	15.8	14.4	31.4	23.2	1.8	24.9	14.7	13.7	27.8
Calcium (Ca)	15.9	6.4	6.1	9.5	6.6	-	15.1	13.3	7.5	12.3
Sodium (Na)	4.4	2.4	1.7	4.6	1.8	-	3.5	1.2	1.0	6.1
Barium (Ba)	22.9	12.1	11.3	22.8	19.3	-	18.8	16.5	14.6	19.7

### 6.1.2 Electrochemical corrosion studies

Potentiodynamic polarization curves of uncoated and coated substrates are presented in Figure 6.3 and the values derived from it are given in Table 6.2. Polarization resistance ( $R_p$ ) was calculated from  $I_{COR}$ ,  $\beta_A$  and  $\beta_c$  values which are given in Table 6.2 using equation 2.30.  $R_p$  of uncoated and coated samples have increased in the order of 316 L < Ti6Al4V < DSS and DSS/Glass < Ti6Al4V/Glass < 316 L/Glass respectively.  $R_p$  of 316 L substrate has increased after coating, whereas it has decreased in case of DSS and Ti6Al4V.

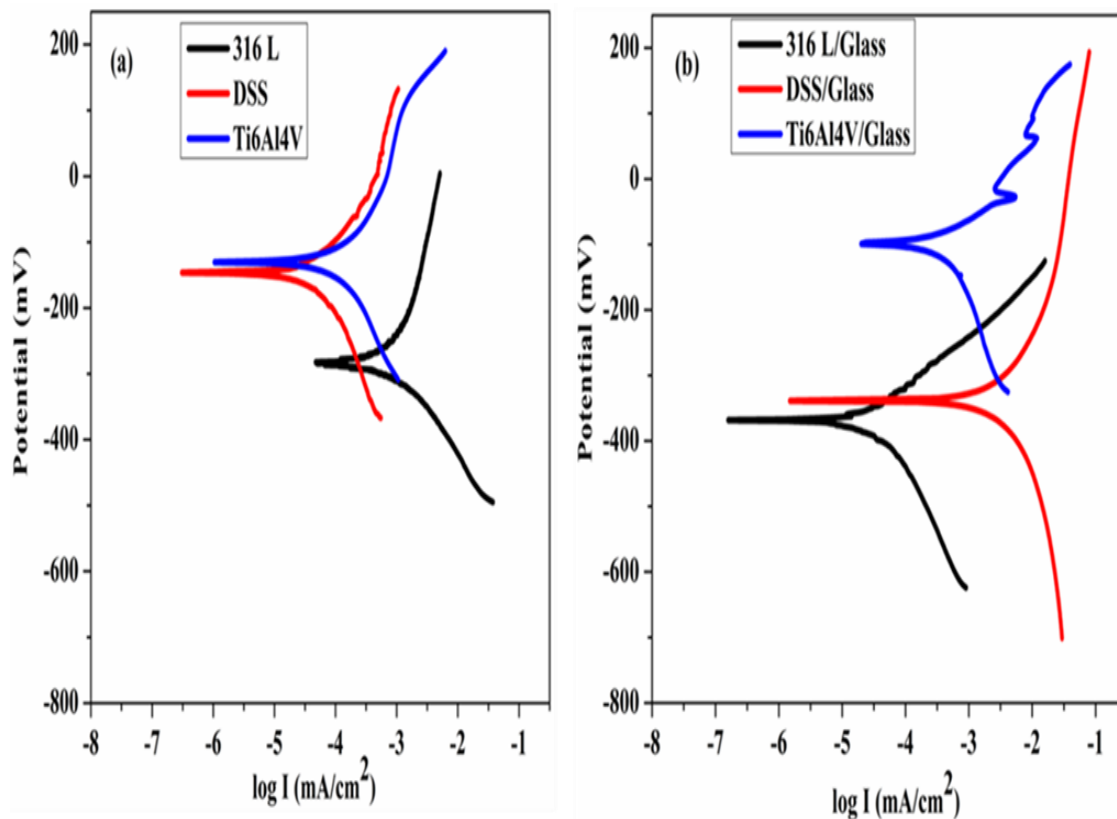


Figure 6.3: Polarization curves of (a) uncoated and (b) glass coated substrates

Table 6.2: Corrosion current ( $I_{COR}$ ), corrosion potential ( $E_{COR}$ ), anodic ( $\beta_A$ ) & cathodic ( $\beta_C$ ) Tafel slopes and polarization resistance ( $R_p$ ) derived from the polarization curve

Sample code	$I_{COR}$ mA/cm <sup>2</sup> ( $\times 10^{-3}$ )	$E_{COR}$ mV	$\beta_A$ mV	$\beta_C$ mV	$R_p$ $\Omega\text{cm}^2$ ( $\times 10^4$ )
316 L	$0.65 \pm 0.16$	$-283 \pm 19$	$204 \pm 19$	$96 \pm 12$	4.39
316 L/Glass	$0.03 \pm 0.01$	$-368 \pm 21$	$76 \pm 9$	$103 \pm 15$	66.4
DSS	$0.04 \pm 0.01$	$-144 \pm 16$	$118 \pm 15$	$158 \pm 16$	71.9
DSS/Glass	$5.58 \pm 1.80$	$-341 \pm 20$	$304 \pm 19$	$386 \pm 20$	1.32
Ti6Al4V	$0.08 \pm 0.02$	$-130 \pm 13$	$104 \pm 14$	$125 \pm 14$	30.2
Ti6Al4V/Glass	$0.45 \pm 0.14$	$-98 \pm 11$	$77 \pm 9$	$233 \pm 18$	5.60

When comparing the electrochemical corrosion resistance ( $R_p$ ) of coated substrates, the difference in their corrosion resistance can depend on various factors such as microstructure, composition and porosity of coatings (Chen et al. 2017).

The bioactive crystalline phases such as  $\text{Ca}_2\text{P}_2\text{O}_7$  and  $\text{Ca}(\text{PO}_3)_2$  present in all coated samples can support their bioactivity due to the biodegradation of such phases into HAp (Putlyaev and Safronova 2006). Formation of HAp on the surface of coating can favorably affect their corrosion resistance (Huang et al. 2013). The crystalline structure of coating is more suitable for improving their corrosion resistance rather than amorphous structure due to the closely packed atomic structure of crystals (Chen et al. 2004). Glasses

are bioactive than ceramics due their higher dissolution rate in solutions (Hench and Jones 2015), whereas it is having poor mechanical strength in comparison with ceramics (Kaur 2017). Embedding of crystalline phases in the glassy phase of coating (glass-ceramic) provides the unusual combination of properties of both glasses and ceramics. It was reported that higher crystallinity leads to lower dissolution (Islam et al. 2017) and crystals inhibit the precipitation or adhesion of Ca-P layer on the surface (Massera et al. 2015).

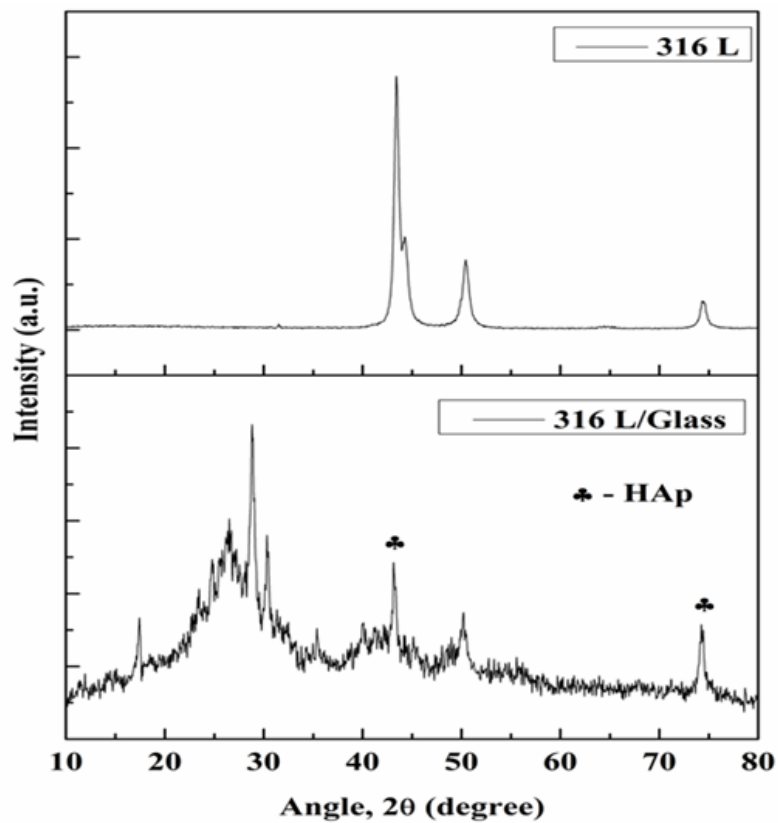


Figure 6.4: XRD image of coated and uncoated 316 L after the electrochemical corrosion studies

XRD patterns of corroded coated and uncoated 316 L substrate are given in Figure 6.4 as a representative image. Some extra crystalline reflections have appeared after electrochemical corrosion test on the surface of all coated substrates, which

correspond to hydroxyapatite (HAp) phase,  $\text{Ca}_5(\text{PO}_4)_3\text{OH}$  [JCPDS Card No. 01-073-1731 and 01-072-1243]. Pores on the coating can be filled by HAp layer which prevented the reaching of solution to substrate surface and thereby increased the corrosion resistance (Wang and Wen 2014). Intense HAp reflection was observed on the coated 316 L after corrosion test among other coated substrates indicating the formation of slightly higher quantity of HAp layer on their surface and thus higher corrosion resistance.

The surface morphology of the corroded coated substrates was studied by SEM and a representative image for coated Ti6Al4V is given in Figure 6.5 (a). The needle shaped particles appeared on coated DSS and Ti6Al4V after the electrochemical corrosion studies and their magnified images are given in Figure 6.5 (b). These needle shaped particles mainly constituted Calcium and Phosphorous according to EDS data.

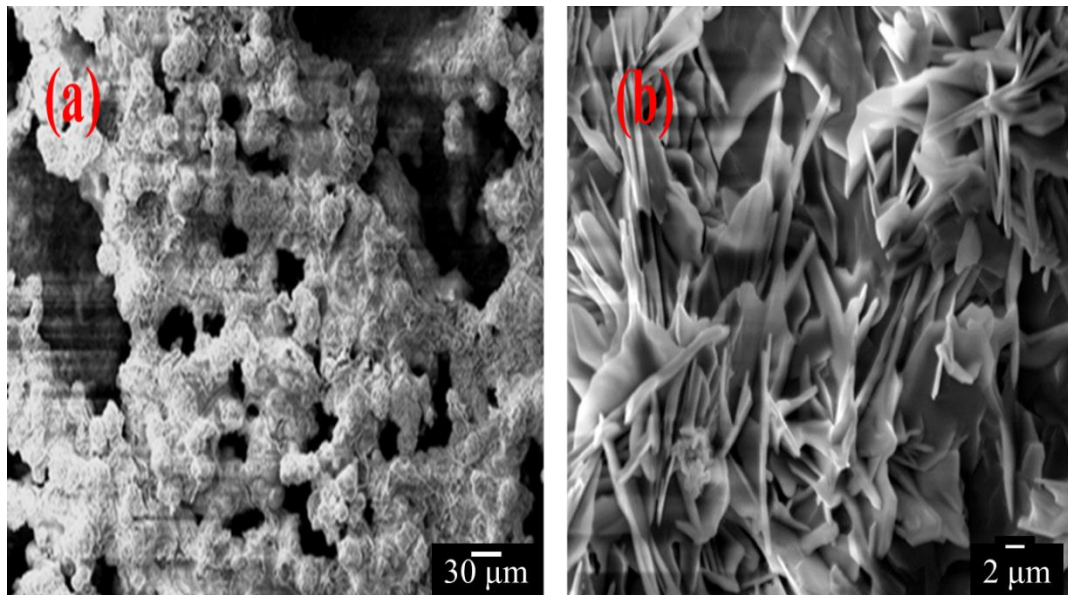


Figure 6.5: SEM images of (a) coated Ti6Al4V and (b) magnified image of needle shaped particles formed on it after the electrochemical corrosion studies

EDS data which was taken on the surface of coated samples after electrochemical corrosion test is given in Table 6.3. As mentioned earlier, the composition of the coated samples also can affect its corrosion resistance. Coated 316 L was having higher corrosion resistance than that of DSS due to the presence of more amount of Calcium in coated 316 L as shown in Table 6.1. The presence of divalent ions such as  $\text{Ca}^{2+}$  in glasses led to the formation of stronger ionic-crosslinks and thus decreased the dissolution or increased the corrosion resistance of glasses (Hafid et al. 2002). The corrosion resistance of coated DSS was lower than that of other two coated samples due to the presence of slightly higher quantity of Phosphorous and lower amount of Calcium on their surface.

Table 6.3: Mass % of elements on the surface of coated substrates as determined from EDS after the electrochemical corrosion test along with the thickness of coatings before and after the electrochemical corrosion test

Sample code	316 L/Glass	DSS/Glass	Ti6Al4V/Glass
Oxygen (O)	43.0	47.8	57.5
Phosphorous (P)	32.5	36.8	26.1
Calcium (Ca)	20.8	14.2	18.6
Sodium (Na)	4.5	2.2	3.0
Barium (Ba)	22.6	18.8	24.7
Chlorine (Cl)	1.2	3.3	2.8
Coating thickness (before), $\mu\text{m}$	~158	~179	~230
Coating thickness (after), $\mu\text{m}$	~135	~74	~121
% Reduction in coating thickness	14.6	58.7	47.4



Comparison of EDS data before and after electrochemical corrosion test (Table 6.1 and 6.3) indicated that concentration of Calcium (Ca) on the coated substrates has increased after the corrosion test, which substantiated the formation of HAP layer as confirmed by XRD and SEM. The percentage reductions in the thickness of coated substrates after corrosion test are given in Table 6.3. The rate of reduction in the thickness was less for coated 316 L indicating their lesser dissolution/corrosion and higher electrochemical corrosion resistance among other coated substrates.

All the coated substrates were porous in nature and the pores can act as a localized zone for corrosion where the electrolyte can enter and the internal part of these pores may get covered with corrosion products.  $\text{Cl}^-$  ions present in the solution accumulate in those pores and it becomes a localized area where the maximum dissolution occurs (Say and Aksakal 2016). The adsorption of Chlorine ( $\text{Cl}^-$ ) ions on the surface of all coated substrates was verified by the EDS data as shown in Table 6.3.

The cathodic current density has increased in a gradual manner in all the coated substrates as observed from the polarization curve which is given in Figure 6.3 (b). Passivation-like region was observed in the anodic part of polarization curve of coated Ti6Al4V indicating their slower corrosion rate at those potentials due to the formation of passive (protective) layer on their surface (Huang et al. 2013). Passivity can be considered as an anodic inhibition to the corrosion process and the rate of substrate dissolution or corrosion is usually reduced by passive layer formation.

When comparing the electrochemical corrosion data of uncoated substrates, it can be observed that uncoated DSS is having higher corrosion resistance ( $R_p$ ), whereas 316 L is having lower corrosion resistance in HBS solution. Passive (protective) layer was formed on the surface of all uncoated substrates during the electrochemical corrosion test and a representative image of uncoated Ti6Al4V is given in Figure 6.6 (a). Measured thickness of these passive layers increased in the order of DSS ( $\sim 7 \mu\text{m}$ ) < Ti6Al4V ( $\sim 30 \mu\text{m}$ ) < 316 L ( $\sim 34 \mu\text{m}$ ) and it supported the electrochemical corrosion data obtained from

the polarization curves. A thicker corrosion layer indicated the severe corrosion and thus lower corrosion resistance (Wang and Wen 2014).

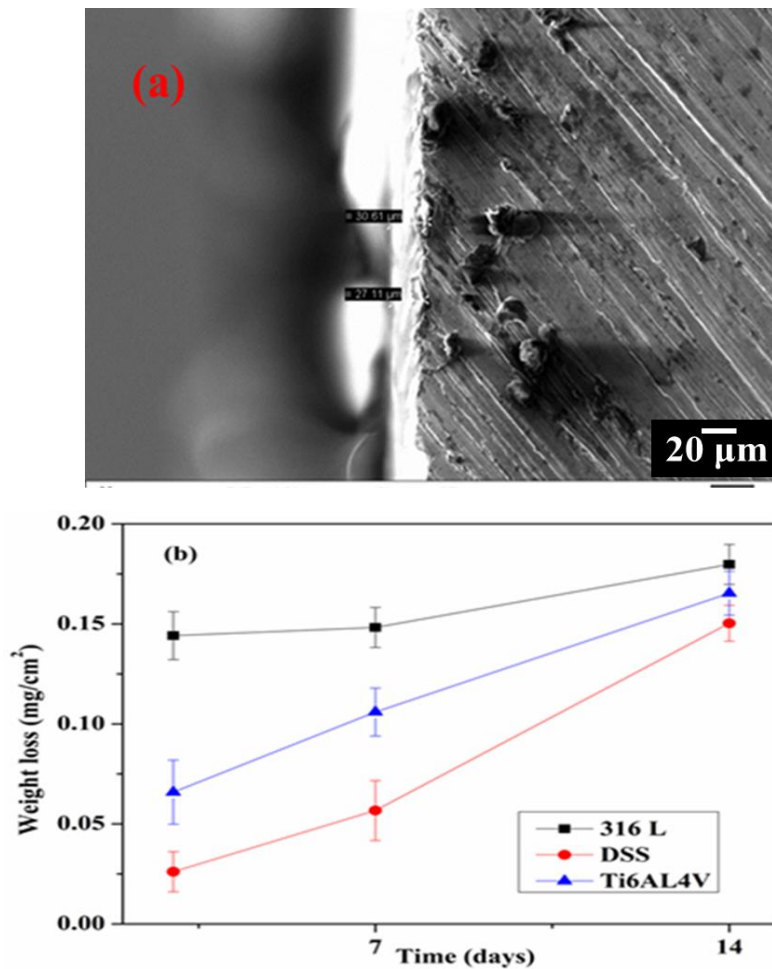


Figure 6.6: (a) SEM image of uncoated Ti6Al4V after electrochemical corrosion test and (b) weight losses of uncoated samples after *in vitro* bioactivity test

To confirm the electrochemical corrosion results, weight losses of uncoated substrates in HBS solution were measured at frequent intervals of 3, 7, 14 days and are given in Figure 6.6 (b). The dissolution/corrosion of ions from the uncoated surfaces reduced their weight and so weight losses increased in accordance with higher

electrochemical corrosion rate or lower corrosion resistance (Wang and Wen 2014). Increase in pH of solution with time and the obtained basic pH in the range of 8.8 -9.1 indicated the dissolution of substrates (Wang and Wen 2014).

The increase in the mass % of elements on the metal substrate after corrosion when compared with initial composition indicates that the element was oxidized and vice versa (Kocijan et al. 2011). Table 6.4 indicates that Cr<sub>2</sub>O<sub>3</sub> and Ni<sub>2</sub>O<sub>3</sub> were formed on uncoated DSS and 316 L after electrochemical corrosion test. The passive layer on these uncoated substrates mainly constituted Chromium (Cr) and Nickel (Ni) similar to observations made by Kocijan et al. (2011). The alloyed Cr can enhance the passivation of stainless steel as explained by the percolation model of passivation (Souto et al. 2001). The formation of insoluble Cr<sub>2</sub>O<sub>3</sub> and continuous network of Cr—O—Cr—O prevented the dissolution of Iron (Fe) ions from the stainless steels. Small variations from the bulk composition was observed in Fe concentration after corrosion test indicating the presence of Fe-oxide in the passive layer as reported in case of Kocijan et al. (2011).

Table 6.4: Mass % of elements from EDS on uncoated 316 L and DSS before and after electrochemical corrosion test

Composition		Cr	Ni	Mn	Si	P	S	C	Mo	N	Fe
316 L	before	17.0	10.0	1.4	0.38	0.041	<0.005	0.021	2.1	0.1	Balance
	after	18.7- 19.5	10.0- 13.5	-	-	0.1	-	2.4- 4.5	-	-	63.7- 65.2
DSS 2205	before	22.7	5.7	1.37	0.38	0.032	0.001	0.03	2.57	0.18	Balance
	after	11.7- 24.8	4.7- 8.2	-	2.3	0.05- 0.2	-	3.3- 6.1	-	-	28.2- 63.0

The observed corrosion results of these two stainless steels substrates was also supported by the work of Kocijan et al. (2011) and Conradi et al. (2011) in which higher corrosion resistance was observed for DSS than that of 316 L in physiological solutions such as HBS solution and artificial saliva. The presence of higher Cr content in the uncoated DSS improved their corrosion resistance through the formation of complex passive layer (Conradi et al. 2011). The amount of Chlorine (Cl) adsorbed on uncoated 316 L and DSS surfaces after corrosion test was 1.3-1.8 and 1.0-1.5 mass % respectively. The amount of Calcium (Ca) adsorbed on 316 L and DSS surfaces after corrosion test was 1.6-2.5 and 1.2-2.8 mass % respectively. The amount of Oxygen (O) observed on 316 L and DSS surfaces after corrosion test was 1.2-2.3 and 1.0-9.5 mass % respectively.

The increase in mass % of Vanadium (V) and presence of Cl<sup>-</sup> ions on the surface of uncoated Ti6Al4V alloy were identified after corrosion in HBS solution as shown in Table 6.5. It indicated that passive layer on uncoated Ti6Al4V constituted with V and some amount of Carbon (2.6-10.3 mass %), Potassium (2.8-3.0 %), Sodium (2.0-4.6 %), Phosphorous (0.07-0.15 %) and Chlorine (0.8-1.7 %) ions were also adsorbed from HBS solution on to the metal surface. It has been reported that passive layer of Vanadium oxide was formed on Ti6Al4V in HBS solution and the Cl<sup>-</sup> ions can increase the dissolution of V ions (Metikoš-Huković et al. 2003, Shukla et al. 2005). Dissolution of Vanadium oxide can support the formation and diffusion of vacancies in oxide layer of Ti6Al4V (Shukla et al. 2005). Dissolution of vanadyl ions (VO<sup>2+</sup>) from Ti6Al4V substrate during corrosion test forms cation vacancies in this substrate. The presence of Cl<sup>-</sup> ions in HBS solution can support the diffusion of these cation vacancies and it can reduce the pitting potential of Ti6Al4V. This lead to the higher susceptibility to localized corrosion (Metikoš-Huković et al. 2003). Electrochemical corrosion resistance of uncoated DSS was higher than that of uncoated Ti6Al4V from the observed result of present work and Sathiyarayanan et al. (2002) have also reported that localized corrosion resistance of DSS is as good as Ti6Al4V.

Table 6.5: Mass% of elements measured using EDS on uncoated Ti6Al4V before and after electrochemical corrosion test

Composition	Al	V	O	C	H	N	Fe	Ti
before	5.5– 6.5	3.5– 4.5	0.13	0.08	0.012	0.05	0.25	Balance
after	2.0- 5.4	1.0- 6.6	1.0- 2.1	2.6- 10.3	-	-	-	69.0- 78.6

While comparing the electrochemical corrosion resistance ( $R_p$ ) of a particular substrate before and after coating, corrosion resistance of 316 L has increased after coating, whereas it has decreased in case of DSS and Ti6Al4V. The corrosion resistance of substrates may increase or decrease after coating based on porosity and composition of coating. The porous structure of coated substrates was the reason for reduction in the corrosion resistance of DSS and Ti6Al4V after coating and solution penetrated through pores attacked the substrate metals (Say and Aksakal 2016). In case of coated 316 L, the adverse effect of porosity on corrosion resistance might be overcome by the formation of higher quantity of protective HAp layer during electrochemical corrosion test as indicated by intense HAp reflections observed in them in comparison with other two coated samples. It can be seen from EDS that presence of  $Cl^-$  ions on uncoated and coated 316 L was same. Whereas higher quantity of  $Cl^-$  was present in coated DSS and Ti6Al4V when compared to uncoated DSS and Ti6Al4V as mentioned earlier, which might indicate the higher rate of attack of  $Cl^-$  ions on these coated samples and thus lower corrosion resistance with respect to their uncoated substrates.

### 6.1.3 *In vitro* bioactivity test of coatings

The *in vitro* bioactivity test of coated substrates supported the electrochemical corrosion results as discussed below.

The representative SEM image of coated Ti6Al4V after immersion in HBS solution for 14 days is given in Figure 6.7. Formation of white layer and thus disappearance of most of pores in the coated surfaces were observed after the immersion.

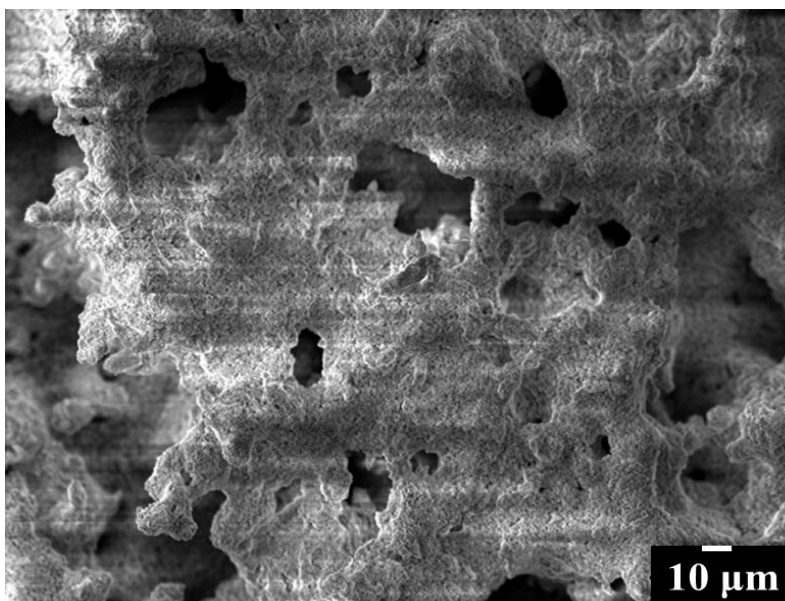


Figure 6.7: SEM images of coated Ti6Al4V after HBS immersion for 14 days

The increase in the concentration of Calcium on the coated surfaces as shown in Table 6.6 proved the accumulation of those ions on their surfaces and thus calcium phosphate (Ca-P) layer formation. The increase in the mass % of Barium on the coated surface after bioactivity test indicated the incorporation of some amount of Barium into the formed Ca-P layer. Some amount of Carbon and Cl<sup>-</sup> ions were also adsorbed on glass

coated surfaces from HBS solution. Composition of Calcium and Phosphorous obtained from EDS data was not representative for the formed surface layer composition alone because the signal came from several microns and could be influenced substantially by the composition of original glass coating if the thickness of layer was less.

Table 6.6: Mass% of elements on coated substrates after HBS immersion for 14 days

Sample code	316 L/Glass	DSS/Glass	Ti6Al4V/Glass
Oxygen (O)	43.52	39.93	37.65
Phosphorous (P)	21.53	30.58	25.00
Calcium (Ca)	19.90	14.89	18.63
Sodium (Na)	3.95	3.64	2.48
Barium (Ba)	23.53	23.26	24.71
Chlorine (Cl)	1.50	3.93	3.79
Carbon (C)	3.10	4.64	4.37

XRD patterns of HBS immersed coated samples indicated the absence of sharp reflections of bioactive crystalline phases after 14 days and thus the layer formed on coated samples was amorphous calcium-phosphate (ACP). ACP layer can be converted into crystalline HAp as the days of immersion increases by consuming more  $\text{Ca}^{2+}$  and  $\text{PO}_4^{3-}$  ions from the solution (N. Gunawidjaja et al. 2012). The formation of HAp is an indication of glass or coating to be a bioactive material. The porous structure of coating helps to nucleate HAp easily and it can attract Calcium and Phosphorous ions from

solutions due to the higher surface area of porous structure. The porous structure can reduce the contact angle between HAp crystal nucleus and liquid-solid interface and thus reduces the Gibb's free energy in the HAp nucleation process. And the HAp deposition process on surface speeds up with the increase in the specific area of solid-liquid interface (Chen et al. 2017).

The basic range of pH (8.7-8.8) of HBS solution was attributed to the cation release ( $\text{Na}^+$  and  $\text{Ca}^{2+}$ ) from coated samples as shown in Figure 6.8. Variations in the ion release rate were within error limit and such steady rate of cation ( $\text{Na}^+$  and  $\text{Ca}^{2+}$ ) and anion ( $\text{PO}_4^{3-}$ ) releases in the final days of immersion supported the accumulation of these ions on coated surfaces and thus formation of Ca-P layer (Al-Rashidy et al. 2017). Franks et al. (2000) have reported that the layer formation on the glass surface when immersed in solution hindered the ion diffusion and ion exchange process from the glasses and so, steady rate of ions release observed in the final days of immersion in HBS solution supported the calcium-phosphate layer formation on the surface of coated samples.

In the initial process of dissolution,  $\text{Na}^+$  ions were exchanged with  $\text{H}^+$  ions in the HBS solution and this increased pH of solution as observed in the initial days of immersion (Kheirkhah et al. 2015). The ion release rate is inversely related to the corrosion resistance (López et al. 2016) and it was substantiated by the observed cation release profile. Lower amount of  $\text{Ca}^{2+}$  and  $\text{Na}^+$  ions were released from coated 316 L, which supported their higher electrochemical corrosion resistance among other two coated substrates. The cations are released during the initial days of dissolution and it leads to the dissolution of entire phosphate chains in the glass structure and finally the dissolution of bulk coating material will happen. As the ions were dissolved into HBS solution, ionic strength of solution increased which can hinder the further dissolution of  $\text{PO}_4^{3-}$  ions from the glass due to the electrostatic interactions (Delahaye et al. 1998). Thus lower amount of cation releases from coated 316 L decreased the cationic strength of solution and so maximum  $\text{PO}_4^{3-}$  ions release was observed here in comparison with other two coated samples (Delahaye et al. 1998).



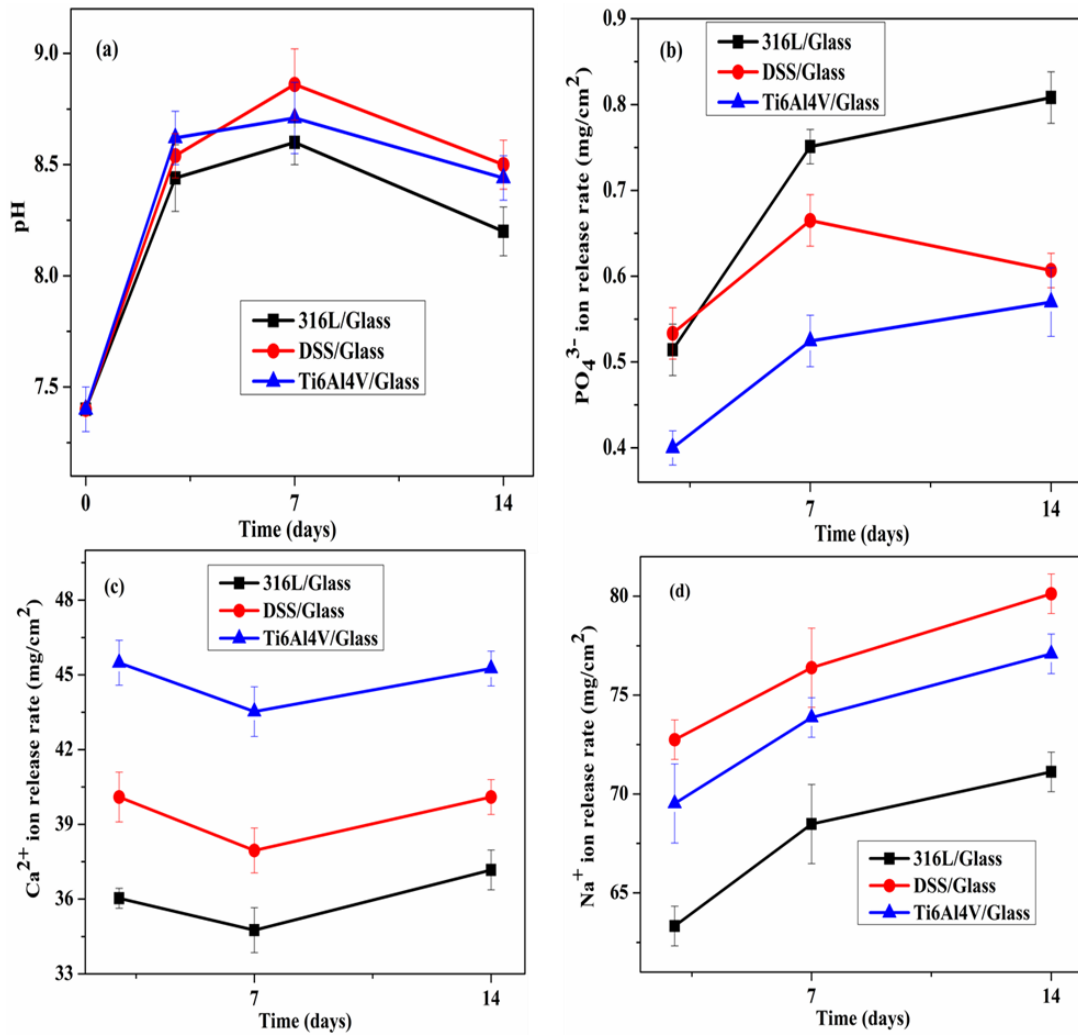


Figure 6.8: (a) pH, (b) PO<sub>4</sub><sup>3-</sup>, (c) Ca<sup>2+</sup> and (d) Na<sup>+</sup> ion release rate from coated substrates after immersion in HBS for 14 days

The reduction in the mass % of Sodium (Na) after electrochemical corrosion test was comparatively lesser in coated 316 L than other two coated samples, which was supported by the lower release of Na<sup>+</sup> ions after immersion test. The lower release rate of ions from coated 316 L was responsible for its lower corrosion (dissolution) rate or higher electrochemical corrosion resistance among other coated samples.

Duplex stainless steel (DSS) 2205 can be an alternative for 316 L for biomedical applications due to its higher electrochemical corrosion resistance and presence of lower amount of Nickel. Presence of Nickel causes hypersensitivity effect in patients (Conradi et al. 2011). DSS can also be an alternative for Ti6Al4V for biomedical applications due to the same order of magnitude of corrosion resistance of these two materials and lower cost of DSS than Ti6Al4V.

## 6.2 SUMMARY

Phosphate glass with composition  $11\text{Na}_2\text{O}-15\text{BaO}-29\text{CaO}-45\text{P}_2\text{O}_5$  was coated on stainless steel 316 L, DSS 2205 and Ti6Al4V alloy using thermal enamelling technique. Coatings were partially crystalline in nature with porous morphology. The variations in the thickness of coatings were related to the difference in diffusion of elements across the interface. The corrosion resistance of glass coated and uncoated substrates has been studied by electrochemical corrosion test in HBS solution. Corrosion resistance of uncoated 316 L has increased after coating, whereas it has decreased in case of DSS and Ti6Al4V substrates. DSS is having higher corrosion resistance among the uncoated substrates, whereas coated 316 L is having higher corrosion resistance among the coated substrates. Amorphous calcium-phosphate layer (ACP) was formed on the surface of all coated substrates after *in vitro* bioactivity in HBS solution. Duplex stainless steel (DSS) 2205 can be an alternative for 316 L and Ti6Al4V for biomedical applications due to its better corrosion resistance. Though the glass-ceramic coating did not improve the electrochemical corrosion resistance of DSS and Ti6Al4V, it helped in the formation of amorphous calcium-phosphate layer which can get converted into crystalline HAp on prolonged duration of immersion. However these conclusions have to be further confirmed by *in vivo* bioactivity studies.

## Chapter 7

### SUMMARY AND CONCLUSIONS

The results of work presented in different chapters of the thesis are summarized as given below. This chapter ends with the conclusion of major findings and scope for the future work.

#### 7.1 SUMMARY

Phosphate glasses with composition  $(26-x)\text{Na}_2\text{O}-x\text{BaO}-29\text{CaO}-45\text{P}_2\text{O}_5$  ( $x = 0, 5, 10, 15$  mol%) were prepared at three different melting temperatures, 1000, 1100 and 1200°C. Effect of BaO content and melting temperature on the structural and mechanical properties of these glasses were subjected to study. All the synthesized glass samples were homogeneous and have amorphous structure. The density and compactness of glasses have increased with BaO content, whereas molar volume was independent of composition. According to FTIR studies, the glass structure mainly constitutes  $Q^1$  and  $Q^2$  structural units. Hardness and fracture toughness were found to be independent of BaO content. The brittleness and crack-length have increased with BaO content in glasses prepared at 1000°C, whereas it has decreased in glasses prepared at 1100 and 1200°C, which are mainly due to the plastic flow of deformation. Lower density and higher molar volume have obtained for glasses prepared at higher melting temperature. Lower brittleness and crack-length was found in glasses prepared at higher melting temperature attributing to the changes in density and plastic flow of deformation in glasses.

Depending on the above mentioned studies glasses prepared at 1200°C were found to have better mechanical properties such as lower brittleness and crack-length and they were selected for optical, thermal, dissolution and in-vitro bioactivity studies.

Effect of BaO addition on the thermal and optical properties of Na<sub>2</sub>O-CaO-P<sub>2</sub>O<sub>5</sub> glasses prepared at 1200°C has been studied. Glass transition temperature, crystallization temperature and thermal stability of glasses have increased with BaO content. Glass forming ability has increased with initial addition of BaO. All the synthesized glasses were having higher thermal stability values greater than 100°C and thus they are suitable for fiber drawing. The refractive index of glasses was increased with BaO content. The initial addition of BaO increased the optical band gap energy, whereas the increase in BaO content has negligible effect on it. The changes in the optical basicity and metallization criteria of glasses supported the variation in band gap energy values. The decrease in the Urbach energy values with BaO addition indicated the presence of less number of defects and/or interstitial bonds in the glass structure.

Effect of BaO addition on the dissolution and *in vitro* bioactivity properties of Na<sub>2</sub>O-CaO-P<sub>2</sub>O<sub>5</sub> glasses was studied in deionized water and phosphate buffer saline (PBS) as well as Hank's balanced salt (HBS) solutions under static dissolution conditions for 28 days. Dissolution rate of glasses in deionized water was found to increase with time, whereas it was decreased by three orders of magnitude with increase in BaO content. All the glass samples were in amorphous nature even after 28 days of immersion in deionized water according to XRD studies. Selective or incongruent type of dissolution in deionized water was found in all the glasses. FTIR studies indicated the depolymerization of glass network after immersion in deionized water. Na<sup>+</sup>, Ca<sup>2+</sup> and PO<sub>4</sub><sup>3-</sup> ions were accumulated on the glass surface indicating the formation of calcium-phosphate layer. Bioactivity of glasses did not improve with BaO composition after immersion in PBS solution, whereas the addition of 15 mol % of BaO supported the formation of crystalline HAp. All the glasses showed the bioactivity in HBS solution by the formation of crystalline HAp and bioactivity was improved with BaO content. Faster HAp formation was happened in HBS when compared to PBS. pH of both PBS and HBS solutions were increased with increase in BaO content, which might reduce the cytotoxicity and improve the biocompatibility of glasses.

Phosphate glass with composition  $11\text{Na}_2\text{O}-15\text{BaO}-29\text{CaO}-45\text{P}_2\text{O}_5$  was coated on stainless steel 316 L, DSS 2205 and Ti6Al4V alloy using thermal enamelling technique. Coatings have partially crystalline structure with porous morphology. The thickness of coatings was varied due to the difference in the diffusion of elements across the interface. The electrochemical corrosion resistance of glass coated and uncoated substrates has been studied by electrochemical corrosion test in HBS solution. Corrosion resistance of uncoated 316 L has increased after coating, whereas it has decreased in case of DSS and Ti6Al4V substrates. DSS is having higher corrosion resistance among the uncoated substrates, whereas coated 316 L is having higher corrosion resistance among the coated substrates. Amorphous calcium-phosphate layer (ACP) was formed on the surface of all coated substrates after *in vitro* bioactivity studies for 14 days in HBS solution. Duplex stainless steel (DSS) 2205 can be an alternative for 316 L and Ti6Al4V for biomedical applications due to its better corrosion resistance. Though the electrochemical corrosion resistance of DSS and Ti6Al4V was not improved with coating which helped in the formation of amorphous calcium-phosphate (ACP) layer.

## 7.2 CONCLUSIONS

- Density of glasses has increased by 13% with BaO content. Glasses prepared at higher melting temperature ( $1200^\circ\text{C}$ ) were having better properties such as lower brittleness. Addition of BaO improved the mechanical properties of  $\text{Na}_2\text{O}-\text{CaO}-\text{P}_2\text{O}_5$  glasses prepared at  $1200^\circ\text{C}$  such as decrease in brittleness by 22%.
- Thermal properties of  $\text{Na}_2\text{O}-\text{CaO}-\text{P}_2\text{O}_5$  glasses have improved with increase in BaO content such as increase in glass transition temperature (by 11%), crystallization temperature (by 18%), thermal stability (by 35%) and glass forming ability (by 33%). All the synthesized glasses are having fiber drawing capability due to their higher thermal stability values greater than  $100^\circ\text{C}$ .
- The refractive indices of glasses increased by 2% with BaO content. The initial addition of BaO increased the optical band gap energy by 83%, whereas further

increase in BaO content has negligible effect on it. Urbach energy has decreased by 78% with increase in BaO content.

- Dissolution rate of Na<sub>2</sub>O-CaO-P<sub>2</sub>O<sub>5</sub> glasses in deionized water decreased by three orders of magnitude with increase in BaO content up to 15 mol%.
- HAp was formed on all the composition of glasses in HBS solution and bioactivity was improved with increase in BaO content. HAp was formed faster (within 7 days) in HBS solution than that of PBS (within 14 days).
- Phosphate glass with composition 11Na<sub>2</sub>O-15BaO-29CaO-45P<sub>2</sub>O<sub>5</sub> was coated on stainless steel 316 L, DSS 2205 and Ti6Al4V alloy using thermal enamelling technique. Coatings have glass-ceramic structure with porous morphology.
- DSS 2205 is having higher electrochemical corrosion resistance among the uncoated samples. Coated 316 L is having higher corrosion resistance among glass coated samples.
- Amorphous calcium-phosphate (ACP) layer was formed on the surface of all coated substrates after *in vitro* bioactivity studies in HBS solution for 14 days, which can get converted into crystalline HAp on prolonged duration of immersion.
- Among the synthesized samples, 11Na<sub>2</sub>O-15BaO-29CaO-45P<sub>2</sub>O<sub>5</sub> glass and coated 316 L are more suitable for biomedical and various technological applications based on their improved properties. Duplex stainless steel (DSS) 2205 can be an alternative for 316 L and Ti6Al4V for biomedical applications due to its better corrosion resistance.

### 7.3 SCOPE FOR THE FUTURE WORK

The efforts that can be made in future are,

- to study the biocompatibility properties and *in vitro* cell culture analysis of synthesized glasses and glass coatings for designing a suitable material or implant for biomedical applications
- to dope the various transition metal ions to the synthesized glass matrix for designing glasses for biomedical optical applications
- to develop the magnetic properties in the synthesized glass matrix by adding suitable ions for cancer treatments
- to embed metallic nano-particles in the synthesized glass matrix for tissue engineering applications
- to check the suitability of present system of glasses for applications other than biomedical fields
- to compare the properties of coating prepared by thermal enamelling technique with other techniques in order to make a practically successful coating

## REFERENCES

- Abd El-Moneim, A. (2001). "Bond compression bulk modulus and Poisson's ratio of the polycrystalline silicate glasses." *Mater. Chem. Phys.*, 70(3), 340–343.
- Ahmad, T., Ubaidullah, M., Shahazad, M., Kumar, D., and Al-Hartomy, O. A. (2017). "Reverse micellar synthesis, structural characterization and dielectric properties of Sr-doped BaZrO<sub>3</sub> nanoparticles." *Mater. Chem. Phys.*, 185, 31–8.
- Ahmed, I., Lewis, M., Olsen, I., and Knowles, J. C. (2004). "Phosphate glasses for tissue engineering: Part 2. Processing and characterisation of a ternary-based P<sub>2</sub>O<sub>5</sub>-CaO-Na<sub>2</sub>O glass fibre system." *Biomaterials*, 25(3), 501–507.
- Ahmed, I., Lewis, M. P., Nazhat, S. N., and Knowles, J. C. (2005). "Quantification of anion and cation release from a range of ternary phosphate-based glasses with fixed 45 mol% P<sub>2</sub>O<sub>5</sub>." *J. Biomater. Appl.*, 20(1), 65–80.
- Ali, S., Farooq, I., and Iqbal, K. (2014). "A review of the effect of various ions on the properties and the clinical applications of novel bioactive glasses in medicine and dentistry." *Saudi Dent. J.*, 26(1), 1–5.
- Al-Noaman, A., Rawlinson, S. C. F., and Hill, R. G. (2012). "The role of MgO on thermal properties, structure and bioactivity of bioactive glass coating for dental implants." *J. Non-Cryst. Solids.* 358(22), 3019–3027.
- Al-Rashidy, Z. M., Farag, M. M., Ghany, N. A. A., Ibrahim, A. M., and Abdel-Fattah, W. I. (2017). "Aqueous electrophoretic deposition and corrosion protection of borate glass coatings on 316L stainless steel for hard tissue fixation." *Surf. Interfaces*, 7 (Supplement C), 125–133.



Altaf, M., Chaudhry, M. A., and Siddiqi, S. A. (2005). "Effect of  $\text{Li}_2\text{O}$  on the Refractive Index and Optical Band Gap of Cadmium Phosphate Glasses." *Glass Phys. Chem.*, 31(5), 597–601.

Anstis, G. r., Chantikul, P., Lawn, B. r., and Marshall, D. b. (1981). "A Critical Evaluation of Indentation Techniques for Measuring Fracture Toughness: I, Direct Crack Measurements." *J. Am. Ceram. Soc.*, 64(9), 533–538.

Arepalli, S. K., Tripathi, H., Vyas, V. K., Jain, S., Suman, S. K., Pyare, R., and Singh, S. P. (2015). "Influence of barium substitution on bioactivity, thermal and physico-mechanical properties of bioactive glass." *Mater. Sci. Eng. C*, 49, 549–559.

"ASTM G102 - 89(2015)E1 - Standard Practice for Calculation of Corrosion Rates and Related Information from Electrochemical Measurements."

<<https://shop.bsigroup.com/ProductDetail/?pid=000000000030336338>> (Feb. 3, 2018).

Austin, C., Smith, T. M., Bradman, A., Hinde, K., Joannes-Boyau, R., Bishop, D., Hare, D. J., Doble, P., Eskenazi, B., and Arora, M. (2013). "Barium distributions in teeth reveal early-life dietary transitions in primates." *Nature*, 498(7453), 216–219.

Azeem, B., KuShaari, K., and Man, Z. (2016). "Effect of Coating Thickness on Release Characteristics of Controlled Release Urea Produced in Fluidized Bed Using Waterborne Starch Biopolymer as Coating Material." *Procedia Eng.*, Proceeding of 4th International Conference on Process Engineering and Advanced Materials (ICPEAM 2016), 148(Supplement C), 282–289.

B Edathazhe, A., and Shashikala, H. D. (2016). "Effect of  $\text{BaO}$  addition on the structural and mechanical properties of soda lime phosphate glasses." *Mater. Chem. Phys.*, 184, 146–154.

Baino, F., and Verné, E. (2017). "Glass-based coatings on biomedical implants: a state-of-the-art review." *Biomed. Glas.*, 3(1), 1–17.

- Beckham, C. A., Greenlee, T. K., and Crebo, A. R. (1971). "Bone formation at a ceramic implant interface." *Calcif. Tissue Res.*, 8(2), 165–171.
- Brauer, D. S., Karpukhina, N., O'Donnell, M. D., Law, R. V., and Hill, R. G. (2010). "Fluoride-containing bioactive glasses: effect of glass design and structure on degradation, pH and apatite formation in simulated body fluid." *Acta Biomater.*, 6(8), 3275–3282.
- Brow, R. K. (2000). "Review: the structure of simple phosphate glasses." *J. Non-Cryst. Solids*, 263–264 (Supplement C), 1–28.
- Bunker, B. C., Arnold, G. W., and Wilder, J. A. (1984). "Phosphate Glass Dissolution in Aqueous Solution." *J. Non-Cryst. Solids*, 64(3), 291–316.
- Burling, L. D. (2006). "Novel phosphate glasses for bone regeneration applications." <<http://eprints.nottingham.ac.uk/10161/>> (Dec. 18, 2016).
- Byun, J.-O., Kim, B.-H., Hong, K.-S., Jung, H.-J., Lee, S.-W., and Izyneev, A. A. (1995). "Properties and structure of RO-Na<sub>2</sub>O-Al<sub>2</sub>O<sub>3</sub>-P<sub>2</sub>O<sub>5</sub> (R = Mg, Ca, Sr, Ba) glasses." *J. Non-Cryst. Solids*, 190(3), 288–295.
- Carta, D., Knowles, J. C., Smith, M. E., and Newport, R. J. (2007). "Synthesis and structural characterization of P<sub>2</sub>O<sub>5</sub>-CaO-Na<sub>2</sub>O sol-gel materials." *J. Non-Cryst. Solids*, 353(11), 1141–1149.
- Ceci-Ginistrelli, E., Pugliese, D., Boetti, N. G., Novajra, G., Ambrosone, A., Lousteau, J., Vitale-Brovarone, C., Abrate, S., and Milanese, D. (2016). "Novel biocompatible and resorbable UV-transparent phosphate glass based optical fiber." *Opt. Mater. Express*, 6(6), 2040–2051.
- Çelikbilek, M., Ersundu, A. E., and Aydin, S. (2013). "Preparation and characterization of TeO<sub>2</sub>-WO<sub>3</sub>-Li<sub>2</sub>O glasses." *J. Non-Cryst. Solids*, 378, 247–253.

Chanthima, N., Kaewkhao, J., Tariwong, Y., Sangwaranatee, N., and Sangwaranatee, N. W. (2017). “Luminescence study and Judd-Ofelt analysis of CaO-BaO-P<sub>2</sub>O<sub>5</sub> glasses doped with Nd<sup>3+</sup> ions.” *Mater. Today Proc.*, International Conference on Science and Technology of the Emerging Materials (July 27-29, 2016), Pattaya, Thailand, 4(5, Part 2), 6091–6098.

Chen, C. C., Huang, T. H., Kao, C. T., and Ding, S. J. (2004). “Electrochemical study of the in vitro degradation of plasma-sprayed hydroxyapatite/bioactive glass composite coatings after heat treatment.” *Electrochimica Acta*, 50(4), 1023–1029.

Chen, S., Tu, J., Hu, Q., Xiong, X., Wu, J., Zou, J., and Zeng, X. (2017). “Corrosion resistance and in vitro bioactivity of Si-containing coating prepared on a biodegradable Mg-Zn-Ca bulk metallic glass by micro-arc oxidation.” *J. Non-Cryst. Solids*, 456 (Supplement C), 125–131.

Conradi, M., Schön, P. M., Kocijan, A., Jenko, M., and Vancso, G. J. (2011). “Surface analysis of localized corrosion of austenitic 316L and duplex 2205 stainless steels in simulated body solutions.” *Mater. Chem. Phys.*, 130(1), 708–713.

Da Costa, Z. M., Pontuschka, W. M., Giehl, J. M., and Da Costa, C. R. (2006). “ESR dosimeter based on P<sub>2</sub>O<sub>5</sub>-CaO-Na<sub>2</sub>O glass system.” *J. Non-Cryst. Solids, Glasses and Related Materials* 7, 352(32), 3663–3667.

Davis, E. A., and Mott, N. F. (1970). “Conduction in non-crystalline systems V. Conductivity, optical absorption and photoconductivity in amorphous semiconductors.” *Philos. Mag.*, 22(179), 903–922.

Dayanand, C., Bhikshamaiah, G., Tyagaraju, V. J., Salagram, M., and Murthy, A. S. R. K. (1996). “Structural investigations of phosphate glasses: a detailed infrared study of the PbO- P<sub>2</sub>O<sub>5</sub> vitreous system.” *J. Mater. Sci.*, 31(8), 1945–1967.

Delahaye, F., Montagne, L., Palavit, G., Claude Touray, J., and Baillif, P. (1998). "Acid dissolution of sodium–calcium metaphosphate glasses." *J. Non-Cryst. Solids*, 242(1), 25–32.

Dembovsky, S. A., and Chechetkina, E. A. (1982). "To the classification of amorphous solids and the calculation of critical cooling rates for amorphous metals and glasses." *Mater. Res. Bull.*, 17(12), 1531–1538.

Dimitrov, V., and Komatsu, T. (2010). "An interpretation of optical properties of oxides and oxide glasses in terms of the electronic ion polarizability and average single bond strength." *J Univ Chem Technol Met.*, 45(3), 219–250.

Döhler, F., Mandlule, A., Wüllen, L. van, Friedrich, M., and Brauer, D. (2015). "31P NMR characterisation of phosphate fragments during dissolution of calcium sodium phosphate glasses." *J Mater Chem B*, 3, 1125.

Duffy, J. A. (2004). "Abnormal refractivity trends in phosphate glass systems." *Phys. Chem. Glas.*, 45(6), 322–327.

Dunn, A., Zaveri, T., Keselowsky, B., and Sawyer, W. G. (2007). "Macroscopic Friction Coefficient Measurements on Living Endothelial Cells." *Tribol. Lett.*, 27, 233–238.

Franks, K., Abrahams, I., Georgiou, G., and Knowles, J. C. (2001). "Investigation of thermal parameters and crystallisation in a ternary CaO–Na<sub>2</sub>O–P<sub>2</sub>O<sub>5</sub>-based glass system." *Biomaterials*, 22(5), 497–501.

Franks, K., Abrahams, I., and Knowles, J. C. (2000). "Development of soluble glasses for biomedical use Part I: in vitro solubility measurement." *J. Mater. Sci. Mater. Med.*, 11(10), 609–614.

Fu, Q., Saiz, E., Rahaman, M. N., and Tomsia, A. P. (2011). "Bioactive glass scaffolds for bone tissue engineering: state of the art and future perspectives." *Mater. Sci. Eng. C*, 31(7), 1245–1256.

- Gali, S., K., R., Murthy, B. V. S., and Basu, B. (2018). "Zirconia toughened mica glass ceramics for dental restorations." *Dental Materials*, 34(3), e36–e45.
- Gnanavel, S., Ponnusamy, S., Mohan, L., and Muthamizhchelvan, C. (2018). "In Vitro Corrosion Behaviour of Ti–6Al–4V and 316L Stainless Steel Alloys for Biomedical Implant Applications." *J. Bio- Tribo-Corros.*, 4(1), 1.
- Groh, D., Döhler, F., and Brauer, D. S. (2014). "Bioactive glasses with improved processing. Part 1. Thermal properties, ion release and apatite formation." *Acta Biomater.*, 10(10), 4465–4473.
- Hafid, M., Jermoumi, T., Toreis, N., and Ghailassi, T. (2002). "Structure of  $(45-x)\text{Na}_2\text{O}-x\text{BaO}-5\text{ZnO}-50\text{P}_2\text{O}_5$  glasses studied by DSC and infrared spectroscopy." *Mater. Lett.*, 56(4), 486–490.
- Hager, I. Z., and El-Mallawany, R. (2010). "Preparation and structural studies in the  $(70-x)\text{TeO}_2-20\text{WO}_3-10\text{Li}_2\text{O}-x\text{Ln}_2\text{O}_3$  glasses." *J. Mater. Sci.*, 45, 897–905.
- Hammood, A. S., Noor, A. F., and Alkhafagy, M. T. (2017). "Effect of heat treatment on corrosion behavior of duplex stainless steel in orthodontic applications." *Mater. Res. Express*.
- Hench, L. L. (2006). "The story of Bioglass®." *J. Mater. Sci. Mater. Med.*, 17(11), 967–978.
- Hench, L. L., and Jones, J. R. (2015). "Bioactive Glasses: Frontiers and Challenges." *Front. Bioeng. Biotechnol.*, 3.
- Hench, L. L., and Paschall, H. A. (1973). "Direct chemical bond of bioactive glass-ceramic materials to bone and muscle." *J. Biomed. Mater. Res.*, 7(3), 25–42.

Hermansen, C., Matsuoka, J., Yoshida, S., Yamazaki, H., Kato, Y., and Yue, Y. Z. (2013). “Densification and plastic deformation under microindentation in silicate glasses and the relation to hardness and crack resistance.” *J. Non-Cryst. Solids*, 364, 40–43.

Hoppe, A., Güldal, N. S., and Boccaccini, A. R. (2011). “A review of the biological response to ionic dissolution products from bioactive glasses and glass-ceramics.” *Biomaterials*, 32(11), 2757–2774.

Huang, K., Cai, S., Xu, G., Ye, X., Dou, Y., Ren, M., and Wang, X. (2013). “Preparation and characterization of mesoporous 45S5 bioactive glass–ceramic coatings on magnesium alloy for corrosion protection.” *J. Alloys Compd.*, 580 (Supplement C), 290–297.

Ibrahim, M. Z., Sarhan, A. A. D., Yusuf, F., and Hamdi, M. (2017). “Biomedical materials and techniques to improve the tribological, mechanical and biomedical properties of orthopedic implants – A review article.” *J. Alloys Compd.*, 714, 636–667.

Islam, M. T., Felfel, R. M., Abou Neel, E. A., Grant, D. M., Ahmed, I., and Hossain, K. M. Z. (2017). “Bioactive calcium phosphate-based glasses and ceramics and their biomedical applications: A review.” *J. Tissue Eng.*, 8, 2041731417719170.

“ISO 23317:2014 - Implants for surgery -- In vitro evaluation for apatite-forming ability of implant materials.” (n.d.). <<https://www.iso.org/standard/65054.html>> (Feb. 4, 2018).

Ivascu, C., Timar Gabor, A., Cozar, O., Daraban, L., and Ardelean, I. (2011). “FT-IR, Raman and thermoluminescence investigation of P<sub>2</sub>O<sub>5</sub>–BaO–Li<sub>2</sub>O glass system.” *J. Mol. Struct.*, Molecular spectroscopy and Molecular structure 2010, 993(1), 249–253.

Jastrzębski, W., Sitarz, M., Rokita, M., and Bułat, K. (2011). “Infrared spectroscopy of different phosphates structures.” *Spectrochim. Acta. A. Mol. Biomol. Spectrosc.*, The Xth International Conference on Molecular Spectroscopy, 79(4), 722–727.

Jermoumi, T., Hassan, S., and Hafid, M. (2003). “Structural investigation of vitreous barium zinc mixed metaphosphate.” *Vib. Spectrosc.*, 32(2), 207–213.

Jha, P. K., Pandey, O. P., and Singh, K. (2015). “FTIR spectral analysis and mechanical properties of sodium phosphate glass–ceramics.”, *J. Mol. Struct.*, 1083.

Jiang, Z.-H., and Zhang, Q.-Y. (2014). “The structure of glass: A phase equilibrium diagram approach.” *Prog. Mater. Sci.*, 61, 144–215.

Jones, J. R. (2013). “Review of bioactive glass: from Hench to hybrids.” *Acta Biomater.*, 9(1), 4457–4486.

K., P. P., N., D., Manikantan Syamala, K., and N., R. (2018). “Antibacterial effects, biocompatibility and electrochemical behavior of zinc incorporated niobium oxide coating on 316L SS for biomedical applications.” *Appl. Surf. Sci.*, 427, 1166–1181.

Kato, Y., Yamazaki, H., Yoshida, S., and Matsuoka, J. (2010). “Effect of densification on crack initiation under Vickers indentation test.” *J. Non-Cryst. Solids*, 356(35), 1768–1773.

Kaur, G. (2017). *Bioactive Glasses: Potential Biomaterials for Future Therapy*. Springer.

Kaur, G., Pandey, O. p., Singh, K., Homa, D., Scott, B., and Pickrell, G. (2014). “A review of bioactive glasses: Their structure, properties, fabrication and apatite formation.” *J. Biomed. Mater. Res. A*, 102(1), 254–274.

Kaur, G., Sharma, P., Kumar, V., and Singh, K. (2012). “Assessment of in vitro bioactivity of SiO<sub>2</sub>-BaO-ZnO-B<sub>2</sub>O<sub>3</sub>-Al<sub>2</sub>O<sub>3</sub> glasses: An optico-analytical approach.” *Mater. Sci. Eng. C*, 32(7), 1941–1947.

Kaur, M., Singh, A., Thakur, V., and Singh, L. (2015). “Effect of TiO<sub>2</sub> substitution on optical and structural aspects of phosphate glasses.” *J. Mol. Struct.*, 1089, 95–101.

Kheirkhah, M., Fathi, M., Salimijazi, H. R., and Razavi, M. (2015). "Surface modification of stainless steel implants using nanostructured forsterite ( $Mg_2SiO_4$ ) coating for biomaterial applications." *Surf. Coat. Technol.*, 276 (Supplement C), 580–586.

Khor, S. F., Talib, Z. A., Malek, F., and Cheng, E. M. (2013). "Optical properties of ultraphosphate glasses containing mixed divalent zinc and magnesium ions." *Opt. Mater.*, 35(3), 629–633.

Kiani, A., Hanna, J. V., King, S. P., Rees, G. J., Smith, M. E., Roohpour, N., Salih, V., and Knowles, J. C. (2012). "Structural characterization and physical properties of  $P_2O_5$ – $CaO$ – $Na_2O$ – $TiO_2$  glasses by Fourier transform infrared, Raman and solid-state magic angle spinning nuclear magnetic resonance spectroscopies." *Acta Biomater.*, 8(1), 333–340.

Kjeldsen, J., Smedskjaer, M. M., Potuzak, M., and Yue, Y. (2015). "Role of elastic deformation in determining the mixed alkaline earth effect of hardness in silicate glasses." *J. Appl. Phys.*, 117(3), 34903.

Kocijan, A., and Conradi, M. (2010). "The corrosion behaviour of austenitic and duplex stainless steels in artificial body fluids." *Mater. Tehnol.*, 44, 21–24.

Kocijan, A., Merl, D. K., and Jenko, M. (2011). "The corrosion behaviour of austenitic and duplex stainless steels in artificial saliva with the addition of fluoride." *Corros. Sci.*, 53(2), 776–783.

Kokubo, T., and Takadama, H. (2006). "How useful is SBF in predicting in vivo bone bioactivity?" *Biomaterials*, 27(15), 2907–2915.

Krishnan, V., and Lakshmi, T. (2013). "Bioglass: A novel biocompatible innovation." *J. Adv. Pharm. Technol. Res.*, 4(2), 78–83.

Kurkjian, C. R. (2000). "Mechanical properties of phosphate glasses." *Journal of Non-Crystalline Solids*, 263–264, 207–212.



Laeny, A. N. (2008). "Synthesis of Amorphous Calcium Phosphate by Low Temperature-Precipitation Method from Eggshell."

<http://repository.ipb.ac.id/handle/123456789/17432> (accessed December 18, 2016).

Lawn, B. R., and Marshall, D. B. (1979). "Hardness, Toughness, and Brittleness: An Indentation Analysis." *J. Am. Ceram. Soc.*, 62(7–8), 347–350.

Lee, E. T. Y., and Taylor, E. R. M. (2006). "Optical and thermal properties of binary calcium phosphate and barium phosphate glasses." *Opt. Mater.*, 28(3), 200–206.

Lee, I.-H., Foroutan, F., Lakhkar, N. J., Gong, M.-S., and Knowles, J. C. (2013). "Sol-gel synthesis and structural characterization of  $P_2O_5$ -CaO- $Na_2O$  glasses." *Phys. Chem. Glas. - Eur. J. Glass Sci. AndTechnology Part B*, 54(3), 115–120.

Lee, I.-H., Shin, S.-H., Foroutan, F., Lakhkar, N. J., Gong, M.-S., and Knowles, J. C. (2013). "Effects of magnesium content on the physical, chemical and degradation properties in a MgO-CaO- $Na_2O$ - $P_2O_5$  glass system." *J. Non-Cryst. Solids*, 363 (Supplement C), 57–63.

Lee, I.-H., Yu, H., Lakhkar, N. J., Kim, H.-W., Gong, M.-S., Knowles, J. C., and Wall, I. B. (2013). "Development, characterisation and biocompatibility testing of a cobalt-containing titanium phosphate-based glass for engineering of vascularized hard tissues." *Mater. Sci. Eng. C*, 33(4), 2104–2112.

Leenakul, W., Kantha, P., Pisitpipathsin, N., Rujijanagul, G., Eitssayeam, S., and Pengpat, K. (2013). "Structural and magnetic properties of  $SiO_2$ -CaO- $Na_2O$ - $P_2O_5$  containing BaO- $Fe_2O_3$  glass-ceramics." *J. Magn. Magn. Mater.*, 325, 102–106.

Li, Y., Liu, Y.-Z., Long, T., Yu, X.-B., Tang, T.-T., Dai, K.-R., Tian, B., Guo, Y.-P., and Zhu, Z.-A. (2013). "Mesoporous bioactive glass as a drug delivery system: fabrication, bactericidal properties and biocompatibility." *J. Mater. Sci. Mater. Med.*, 24(8), 1951–1961.

López, M. M. M., Fauré, J., Cabrera, M. I. E., and García, M. E. C. (2016). “Structural characterization and electrochemical behavior of 45S5 bioglass coating on Ti6Al4V alloy for dental applications.” *Mater. Sci. Eng. B*, 206 (Supplement C), 30–38.

Lorentz, H. A. (1880). “Ueber die Beziehung zwischen der Fortpflanzungsgeschwindigkeit des Lichtes und der Körperdichte.” *Ann. Phys.*, 245(4), 641–665.

Ma, L. (2014). “Dissolution behavior of phosphate glasses.” *Dr. Diss.*

Maheswaran, A., Hirankumar, G., Heller, N., Karthickprabhu, S., and Kawamura, J. (2014). “Structure, dielectric and bioactivity of  $P_2O_5$ -CaO- $Na_2O$ - $B_2O_3$  bioactive glass.” *Appl. Phys. A*, 117(3), 1323–1327.

Majumdar, A., and Jana, S. (2001). “Glass and glass-ceramic coatings, versatile materials for industrial and engineering applications.” *Bull. Mater. Sci.*, 24(1), 69–77.

Makishima, A., and Mackenzie, J. D. (1973). “Direct calculation of Young’s modulus of glass.” *J. Non-Cryst. Solids*, 12(1), 35–45.

Makishima, A., and Mackenzie, J. D. (1975). “Calculation of bulk modulus, shear modulus and Poisson’s ratio of glass.” *J. Non-Cryst. Solids*, 17(2), 147–157.

Manam, N. S., Harun, W. S. W., Shri, D. N. A., Ghani, S. A. C., Kurniawan, T., Ismail, M. H., and Ibrahim, M. H. I. (2017). “Study of corrosion in biocompatible metals for implants: A review.” *J. Alloys Compd.*, 701, 698–715.

Mandlule, A., Döhler, F., Wüllen, L. van, Kasuga, T., and Brauer, D. S. (2014). “Changes in structure and thermal properties with phosphate content of ternary calcium sodium phosphate glasses.” *J. Non-Cryst. Solids*, 392, 31–38.

Marshall, J. (1990). *Glass source book*. Chartwell Books.

Massera, J., Mayran, M., Rocherullé, J., and Hupa, L. (2015). “Crystallization behavior of phosphate glasses and its impact on the glasses’ bioactivity.” *J. Mater. Sci.*, 50(8), 3091–3102.

Massera, J., Vassallo-Breillot, M., Törngren, B., Glorieux, B., and Hupa, L. (2014). “Effect of CeO<sub>2</sub> doping on thermal, optical, structural and in vitro properties of a phosphate based bioactive glass.” *J. Non-Cryst. Solids*, 402, 28–35.

“Measurement of Crystallinity and Phase Composition of Hydroxyapatite by XRD - Hitpages.” <<https://www.hitpages.com/doc/4785854308417536/7/>> (Dec. 18, 2016).

Merwin, G. E., Atkins, J. S., Wilson, J., and Hench, L. L. (1982). “Comparison of ossicular replacement materials in a mouse ear model.” *Otolaryngol.-Head Neck Surg. Off. J. Am. Acad. Otolaryngol.-Head Neck Surg.*, 90(4), 461–469.

Metikoš-Huković, M., Kwokal, A., and Piljac, J. (2003). “The influence of niobium and vanadium on passivity of titanium-based implants in physiological solution.” *Biomaterials*, 24(21), 3765–3775.

Moore, Wellington. (1964). “Comparative Metabolism of Barium-133 and Calcium-45 by Embryonic Bone Grown in Vitro.” *Radiat. Res.*, 21(3), 376–382.

Morse, D. L., and Evenson, J. W. (2016). “Welcome to the Glass Age.” *Int. J. Appl. Glass Sci.*, 7(4), 409–412.

Müller, L., and Müller, F. A. (2006). “Preparation of SBF with different HCO<sub>3</sub><sup>-</sup> content and its influence on the composition of biomimetic apatites.” *Acta Biomater.*, 2(2), 181–189.

Narayanan, M. K., and Shashikala, H. D. (2015). “Physical, mechanical and structural properties of BaO–CaF<sub>2</sub>–P<sub>2</sub>O<sub>5</sub> glasses.” *Journal of Non-Crystalline Solids*, 430, 79–86.

Narayanan, M. K., and Shashikala, H. D. (2015). “Thermal and optical properties of BaO–CaF<sub>2</sub>–P<sub>2</sub>O<sub>5</sub> glasses.” *Journal of Non-Crystalline Solids*, 422, 6–11.

N. Gunawidjaja, P., Izquierdo-Barba, I., Mathew, R., Jansson, K., García, A., Grins, J., Arcos, D., Vallet-Regí, M., and Edén, M. (2012). “Quantifying apatite formation and cation leaching from mesoporous bioactive glasses in vitro : a SEM, solid-state NMR and powder XRD study.” *J. Mater. Chem.*, 22(15), 7214–7223.

O’Donnell, M. D., Watts, S. J., Hill, R. G., and Law, R. V. (2009). “The effect of phosphate content on the bioactivity of soda-lime-phosphosilicate glasses.” *J. Mater. Sci. Mater. Med.*, 20(8), 1611–1618.

Pradhan, S., and Pokhrel, M. R. (2013). “Spectrophotometric Determination of Phosphate in Sugarcane Juice, Fertilizer, Detergent and Water Samples by Molybdenum Blue Method.” *Sci. World*, 11(11), 58–62.

Prison, J. M., Martinelli, J. R., Sene, F. F., and Bergo, P. (2008). “Crystallization of barium magnesium phosphate glasses determined by differential thermal analysis and X-rays diffraction.” *J. Non-Cryst. Solids, Glass and Related Materials* 8, 354(42), 4723–4726.

Pugliese, D., Boetti, N. G., Lousteau, J., Ceci-Ginistrelli, E., Bertone, E., Geobaldo, F., and Milanese, D. (2016). “Concentration quenching in an Er-doped phosphate glass for compact optical lasers and amplifiers.” *J. Alloys Compd.*, 657, 678–683.

Putlyaev, V. I., and Safronova, T. V. (2006). “A new generation of calcium phosphate biomaterials: The role of phase and chemical compositions.” *Glass Ceram.*, 63(3–4), 99–102.

Radev, L., Hristov, V., Samuneva, B., and Ivanova, D. (2009). “Organic/Inorganic bioactive materials Part II: in vitro bioactivity of Collagen-Calcium Phosphate Silicate/Wollastonite hybrids.” *Cent. Eur. J. Chem.*, 7(4), 711–720.

- Rai, V. N., Sekhar, B. N. R., Phase, D. M., and Deb, S. K. (2014). "Effect of gamma irradiation on the structure and valence state of Nd in phosphate glass." *ArXiv14064686 Cond-Mat Physicsphysics*.
- Rajendran, V., Nishara Begum, A., Azooz, M. A., and El Batal, F. H. (2002). "Microstructural dependence on relevant physical–mechanical properties on SiO<sub>2</sub>–Na<sub>2</sub>O–CaO–P<sub>2</sub>O<sub>5</sub> biological glasses." *Biomaterials*, 23(21), 4263–4275.
- Rajkumar, G., Rajendran, V., and Aravindan, S. (2012). "Role of MgO on the HAp forming ability in phosphate based glasses." *ResearchGate*, 38(5), 3781–3790.
- R. L., E., and Alshathly, M. (2014). "Microstructural characterization and in vitro bioactivity of SrO–SiO<sub>2</sub>–Na<sub>2</sub>O–CaO–B<sub>2</sub>O<sub>3</sub>–P<sub>2</sub>O<sub>5</sub> glasses." *Life Sci.*, 11, 36–46.
- Raouf, G. A., Gashlan, H., Khedr, A., Hamedy, S., and Al-Jabbri, H. (2015). "In vitro new biopolymer for bone grafting and bone cement." *Int. J. Latest Res. Sci. Tech.* 4(2), 2278–5299.
- Rasool, S. N., Rama Moorthy, L., and Jayasankar, C. K. (2013). "Optical and luminescence properties of Dy<sup>3+</sup> ions in phosphate based glasses." *Solid State Sci.*, 22 (Supplement C), 82–90.
- Rocha-Rangel, E. (2011). "Fracture Toughness Determinations by Means of Indentation Fracture." *Nanocomposites Unique Prop. Appl. Med. Ind.*
- Rouxel, T., Ji, H., Guin, J. P., Augereau, F., and Rufflé, B. (2010). "Indentation deformation mechanism in glass: Densification versus shear flow." *J. Appl. Phys.*, 107(9), 94903.
- Salih, V., Franks, K., James, M., Hastings, G. W., Knowles, J. C., and Olsen, I. (2000). "Development of soluble glasses for biomedical use part II: The biological response of human osteoblast cell lines to phosphate-based soluble glasses." *J. Mater. Sci. Mater. Med.*, 11(10), 615–620.

Sandhu, G. S., Simari, R. D., Holmes, D. R., Dragomir, D. M. D., and Parakka, A. P. (2011). "Medical devices including duplex stainless steel."

Sathiyarayanan, S., Marikkannu, C., Srinivasan, P. B., and Muthupandi, V. (2002). "Corrosion behaviour of Ti6Al4V and duplex stainless steel (UNS31803) in synthetic bio-fluids." *Anti-Corros. Methods Mater.*, 49(1), 33–37.

Say, Y., and Aksakal, B. (2016). "Effects of hydroxyapatite/Zr and bioglass/Zr coatings on morphology and corrosion behaviour of Rex-734 alloy." *J. Mater. Sci. Mater. Med.*, 27(6), 105.

Sehgal, J., and Ito, S. (1999). "Brittleness of glass." *J. Non-Cryst. Solids*, 253(1), 126–132.

Sehgal, J., Nakao, Y., Takahashi, H., and Ito, S. (1995). "Brittleness of glasses by indentation." *J. Mater. Sci. Lett.*, 14(3), 167–169.

Sheha, R. R. (2007). "Sorption behavior of Zn(II) ions on synthesized hydroxyapatites." *J. Colloid Interface Sci.*, 310(1), 18–26.

Shelby, J. E. (2007). *Introduction to Glass Science and Technology*. Royal Society of Chemistry.

Shukla, A. K., Balasubramaniam, R., and Bhargava, S. (2005). "Properties of passive film formed on CP titanium, Ti–6Al–4V and Ti–13.4Al–29Nb alloys in simulated human body conditions." *Intermetallics*, 13(6), 631–637.

Sivakumar, M., Mudali, U. K., and Rajeswari, S. (1993). "Compatibility of ferritic and duplex stainless steels as implant materials: in vitro corrosion performance." *J. Mater. Sci.*, 28(22), 6081–6086.

Sola, A., Bellucci, D., and Cannillo, V. (2014). "Enamelled coatings produced with low-alkaline bioactive glasses." *Surf. Coat. Technol.*, 248 (Supplement C), 1–8.

- Souto, R. M., Rosca, I. C. M., and González, S. (2001). "Resistance to Localized Corrosion of Passive Films on a Duplex Stainless Steel." *Corrosion*, 57(4), 300–306.
- Spevak, L., Flach, C. R., Hunter, T., Mendelsohn, R., and Boskey, A. (2013). "FTIRI Parameters describing Acid Phosphate Substitution in Biologic Hydroxyapatite." *Calcif. Tissue Int.*, 92(5), 418–428.
- Stanley, H. R., Hall, M. B., Clark, A. E., King, C. J., Hench, L. L., and Berte, J. J. (1997). "Using 45S5 bioglass cones as endosseous ridge maintenance implants to prevent alveolar ridge resorption: a 5-year evaluation." *Int. J. Oral Maxillofac. Implants*, 12(1), 95–105.
- Stern, M., and Geary, A. L. (1957). "Electrochemical Polarization I . A Theoretical Analysis of the Shape of Polarization Curves." *J. Electrochem. Soc.*, 104(1), 56–63.
- Suguna, K., and Sekar, C. (2011). "Role of Strontium on the Crystallization of Calcium Hydrogen Phosphate Dihydrate (CHPD)." *J. Miner. Mater. Charact. Eng.*, 10(7), 625.
- Tai, B. J., Bian, Z., Jiang, H., Greenspan, D. C., Zhong, J., Clark, A. E., and Du, M. Q. (2006). "Anti-gingivitis effect of a dentifrice containing bioactive glass (NovaMin) particulate." *J. Clin. Periodontol.*, 33(2), 86–91.
- Tang, E., Tommaso, D. D., and Leeuw, N. H. de. (2010). "An Ab Initio Molecular Dynamics Study of Bioactive Phosphate Glasses." *Adv. Eng. Mater.*, 12(7), B331–B338.
- Tariwong, Y., Chanthima, N., Kaewkhao, J., Sangwaranatee, N., and Kim, H. J. (2016). "Photoluminescence Properties of CaO-BaO-P<sub>2</sub>O<sub>5</sub> Glass Systems Doped with Sm<sup>3+</sup>." *Key Eng. Mater.*, 675–676, 368–371.
- Taylor, J. R. (1997). *An Introduction to Error Analysis: The Study of Uncertainties in Physical Measurements*. University Science Books.

Tefft, B. J., Gooden, J. Y., Uthamaraj, S., Harburn, J. J., Klabusay, M., Holmes, D. R., Simari, R. D., Dragomir-Daescu, D., and Sandhu, G. S. (2013). “Magnetizable Duplex Steel Stents Enable Endothelial Cell Capture.” *IEEE Trans. Magn.*, 49(1), 463–466.

Tefft, B. J., Uthamaraj, S., Harburn, J. J., Hlinomaz, O., Lerman, A., Dragomir-Daescu, D., and Sandhu, G. S. (2017). “Magnetizable stent-grafts enable endothelial cell capture.” *J. Magn. Magn. Mater.*, 427, 100–104.

Toma, S. L., Gheorghiu, D. A., Radu, S., and Bejinariu, C. (2013). “The Influence of the Diffusion on Adherence of the 60T Deposits Obtained by Thermal Spraying in Electric Arc.” *Appl. Mech. Mater.*, 371, 270–274.

Tošić, M. B., Nikolić, J. D., Grujić, S. R., Živanović, V. D., Zildžović, S. N., Matijašević, S. D., and Ždrale, S. V. (2013). “Dissolution behavior of a polyphosphate glass into an aqueous solution under static leaching conditions.” *J. Non-Cryst. Solids*, 362(1), 185–194.

Tulyaganov, D. U., Agathopoulos, S., Ventura, J. M., Karakassides, M. A., Fabrichnaya, O., and Ferreira, J. M. F. (2006). “Synthesis of glass–ceramics in the CaO–MgO–SiO<sub>2</sub> system with B<sub>2</sub>O<sub>3</sub>, P<sub>2</sub>O<sub>5</sub>, Na<sub>2</sub>O and CaF<sub>2</sub> additives.” *J. Eur. Ceram. Soc.*, 26(8), 1463–1471.

Uo, M., Mizuno, M., Kuboki, Y., Makishima, A., and Watari, F. (1998). “Properties and cytotoxicity of water soluble Na<sub>2</sub>O–CaO–P<sub>2</sub>O<sub>5</sub> glasses.” *Biomaterials*, 19(24), 2277–2284.

Urbach, F. (1953). “The Long-Wavelength Edge of Photographic Sensitivity and of the Electronic Absorption of Solids.” *Phys. Rev.*, 92(5), 1324–1324.

Uthamaraj, S., Tefft, B. J., Hlinomaz, O., Sandhu, G. S., and Dragomir-Daescu, D. (2015). “Ferromagnetic Bare Metal Stent for Endothelial Cell Capture and Retention.” *J. Vis. Exp. JoVE*, (103).



- Venkateswara Rao, G., and Shashikala, H. D. (2014). "Structural, optical and mechanical properties of ternary CaO-CaF<sub>2</sub>-P<sub>2</sub>O<sub>5</sub> glasses." *J Adv Ceram*, 3(2), 109–116.
- Wang, X., and Wen, C. (2014). "Corrosion protection of mesoporous bioactive glass coating on biodegradable magnesium." *Appl. Surf. Sci.*, 303 (Supplement C), 196–204.
- Welch, R. C., Smith, J. R., Potuzak, M., Guo, X., Bowden, B. F., Kiczanski, T. J., Allan, D. C., King, E. A., Ellison, A. J., and Mauro, J. C. (2013). "Dynamics of glass relaxation at room temperature." *Phys. Rev. Lett.*, 110(26), 265901.
- Wilson, J., and Low, S. B. (1992). "Bioactive ceramics for periodontal treatment: comparative studies in the Patus monkey." *J. Appl. Biomater. Off. J. Soc. Biomater.*, 3(2), 123–129.
- Wilson, J., Pigott, G. H., Schoen, F. J., and Hench, L. L. (1981). "Toxicology and biocompatibility of bioglasses." *J. Biomed. Mater. Res.*, 15(6), 805–817.
- Xiang, Q., Liu, Y., Sheng, X., and Dan, X. (2007). "Preparation of mica-based glass-ceramics with needle-like fluorapatite." *Dental Materials*, 23(2), 251–258.
- Zanotto, E. D., and Mauro, J. C. (2017). "The glassy state of matter: Its definition and ultimate fate." *J. Non-Cryst. Solids*, 471 (Supplement C), 490–495.

## **LIST OF PUBLICATIONS FROM THESIS WORK**

### **PAPERS PUBLISHED IN PEER-REVIEWED JOURNALS**

- Edathazhe, A. B., and Shashikala, H. D. (2018). “Corrosion resistance and in-vitro bioactivity of BaO containing Na<sub>2</sub>O-CaO-P<sub>2</sub>O<sub>5</sub> phosphate glass-ceramic coating prepared on 316 L, duplex stainless steel 2205 and Ti6Al4V.” *Mater. Res. Express*, 5(3), 35404.
- Edathazhe, A. B., and Shashikala, H. D. (2018). “Dissolution and in vitro bioactive properties of BaO added Na<sub>2</sub>O–CaO–P<sub>2</sub>O<sub>5</sub> glasses.” *Physics and Chemistry of Glasses - European Journal of Glass Science and Technology Part B*, 59(1), 34–48.
- B Edathazhe, A., and Shashikala, H. D. (2016). “Effect of BaO addition on the structural and mechanical properties of soda lime phosphate glasses.” *Materials Chemistry and Physics*, 184, 146–154.

### **PAPERS PUBLISHED IN INTERNATIONAL CONFERENCE PROCEEDINGS**

- Akhila B Edathazhe and Shashikala, H. D. (2015). “The Effect of BaO Content and Soaking Temperature on Basis Structural Properties of Alkali-Alkaline Earth Phosphate Glasses.” *Bonfring*, 6.

### **MANUSCRIPT UNDER REVIEW IN INTERNATIONAL CONFERENCE PROCEEDINGS**

- Akhila B Edathazhe, H.D. Shashikala, (2016). “Dissolution studies of Na<sub>2</sub>O-BaO-CaO-P<sub>2</sub>O<sub>5</sub> glasses in deionized water under semi-dynamic conditions for bioactive applications.” *Material Today Proceedings*

## **MANUSCRIPT HAS TO BE COMMUNICATED**

- Akhila B Edathazhe, H.D. Shashikala, “Thermal and optical properties of BaO added Na<sub>2</sub>O-CaO-P<sub>2</sub>O<sub>5</sub> glasses”, compiled to communicate to an SCI journal

## **PAPERS PRESENTED IN INTERNATIONAL CONFERENCES**

- Akhila B Edathazhe, H.D. Shashikala, “Dissolution studies of Na<sub>2</sub>O-BaO-CaO-P<sub>2</sub>O<sub>5</sub> glasses in deionized water under semi-dynamic conditions for bioactive application”, International Conference on smart Engineering Materials (ICSEM-2016), R.V. College of Engineering, Bangalore, India, October 2016, (*Oral Presentation*).
- Akhila B Edathazhe, H.D. Shashikala, “The effect of BaO content and soaking temperature on basic structural properties of calcium sodium phosphate glasses”, International conference on advances in materials, manufacturing and applications (AMMA-2015), NIT Trichy, India, ISBN: 978-93-84743-62-8, April 2015, (*Oral Presentation*).

## **LIST OF PUBLICATIONS OTHER THAN THESIS WORK**

### **PAPERS PUBLISHED IN INTERNATIONAL CONFERENCE PROCEEDINGS**

- Edathazhe, A. B., and Shashikala, H. D. (2018). “Optical properties of BaO added bioactive Na<sub>2</sub>O-CaO-P<sub>2</sub>O<sub>5</sub> glasses.” *AIP Conference Proceedings*, 1943(1), 20072.

- Kumar, N. M., Rao, G. V., Akhila, B. E., and Shashikala, H. D. (2014). “Effect of CaF<sub>2</sub> addition on optical properties of barium phosphate glasses.” *AIP Conference Proceedings*, 1591(1), 733–735.

#### **PAPERS PRESENTED IN INTERNATIONAL CONFERENCES**

- Akhila B Edathazhe, H.D. Shashikala, “Optical Properties of BaO Added Bioactive Na<sub>2</sub>O-CaO-P<sub>2</sub>O<sub>5</sub> Glasses”, International Conference on Design, Materials & Manufacture (IcDeM 2018), NIT Karnataka, India, January 2018, (*Oral Presentation*).
- Manoj Kumar N., G.Venkateswara Rao., Akhila B.E., H. D. Shashikala, “Effect of CaF<sub>2</sub> Addition on Optical Properties of Barium Phosphate Glasses”, 58<sup>th</sup> DAE-Solid state physics symposium, Thapar University, Patiala, Punjab, India, December 2013, (*Poster Presentation*).

#### **PAPERS PRESENTED IN NATIONAL CONFERENCES**

- Akhila B Edathazhe, H.D. Shashikala, “Synthesis and characterization of barium phosphate glass with fly ash” National conference on condensed matter physics (CMPA-2013), MIT Manipal, India, December 2013, (*Best Oral Presentation Award*).
- Monisha G N, Akhila B Edathazhe, H. D. Shashikala, “Synthesis and characterization of phosphate glass thin film on metal substrate” National conference on condensed matter physics (CMPA-2015), MIT Manipal, India, April 2016, (*Best Poster Presentation Award*).

## **CURRICULAM VITAE**



**AKHILA B EDATHAZHE**

### **Permanent address**

Kaviyil (House),

Phone: +91- 9164706310, +91- 9632867001

Naduvil (P.O.), Vilakkannur,

Email id: akhilabilly@gmail.com

Kannur (District.), Kerala,

Secondary Email id: sijo.kaviyiljoseph@gmail.com

India, PIN- 670 582

### **Education**

- Ph.D. in Physics, National Institute of Technology (NIT) Karnataka, Surathkal, India, (2012 - 2018)
- M.Phil. in Physics, CGPA- 8.47, (University 3<sup>rd</sup> Rank), Periyar University, Tamil Nadu, India, (2011 - 2012)
- M.Sc. in Physics, CGPA- 8.41, Bharathiar University, Tamil Nadu, India, (2009 - 2011)

- B.Sc. in Physics, Total mark - 63.4%, Kannur University, Kerala, India, (2006 - 2009)
- Plus-two (Science), Total mark - 77.3%, Board of Higher Secondary Examination, Govt. of Kerala (2003 - 2005)
- SSLC, Total mark - 86.5%, Kerala State Board (2003)

### **Honors and Awards**

- MHRD (Ministry of Human Resource Development, Government of India) Fellowship for doing Ph. D. (2012-2017)
- 3<sup>rd</sup> Rank in M. Phil. Physics from Periyar University, Tamil Nadu
- ‘Outstanding Reviewer Award’ from journal ‘Material Science and Engineering C’ (Elsevier) in 2016
- Reviewed articles for journal ‘Biomedical Physics and Engineering Express’ (IOP), ‘Materials Research Express’ (IOP) and ‘Material Science and Engineering C’ (Elsevier)
- Best Oral presentation award in a National conference conducted in MIT Manipal, India (2013)
- Best Poster presentation award in National conference conducted in MIT Manipal, India (2016)

### **Research Experience**

- **Ph. D.** - Thesis Title: Investigation of properties, corrosion and bioactivity of novel BaO added phosphate glasses and glass-ceramic coating on biomedical metallic implant materials

- **M. Phil.** - Thesis Title: CTAB-Assisted synthesis of  $\text{Co}_3\text{O}_4$  nano powders by Hydrothermal method
- **M. Sc.** - Project Title: Synthesis and characterization of multiferroic  $\text{BiMnO}_3$  thin film by RF sputtering method

### Publications

Category	Published	Under communication	To be communicated
International Journals (SCI-Indexed)	3	-	2
International Conference Proceedings	3	1	-
National Conference Proceedings	2	-	-